Extraction of Energy-Dependent Information in Radiography

Robert E. Alvarez

With the renewed interest in dual energy imaging, I decided to make my Ph.D. dissertation available on the Internet. This took some doing since it was written in 1976, just before the day of electronic document preparation. This is the result converted from the paper copy. There are some slight changes to correct typographical errors and some of the figures have been re-computed instead of being taken from references (I couldn't resist) but it is mainly as originally written. In particular no more modern results have been added.

I did not find any obvious errors. There has been a lot of progress in the field but the fundamental results remain valid since they are based x-ray physics. I am working on updating to cover developments in the field of dual energy imaging but more on that later. I will periodically make corrections for typos but will not change the contents of this document and put updates in new documents.

Last updated February 16, 2015

Robert E. Alvarez
Mountain View, California
2007

Contents

1. An overview of the thesis

1.1. Introduction

A conventional single projection medical x-ray imaging system is shown in Fig. 1.1. This system is used in a large number of radiological examinations and is, perhaps, the apparatus that comes to mind when medical radiography is mentioned. The purpose of the system is to form an image of the x-ray shadows cast by the various parts of the body. It consists of three main parts: an x-ray tube, which is the source of x-ray photons; a collimating grid, which removes scattered photons so the image consists primarily of the photons which have not interacted with the body, and an imaging detector, which is usually a film screen cassette.

Although this system is widely used, it does not completely extract the information present in the transmitted x-ray photons. Rather, the information is an average value over both depth and x-ray energy. Spatially, it is an average value because the output is the projection of the transmission of a three-dimensional object onto a two-dimensional image. It is an average in energy because the transmission at any point is a function of x-ray energy. The image represents the transmission at a single average energy and thus ignores the information that can be extracted by making measurements at many different energies.

The averaging processes can be a serious limitation in many applications. Because of the spatial averaging, structures of interest are many times shadowed by other objects within the same line of sight. Also, the projection process makes it difficult to visualize subtle variations of the size or density of a large object. The averaging over energy removes significant information from the image. For example, a lesion exhibiting a high attenuation could have either a high density or be composed of a material with a relatively high average atomic number. By using energy dependent measurements, these two alternatives can be distinguished. The extra information gained by removing these averaging processes could have important clinical significance.

Recently, a highly successful technique has been introduced which removes the spatial averaging. This technique, known as computerized tomography [Ambrose and Hounsfield 1973], forms an image of a slice through an object by making measurements at many different positions and angles around the object and processing the measurements on a computer. Other forms of tomography had existed previously but none removed the spatial averaging completely. Their effect was to blur the contribution of objects not in the desired slice. Computerized tomography gives an accurate image of a slice through

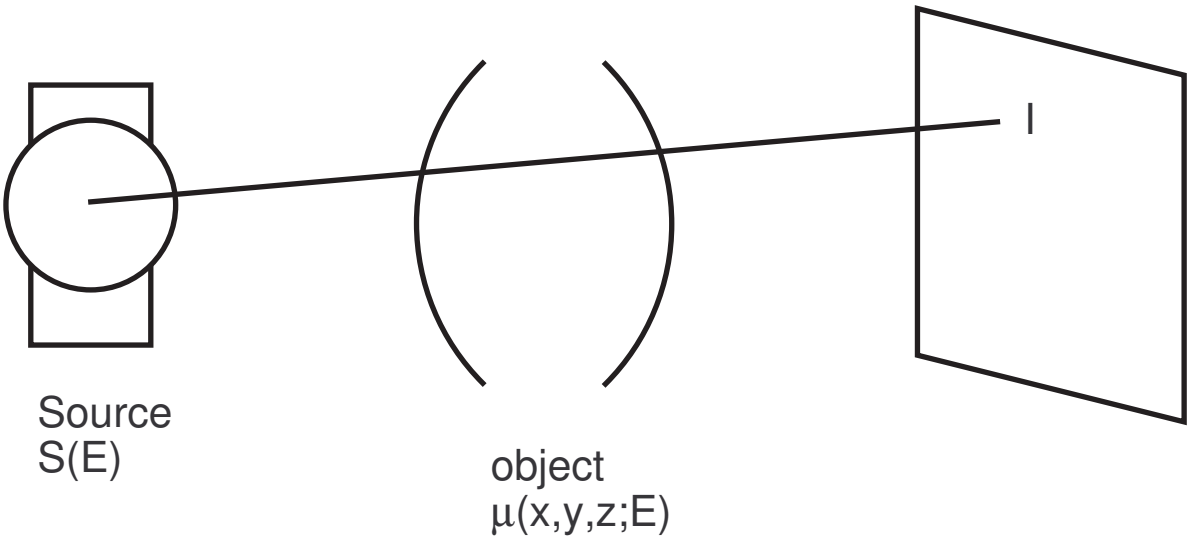

Figure 1.1.: Single projection medical x-ray imaging system. The x-ray flux at a point on the detector is $I = \int S(E) exp\left[-\int \mu(x,y,z;E) ds\right] dE$

a cross section of an object. Using this technique, radiologists have been able to see objects that had never been seen in a transmission x-ray image. Although it was recently introduced, this technique has had a significant impact on medical radiology.

This thesis describes techniques for extracting energy dependent information and, thus, removing the remaining averaging process. It will be shown that an image of the energy dependent information contains a significantly greater amount of useful data than an image which represents a single average energy. The usefulness of a technique to extract this information depends on factors such as the complexity of the system and the required patient dose. It will be shown that relatively simple measurements are sufficient to extract the information completely and that the resultant patient dose is comparable to that resulting from a conventional examination.

1.2. Previous Work in Extraction of Energy Dependent Information

There has been relatively little work in the extraction of energy dependent information. The work has been concentrated in three main areas: K edge techniques, imaging with radioisotope sources, and techniques based on changing x-ray tube voltage.

As early as 1925, Glocker and Frohnmayer used K edge techniques to increase the contrast of a specific element. The operation of this method may be understood by con-

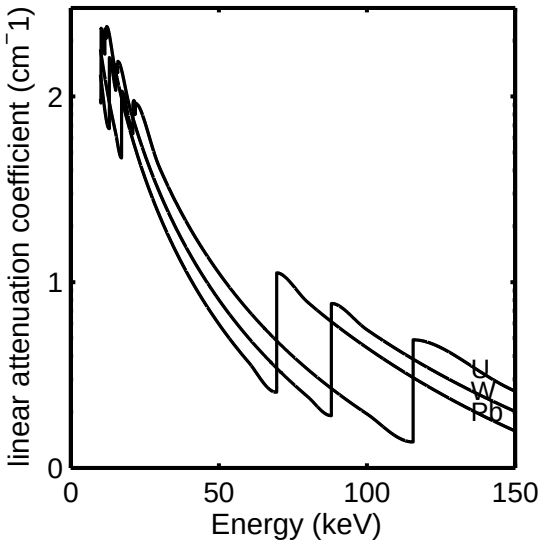

Figure 1.2.: Plot of the linear attenuation coefficients of several elements (W, Pb, U) showing their discontinuous behavior

sidering the attenuation coefficient function of energy of a typical element. As shown in Fig. 1.2, this is a decreasing function except at certain energies where the attenuation coefficient suddenly increases. These energies are characteristic of the element. The highest energy discontinuity is called the K edge. It is evident that, if the transmission is measured at energies just above and just below the K edge, only regions containing the specific element of interest will show a large change. By taking the difference between the transmissions, the contrast of this element can be greatly increased.

Various systems have been developed which use the K edge technique. In the 1950's Jacobson [Jacobson, 1958] developed a system capable of imaging the iodine in the thyroid gland. This was an elaborate system using analog electronics and containing wedges of material which had to be adjusted at each point in the image. Although accurate, it was apparently too slow to be useful in a clinical situation. Recently, Mistretta and others [Mistretta, et. al., 1974] have also introduced a system for K edge imaging. The system uses a highly filtered x-ray tube source and television techniques to produce an accurate difference image. The system is still in the experimental stage. Under controlled circumstances it has shown the capability of imaging 1-2 mg/cm2 of iodine.

Other than iodine, the elements occurring in the body in larger than trace amounts have K edges below 10 Key. The body transmission at these energies is so low that the technique cannot be applied. An accurate measurement of the transmission below and above the K edge would require a very large dose. Iodine, however, is an important case not only because it is naturally occurring but because it is used in many contrast materials.

Even at energies above the K edge, body materials have sufficiently different attenu-

ation coefficient functions of energy so that energy dependent measurements are very useful. Techniques have been developed which use measurements with radioactive isotope sources. These measurements are used to calculate the amount of bone calcification [Cameron and Sorenson,1963] and the relative amount of fat and muscle [Mazess, Cameron, Sorenson, 1970] along a straight line path through the body. The isotope sources do not produce enough photons per second to allow an imaging detector to be used. They are used in scanned systems.

Various techniques have been invented to extract energy dependent information in an imaging system. These techniques have been ad hoc and almost purely experimental.

Several workers have made measurements with different x-ray tube voltages to extract the energy dependent information. In the early 1950's several "color" x-ray imaging systems were produced [Takahashi, 1952; Donovan, 1951; Donovan and Jones, 1951]. In these systems, three exposures were taken with different x-ray voltages. The resultant images could be used to expose the three layers of a color film or projected using a triple projector with different color filters. Recently, a similar approach has been taken with computerized tomography systems [Ambrose and Hounsfield, 1973; Zatz, 1976]. Two scans are taken with different x-ray tube voltages. The technique has shown great sensitivity to iodine contrast materials.

An interesting color x-ray imaging system is described by Jacobson and Mackay (1958). This system utilizes the fact that x-rays with lower energies are stopped in smaller distances of a given material. A special cassette consisting of slabs of fluorescent material which emit light of different colors and a color film is used to extract the energy dependent information.

All these systems suffer from the lack of a sound theoretical basis. The type of information that can be extracted is not precisely known. Thus the signal processing used must be relatively simple and it is difficult to compare the various systems or to optimize any particular system.

1.3. Overview of the Thesis

The techniques for the extraction of energy dependent information are presented in two steps. First, the information that can be derived from energy dependent measurements is discussed. It is shown that complete energy dependent information can be obtained from low resolution measurements. Next, techniques for incorporating the necessary measurements in both single projection and computerized tomography systems are described.

Chapter 2 discusses the information available from energy dependent x-ray transmission measurements. First, the physics of the interactions of x-rays and matter are summarized. Next, it is shown that a set of functions, $f_1(E)$ and $f_2(E)$, exist so that for materials with atomic number less than 20 and in the diagnostic energy region, any attenuation

coefficient function of energy $\mu(E)$ can be expressed as

$$\mu(E) = a_1 f_1(E) + a_2 f_2(E) \tag{1.3.1}$$

to an accuracy better than that of an x-ray measurement. Thus the problem of extracting energy dependent information has been transformed from one of estimating a complete function of energy to one of estimating two constants. This provides a theoretical framework for extracting energy dependent information.

Since only two constants must he estimated, low energy-resolution measurements should be sufficient to determine these constants. In Chapter 3 we discuss the extraction of the energy dependent information from low resolution measurements. In fact, a technique is described for gathering the information using detectors that measure the total energy or total number of the incident photons and have no energy resolution. This is done by making measurements with two different incident spectra. A statistical model is developed for the measurement process. This model is used to find expressions for the errors due to the fundamental limiting noise source, Poisson counting noise.

Energy dependent information can be measured in a single projection system. Since the system still has spatial averaging, the quantities that can be measured are the line integrals of the coefficients a_1 and a_2. In Chapter 4, the techniques for measuring these line integrals are described. These techniques are used to form an image equivalent to a high voltage radiograph but without the difficulties encountered in high energy measurements. Also, the conditions under which an image of a particular substance can be formed are discussed. Two experiments are described which show the validity of these ideas. One experiment shows selective material imaging using the scanned x-ray source and detector of the EMI scanner. Another experiment shows a system to make an image of bone only or soft tissue only. Finally, the techniques for measuring the two intensities that are necessary to calculate the line integrals in an imaging system are summarized.

A computerized tomography system provides an excellent framework for making energy dependent measurements because electronic rather than film detectors are used. By using the techniques described in Chapters 3 and 4, the line integrals of the coefficients a_1 and a_2 can be calculated. In chapter 5, we show that the techniques of computerized tomography can then be used to calculate a_1 and a_2 at every point in the cross section of an object. A computer simulation is used to illustrate this procedure. Expressions are derived for the errors in the reconstructed values due to counting noise. Energy dependent techniques can be used to avoid an important error that occurs in conventional single average energy computerized tomography systems. This error occurs because there is not enough information present in a single intensity measurement with a broad spectrum source to accurately calculate the line integral of the linear attenuation coefficient. This quantity must be calculated to carry out a reconstruction. In Chapter 6 the techniques used in current systems to calculate the line integrals are discussed. A unified theoretical analysis of these techniques is described which allows them to be compared and which allows their dependence on system parameters to be derived. It is shown that the line

integral cannot be calculated from a single intensity measurement with a broad spectrum source. Finally, we show that energy dependent techniques provide a generally applicable accurate technique for calculating the line integral.

Chapter 7 is a summary of conclusions and final remarks. It includes suggestions for further research.

Appendix A describes a numerical method for solving the equations relating the measured intensities to the desired line integrals of a_1 and a_2. The technique is a generalization of the well-known Newton-Raphson method to the problem of two simultaneous equations. Appendix B describes a least squares curve fitting technique for determining the values of a_1 and a_2 from experimentally measured values of the attenuation coefficient.

2. INFORMATION AVAILABLE FROM X-RAY ATTENUATION MEASUREMENTS

2.1. Introduction

As described in Chapter 1, the information in a conventional radiograph represents an averaging process over energy. In this chapter we will discuss the information that is available from measurements at a great many energies. We will be concerned with the information at a single point in the radiographic image. The radiologist extracts diagnostically useful information from the values at any given point and from the two-dimensional patterns of the data.

This chapter has three main parts. The types of information available depend on the physics of the interactions of x-rays and matter. This will be discussed in the first part of this chapter. Next, we will consider the situation from the point of view of extracting information. This information is summarized by the linear attenuation coefficient function of energy. We will show how to convert the problem from one of estimating a complete function of energy to one of estimating a small number of constants independent of energy. Finally, we will discuss some implications of this theory to medical radiography. The values of the constants for body materials will be shown. The implications of having a two function basis set will be discussed.

2.2. X-Ray Energies Used in Diagnostic Radiology

The interactions of electromagnetic radiation and matter are strongly dependent on the energy of the photons. In order to study the possible types of interactions, the energy region must be specified. The x-rays used in medical diagnostic apparatus have energies from approximately 10 to 300 Key. This energy region is dictated mainly by the transmission properties of the body. For common body materials and thicknesses, the contrast per unit dose has a maximum in this region [Jacobson and Mackay 1958]. The contrast C of a radiographic system is defined to be

$$C = \frac{\delta n}{n} \tag{2.2.1}$$

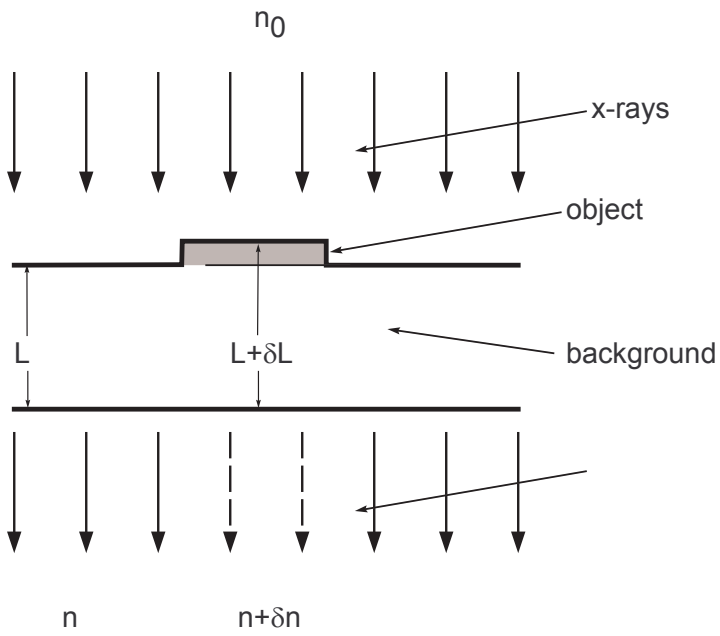

Figure 2.1.: Quantities in the definition of contrast.

where n and δn represent numbers of photons as shown in Fig. 2.1. This definition of contrast is useful because this quantity is equal to the change in attenuation of the object. The attenuation τ is defined by

$$n = n_0 e^{-\tau} \tag{2.2.2}$$

where n is shown in Fig. 2.1 as the number of photons incident on the object. Differentiating this expression

$$\delta n = -(n_0 e^{-\tau})\delta\tau \tag{2.2.3}$$

Thus

$$\delta\tau = -\frac{\delta n}{n} \tag{2.2.4}$$

The dose (or actually the average quantity which is mean specific energy) is proportional to the energy deposited by the photons per mass [ICRU 1971]. This is determined by the number of photons absorbed $n_0 - n$, the energy of each photon E, and the mass, which is the density ρ times the volume, the product of the area A and the thickness L. Thus

$$D = \frac{(n_0 - n)E}{AL\rho} \tag{2.2.5}$$

where A is x-ray cross sectional area, L is the object thickness, and p is the object mass density.

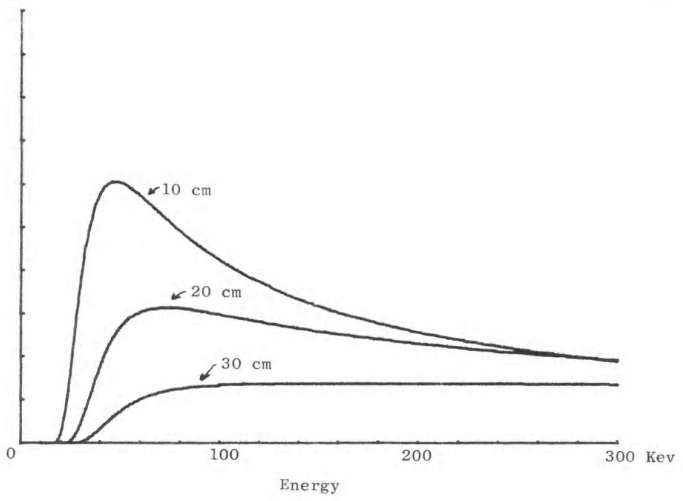

Figure 2.2.: Contrast per unit dose as a function of energy for various body thicknesses

The quantity that should be maximized is the contrast per unit dose

$$\frac{C}{D} = \frac{\delta n A L \rho}{n(n_0 - n)E} \tag{2.2.6}$$

This quantity is plotted as a function of energy in Fig. 2.2 for various thicknesses of water which is a major body constituent. For energies below the diagnostic energy region, the body attenuation is so large that essentially no photons are transmitted. Thus the contrast per unit dose becomes very small. At very low energies (in the microwave region), the body transmission increases but the wavelength of the radiation is so large that objects of interest cannot be resolved [Macovski 1975]. At energies above the diagnostic energy region the body attenuation becomes small so the contrast decreases. The dose increases because the energy per photon increases. The contrast per unit dose, therefore, decreases at higher energies. Practical limitations such as obtaining sufficiently high intensity sources and efficient detectors also limit the highest useable energy.

2.3. Definition of Cross Section and Linear Attenuation Coefficient

In the diagnostic energy region, the interactions of radiation with matter take the form of single processes with individual atoms. They can thus be described by cross sections which give the probability interaction of the photons with an atom. These are measured experimentally as shown in Fig. 2.3. Suppose n_0 photons of energy E are incident on a

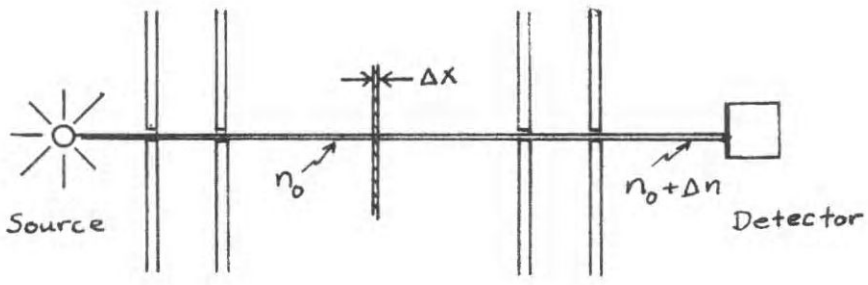

Figure 2.3.: Quantities in the Definition of Cross Section

thin absorber of thickness x. The absorber is assumed to consist of a single element with N atoms per unit volume. If on the average $n_0 + \delta n$ photons pass through the absorber without interacting, then the cross section $\sigma(E)$ is defined by

$$-\frac{\delta n}{n_0} = \sigma(E) N \delta x \tag{2.3.1}$$

Note that the cross section has the units of area.

The number of photons transmitted by a thick absorber may be calculated by integrating equation (2.3.1). The number that have not interacted after a thickness x will be

$$n(x) = n_0 e^{-\sigma(E)Nx} \tag{2.3.2}$$

The linear attenuation coefficient is defined to be

$$\mu(E) = \sigma(E)N \tag{2.3.3}$$

Note that this quantity has the units $(length)^{-1}$. If the material composition varies so $\mu = \mu(x, y, z; E)$, integrating equation (2.3.1) yields

$$n = n_0 e^{-\int \mu(x,y,z;E) ds} \tag{2.3.4}$$

where the line integral is over the path of the x-ray beam.

2.4. Kinds of Interactions in the Diagnostic Energy Region

The processes by which x-rays interact with matter may be classified according to the object with which the photon interacts and the effect of the interaction on the photon. These are summarized in Table 2.1 [Fano 1953].

Table 2.1.: Interactions of X-Rays and Matter

Kinds or Interaction	Effects of interaction
1. Interaction with atomic electrons	a. Complete absorption
2. Interaction with nuclear	b. Elastic scattering
3. Interaction with electric	c. Inelastic scattering
4. Interaction with meson field surrounding nuclear particles	

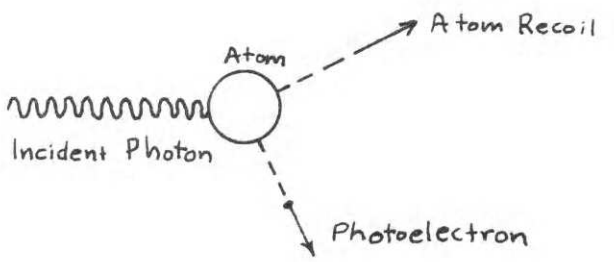

Figure 2.4.: Photoelectric Interaction of an X-Ray Photon with an Atom

There are twelve possible types of interaction processes. Not all of them have been observed and the probabilities of most of them are very small. Only three processes are important in the diagnostic x-ray energy region: the photoelectric effect (Ia), Compton scattering (Ic), and Rayleigh scattering (Ib).

The photoelectric effect involves photon with a bound atomic electron (usually from the inner shells of an atom). As shown in Fig. 2.4, the photon disappears, an electron leaves atom, and the atom as a whole recoils to conserve momentum.

The photoelectric interaction cannot occur unless the photon energy exceeds the binding energy of the electron. As the photon energy increases there are sharp jumps in the cross section at the binding energy of the various shells of the atoms. At these energies more electrons become available to interact. Beyond the binding energy of the innermost shell, the cross section decreases rapidly with energy. Figure 2.5 is a plot of the photoelectric cross section as a function of energy for various elements. Note that, at a given energy, the cross section depends strongly on the atomic number.

Compton scattering is the dominant interaction in the diagnostic range when the photon energy is much greater than the binding energy of the electron. As shown in Fig. 2.6, a scattered photon appears at some angle e with the original photon direction. In this interaction the electron acts as a free particle and recoils to conserve momentum. Because of the energy imparted to the electron, the scattered photon has less energy than the

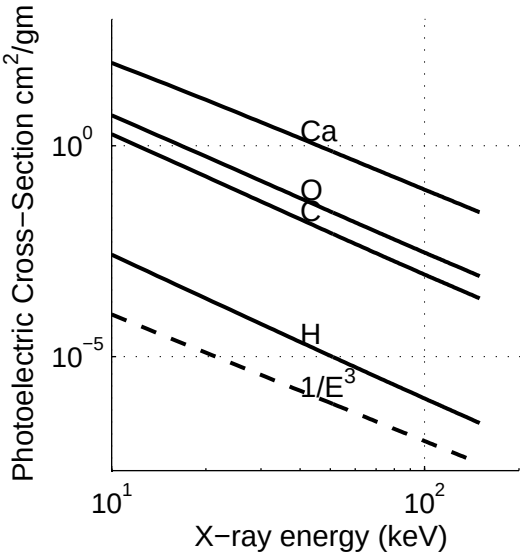

Figure 2.5.: Photoelectric Cross Section as a Function of Photon Energy for several elements. Also plotted is the function $1/E^3$

incident photon. If E is the original and E' is the scattered photon energy, then (m is the elctron rest mass and c is the speed of light)

$$\frac{1}{E'} - \frac{1}{E} = \frac{1}{mc^2}(1 - \cos\theta) \tag{2.4.1}$$

The relative probability for Compton scattering is a function of the scattering angle. The distribution becomes peaked in the forward direction as energy is increased. Thus, for given collimator acceptance angle , more scattered photons are detected the energy increases. This is undesirable and is another reason for limiting the upper energy of the diagnostic energy region The contribution of Compton scattering to the linear attenuation coefficient depends on electron density. The total cross section for scattering into any angle as a function of energy is given by the Klein-Nishina formula [Klein and Nishina 1929]

$$\sigma_C = 2\pi r_0^2 \left\{ \frac{1+\alpha}{\alpha^2} \left[\frac{2(1+\alpha)}{1+2\alpha} - \frac{1}{\alpha}\ln(1+2\alpha) \right] + \frac{1}{2\alpha}\ln(1+2\alpha) - \frac{1+3\alpha}{(1+2\alpha)^2} \right\} \tag{2.4.2}$$

where $r_0 = \frac{\mu_0 e^2}{4\pi m}$ and $\alpha = \frac{h\nu}{mc^2}$. Although this formula appears complicated, it actually defines a smooth, well-behaved function of energy. This function is plotted in Fig. 2.7

Rayleigh scattering is a cooperative effect of all the electrons in an atom The incident electromagnetic field forces all the electrons to vibrate at its frequency. The vibrating electrons in turn radiate electromagnetic energy whose intensity is the square of the sum

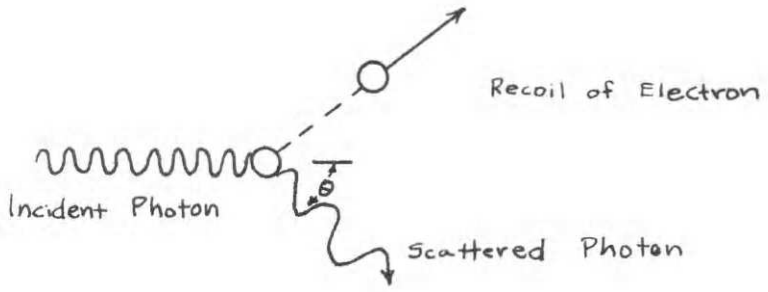

Figure 2.6.: Compton Scattering of a Photon

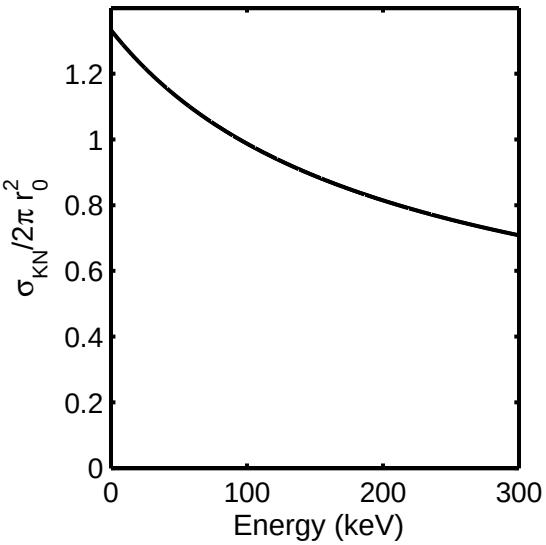

Figure 2.7.: Klein-Nishina Function of Energy

of the amplitudes of the radiation from each electron. The frequency of the scattered and incident radiation is the same. The cross section for this interaction is

$$\sigma_R(E) = \frac{3}{8}\pi r_0^2 f(\theta) \tag{2.4.3}$$

where r_0 is as defined previously, and $f(\theta)$ is an atomic scattering factor which depends strongly on atomic number, energy, and angle. In the forward direction all the amplitudes are in phase and add to give a high intensity. At other angles, the amplitudes are out of phase and give a smaller intensity. The cross section for Rayleigh scattering is thus peaked in the forward direction. It varies with energy as E^{-n} where n is between two and three [Dyson 1973].

The interaction processes act independently and are mutually exclusive [Evans 1955). Thus, the probability of a photon traversing an without any interactions is the product of the probabilities of undergoing any of the individual interactions. This is

$$Probability = e^{-(\mu_P+\mu_C+\mu_R)x} \tag{2.4.4}$$

where x is the object thickness and μ_P, μ_C, μ_R are the linear attenuation coefficients due to photoelectric, Compton, and Rayleigh scattering interactions. The total attenuation coefficient is simply the sum of the attenuation coefficients for the individual processes

$$\mu = \mu_P + \mu_C + \mu_R \tag{2.4.5}$$

2.5. Interactions of Mixtures

Since, in the diagnostic energy region, the x-ray photon energies are much higher than chemical binding energies, the total cross section of a material containing more than one element is simply the sum of the contributions from each element.

$$\sigma = \sum_{i=1}^{N} \sigma_i \tag{2.5.1}$$

If the material contains $N_i$atoms per unit volume of element number i, the linear attenuation coefficient will be

$$\mu = \sum_{i=1}^{N} N_i \sigma_i \tag{2.5.2}$$

This rule is highly accurate except at energies within one or two Key of an absorption edge [Deslattes 1969]. Since common body materials have absorption edges below the diagnostic energy region, the rule applies accurately in almost all cases of medical interest.

2.6. Extraction of Energy Dependent Information from Attenuation Measurements

Radiography systems, including computerized tomography systems, attempt to exclude scattered radiation and base their measurements on the photons that have not interacted with the body. In these systems, if the linear attenuation coefficient function $\mu(x, y, z; E)$ is known at all points and all energies, then equation 2.3.4 can be used to calculate the average number of photons that have not interacted with the body. Since this is the quantity measured, the linear attenuation coefficient function summarizes the information that can be extracted by an x-ray attenuation measurement.

If a high energy resolution detector was used, then one could conceiveably use this detector in a computerized tomography system to reconstruct the function $\mu(x, y, z; E)$ at all points and energies of interest within the body. This would be exceedingly slow and involve complex apparatus. Furthermore, all the information would be of little use because it could not be displayed or utilized by the radiologist.

An alternate approach is to use vector space techniques. This technique involves finding a set of basis functions $\{f_i(E)\}$ such that, to an accuracy limited by the experimental errors in the measurements,

$$\mu(E) = a_1 f_1(E) + a_2 f_2(E) + \dots \tag{2.6.1}$$

Instead of estimating μ at every energy, the problem is one of estimating the coefficients $\{a_i\}$. If this procedure is to result in more simplicity, the set of functions $\{f_i(E)\}$ must be small.

The mixture rule described in section 2.5 has an important effect on the problem of finding a suitable set of basis functions. In general the set $\{f_i(E)\}$ would have an infinite number of functions. The mixture rule, however, states that $\mu(E)$ is the sum of the attenuation coefficient functions of the elements present in significant amounts in the body. If there are N of these elements

$$\mu = \sum_{i=1}^{N} a_i \mu_i \tag{2.6.2}$$

Thus $\mu(E)$ is contained in a space with dimension less than or to N. Except for iodine in the thyroid and various trace elements, materials of the body have atomic number less than 20 [Cho, 1975].

The dimension of the space containing $\mu(E)$ can be reduced further if the attenuation coefficient of any element present in the body can be expressed as the linear combination of a small set of functions. The choice of these basis functions can be guided by the physics of the interactions. As discussed in section 2.4, there are three significant interactions: the photoelectric effect, Compton scattering, and Rayleigh scattering. Furthermore, as shown in Eq. 2.4.5, the contributions of these interactions to the linear attenuation coefficient add. If energy functions could be found to describe these interactions, would

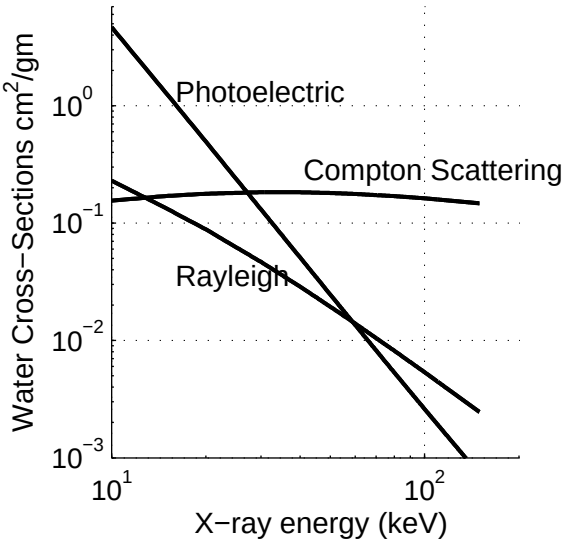

Figure 2.8.: Cross-sections as a function of energy for water

be good candidates for a basis set. The cross section per electron for Compton scattering as a function of energy is given by the Klein-Nishina formula, Eq. 2.4.2. Experimental tests of this formula in the diagnostic energy region have excellent agreement with theory [Bernstein and Mann 1956].

No good theoretical formulas exist to describe the energy dependence of the photoelectric effect. Figure 2.4 shows calculations the photoelectric cross section for various elements as a function of energy. For the atomic number and energy region of interest, a/E^3seems to provide a good fit.

Figure 2.8 shows the relative contributions of the three interactions to the attenuation coefficient of water. The photoelectric effect and Compton scattering clearly predominate Rayleigh scattering. The dominance is even greater for higher average atomic number materials such as bone. The accuracy of computerized tomography is of the order of 0.1%. Thus it might be possible to distinguish Rayleigh scattering at some energies. However, as described in Section 2.4, its dependence on energy is very close to the form of the photoelectric effect.

The ultimate choice of a basis set is empirical. A set of functions must be found which, for the atomic number and energy region of interest, fit experimental data to an accuracy comparable to the measurement accuracy. The basis set will change as the accuracy of the measurement system increases.

Highly accurate measurements on body tissues have recently become available [Phelps, Hoffman, Ter-Pogossian 1975]. The measurement of the attenuation coefficient of a body material is a difficult task. First, because of the accuracy required, the measurement would be difficult for any material. Biological materials present a serious problem. They must be

removed from the donor and inevitably change in this process. In the measurements of Phelps, Hoffman, and Ter-Pogossian steps were taken to minimize these changes. Nevertheless, the relationship between the in-vivo and in-vitro values is still somewhat in doubt. For the purpose of testing the basis set, the measurements are entirely adequate. They represent highly accurate measurements of the attenuation coefficient of a material. If a good fit is found for these materials, the fit will also be good for the in-vivo values. The relationship between the values of the in-vivo and in-vitro measurements is the only matter of doubt.

The measurements were used to test a proposed representation

$$\mu(E) = a_1 f_1(E) + a_2 f_{KN}(E) \tag{2.6.3}$$

where $f_1(E) = 1/E^3$and $f_{KN}(E)$ is the Klein-Nishina function. The results are shown in Tables 2.2 and 2.3. The least squares curve fitting routine described in Appendix B was used. The accuracy is of the order of 0.1% for energies greater than 30 Kev. This is the order of magnitude of the measurement accuracy and also the accuracy of a computerized tomography system. The theoretical curves and the experimental points are shown in Fig. 2.9. The success of the fit with two functions indicates that the contribution of Rayleigh scattering cannot be distinguished. Or else, the value of a_1 contains the contribution of the photoelectric effect plus some contribution from Rayleigh scattering.

2.7. Physical Interpretation of Coefficients

The coefficients a_1 and a_2 can be related to the physical properties of the material. The value of $a_1$is determined mainly by the photoelectric interaction. This term is strongly dependent on the atomic number of the material. The value of a_1 is

$$a_1 \approx K_1 \frac{\rho}{A} Z^n \tag{2.7.1}$$

where K_1 is a constant, ρ is the mass density, A is the atomic weight, and Z is the atomic number. This expression is not exact, but it gives the approximate dependence on the physical parameters [Evans 1955].

The coefficient a_2 gives the contribution of Compton scattering. This coefficient is proportional to the electron density and thus

$$a_2 \approx K_2 \frac{\rho}{A} Z \tag{2.7.2}$$

The quantity Z/A is nearly constant for most elements except hydrogen so a_2 is roughly proportional to the mass density.

The measurements of Phelps, Hoffman, and Ter-Pogossian can be used to calculate values of a_1 and$a_2$for the tissues they measured. These give some indication of the range of values of these coefficients. There are two coefficients for every tissue. These are

Table 2.2.: RESULTS FOR FIT OF THEORETICAL FUNCTIONS TO EXPERIMENTAL DATA (SOFT TISSUE)

Energy (keV)	Fat (meas.)	Fat (Calc)	Brain (Meas.)	Brain (Calc.)	Pancreas(meas)	Pancreas (calc)
17.7	.6647	.6585	1.092	1.076	1.175	1.163
21.1	.4615	.4676	.7106	.7191	.7725	.7737
26.4	.3273	.3311	.4593	.4657	.4927	.4969
27.4	.3169	.3159	.4340	.4375	.4600	.4661
31.1	.2760	.2743	.3517	.3614	.3772	.3831
35.5	.2451	.2439	.3062	.3064	.3219	.3231
41.4	.2189	.2194	.2631	.2632	.2771	.2761
47.2	.2041	.2045	.2387	.2378	.2500	.2485
52.0	.1950	.1958	.2251	.2236	.2332	.2332
59.5	.1843	.1860	.2080	.2032	.2167	.2166
59.6	.1850	.1860	.2079	.2080	.2157	.2164
84.3	.1660	.1671	.1821	.1817	.1899	.1883
97.4	.1608	.1605	.1741	.1735	.1818	.1796
103.2	.1618	.1580	.1711	.1704	.1780	.1764
121.9	.1517	.1507	.1630	.1620	.1679	.1676
136.3	.1465	.1460	.1586	.1566	.1621	.1620

Table 2.3.: RESULTS FOR FIT OF THEORETICAL FUNCTIONS TO EXPERIMENTAL DATA (BONE)

Energy (keV)	Meas.	Calc.
10	20.0	20.2
15	6.28	6.14
20	2.78	2.11
30	.958	.940
40	.510	.505
50	.347	.347
60	.272	.274
80	.208	.212
100	.180	.184
150	.14	.154

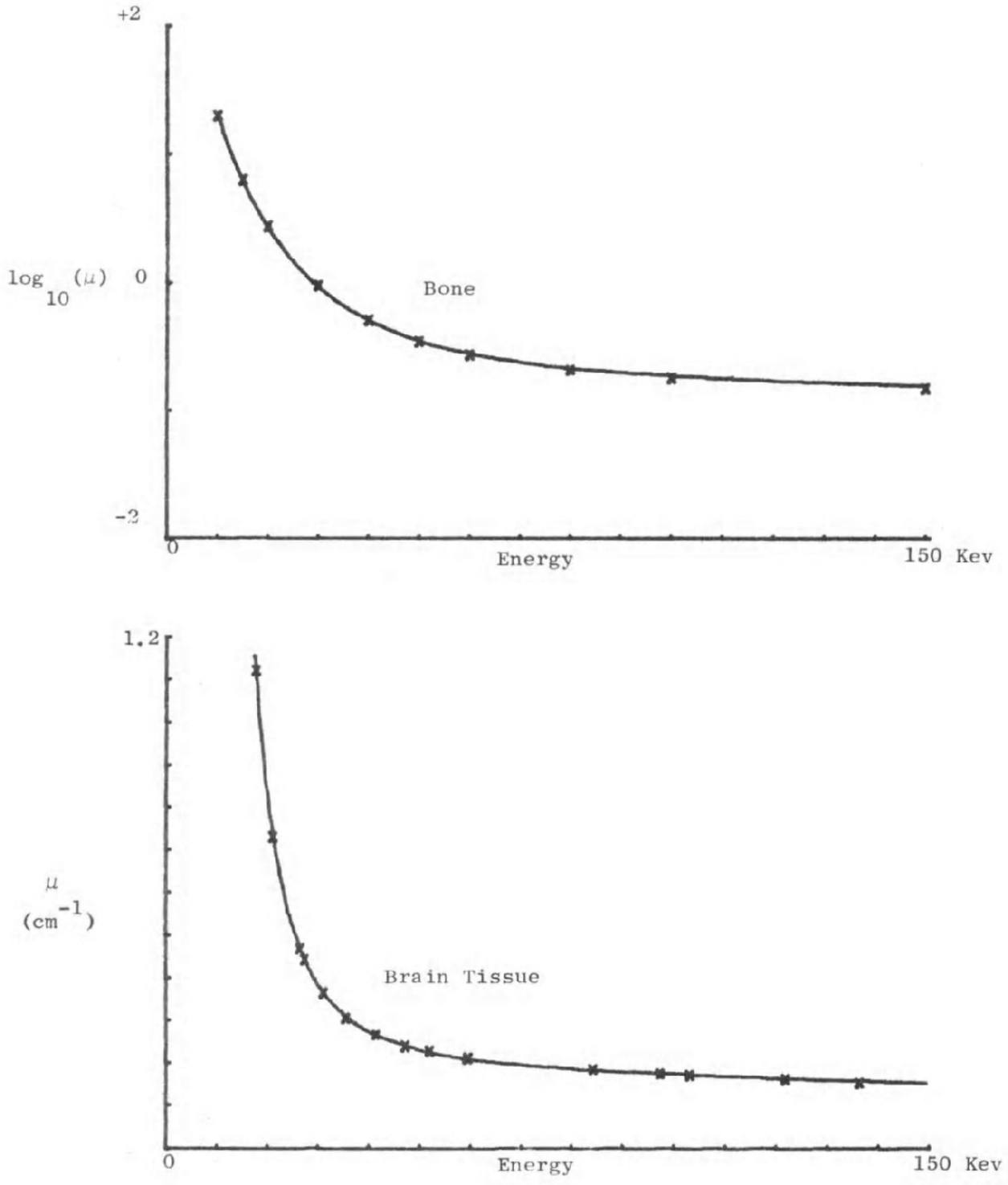

Figure 2.9.: Theoretical curves and experimental values for attenuation coefficients. The crosses are experimental values.

plotted on a two dimensional presentation in Fig. 2.10. A conventional system will give the value of the linear attenuation coefficient at a single energy E_0

$$\mu(E_0) = a_1 f_1(E_0) + a_2 f_{KN}(E_0) \tag{2.7.3}$$

This represents the projection of the data in Fig. 2.10 onto a line passing through the origin with slope $\frac{f_1(E_0)}{f_2(E_0)}$. There is obviously more information in the two dimensional data than in the one dimensional projection.

2.8. Implications of a Two Function Basis Set

The fact that there are only two functions in the basis set has several important implications. First, any basis set is not unique. Mathematically, a set of linear combinations of the functions may also be an adequate basis set. The physical implication of this fact is that the attenuation coefficients of any two distinct materials are also a good basis set. In Chapter 4 this will be shown to have a strong effect on the interpretation and limitations of selective material imaging in a conventional single projection x-ray system.

The two function basis set also has many practical implications. It implies that complete energy dependent information can be extracted from relatively simple measurements. This will be discussed in the next chapter.

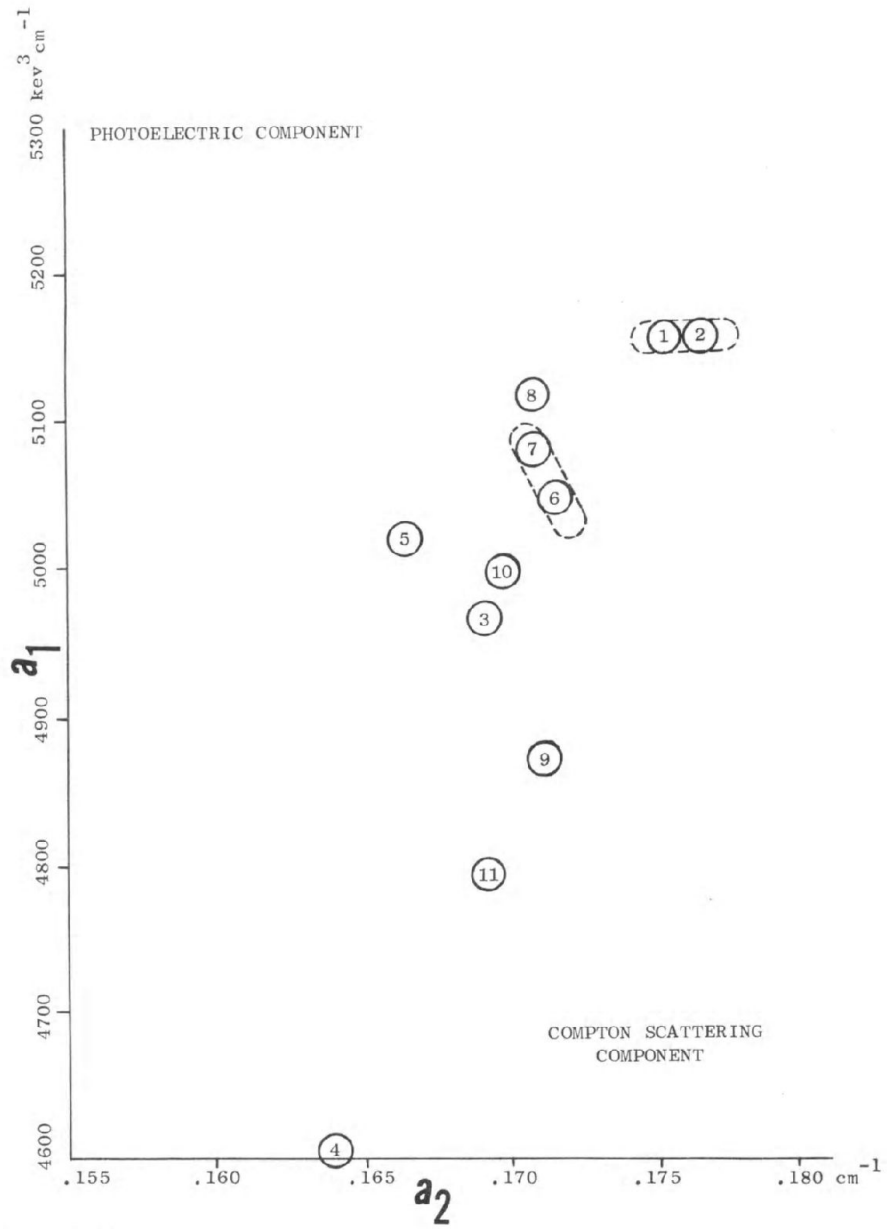

1. Clotted blood
2. Clotted blood
3. Subdural hematoma
4. Water
5. Neuroma
6. Meningioma
7. Meningioma
8. Medullablastoma
9. Astrocytoma
10. Human grey matter
11. Human white matter

Figure 2.10.: Two-dimensional plot of the information available from energy spectral analysis. The values of the coefficients a_1 and a_2 are calculated from measurements of the attenuation coefficients of body materials at 16 energies in the diagnostic region. Each point represents the (a_1, a_2) values for a given body material.

3. Extraction of Energy Dependent Information with Broad Spectrum Measurements

3.1. Introduction

As discussed in Chapter 2, the complete energy dependent information in an x-ray transmission measurement is summarized by two constants which are independent of energy. It should be possible to calculate these constants from measurements having low energy resolution. The detectors that are now commonly used in radiography, such as film screen cassettes or sodium iodide scintillation detectors, integrate over energy and have essentially no energy resolution. These detectors have been perfected over a long period of time and it would be advantageous to design a system configuration that would utilize them.

It might be possible to use integrating detectors to measure energy dependent information because of the analogy of the x-ray system to a color television camera. Both systems attempt to measure information that depends on the energy of electromagnetic radiation. In both cases the information is summarized by a small number of constants. The color television attempts to measure the amounts of three primary colors at any point in the scene. This is sufficient because the receptors in the human eye, apparently, can only distinguish between these three colors and their combinations (Rushton 1969). The color television camera extracts the color information by placing color filters between conventional integrating "black and white" cameras and the scene. The analogy in the x-ray system is to extract energy dependent information by making integrating measurements with different x-ray spectra incident on the patient.

In this chapter we will discuss the use of this type of measurement, as well as other low resolution measurements, to extract complete energy dependent information. First, we will introduce and define the concepts necessary to describe x-ray energy spectra. Next, we will discuss the deterministic considerations for calculating the information from broad spectrum measurements. The, accuracy of these measurements is fundamentally limited by the random nature of measurements on x-rays. In the last part of this chapter, we develop a stochastic model for the measurements and use it to derive an optimum procedure for estimating the energy dependent information. The errors in the estimates are dependent on the number of x-ray photons, and hence the dose, involved in the measurement and expressions relating these quantities are derived.

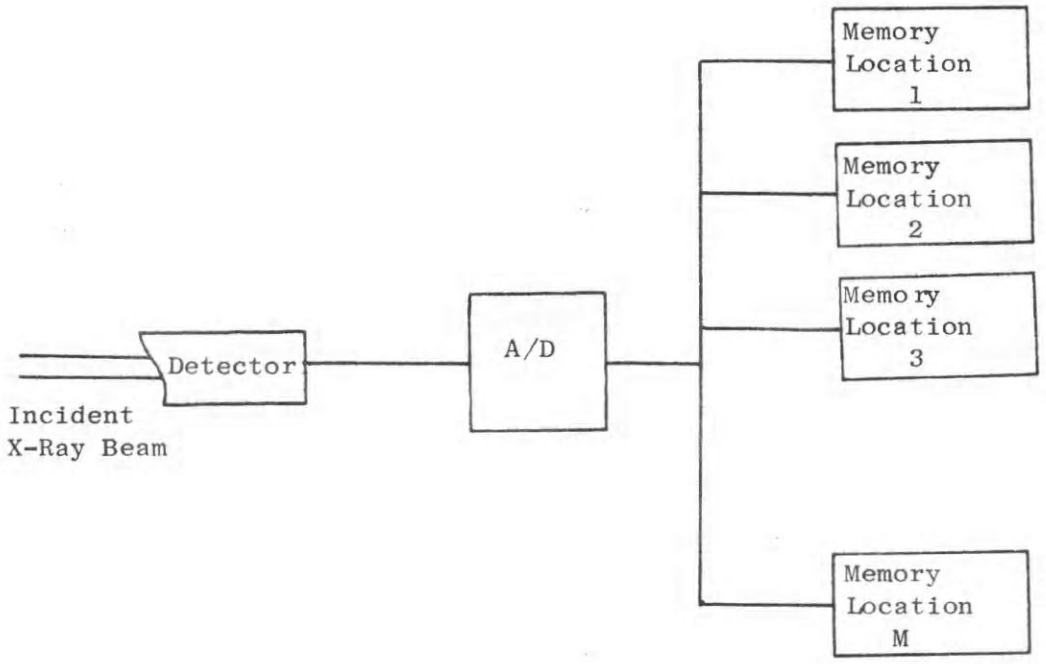

Figure 3.1.: System for measuring an x-ray energy spectrum

3.2. X-ray Spectra and Their Measurement

An x-ray spectrum may be measured using an energy resolving detector and a multichannel analyzer. The measurement system is shown schematically in Fig. 3.1. The system operates as follows:

> For every incident photon, the detector produces a pulse whose size is proportional to the energy of the photon. The A/D converter senses the pulse size and classifies it into one of n energy regions, or channels. The multichannel analyzer contains a memory with a location for each channel and circuitry to add one to the count of the appropriate channel for each measurement from the A/D converter. The system counts for a fixed time and then stops. At this point, the number of counts per channel will be proportional to the x-ray spectrum except for the random nature of the measurement.

A typical x-ray tube spectrum is shown in Fig. 3.2. The x-ray photons are produced by accelerating electrons across a high voltage in a vacuum tube and having them impinge on an anode. Two processes are responsible for the production of x-rays. The most important is bremsstrahlung radiation. This is caused by the deceleration of the electrons as they strike the anode and produces the broad continuous part of the spectrum. It is

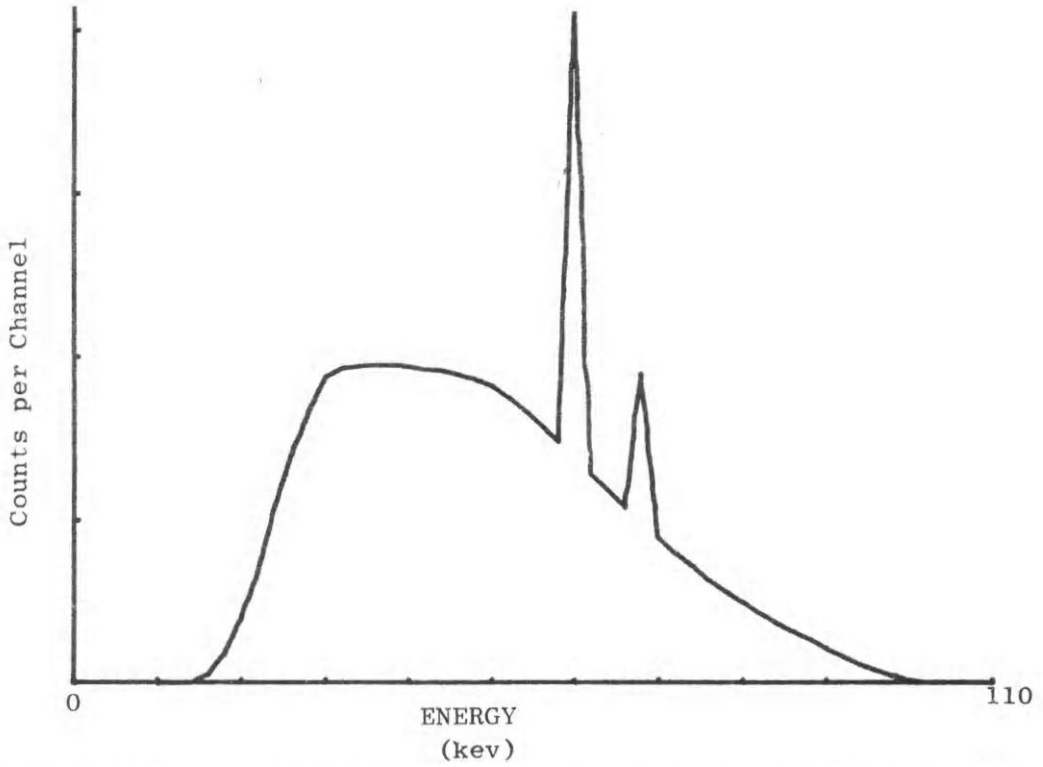

Figure 3.2.: Typical x-ray tube spectrum (from Epp and Weiss 1966)

impossible to produce photons with an energy greater than the electron kinetic energy so the bremsstrahlung spectrum has an upper cutoff energy. The second process produces the sharp spikes in the spectrum from 60 to 70 keV. In decelerating, the high energy electrons knock out inner shell electrons of the anode material. When these vacancies are filled, fluorescent radiation is emitted. The energy of this radiation is sharply defined and characteristic of the anode material (tungsten in the case of Fig. 3.2).

There are many practical difficulties in the measurement of an x-ray tube spectrum. First, no detector system has perfect energy resolution. The measurement is always the convolution of the detector energy impulse response with the desired quantity. Semiconductor detectors have resolution of about 1 keV. Also, high resolution pulse height analysis cannot analyze a large number of photons per second. X-ray tubes produce photons in copious amounts and provisions must be made to reduce the count rate. This is usually done by separating the detector and tube. Finally, the anode voltage of the x-ray tube is usually poorly filtered. The tube spectrum is not constant but varies with time. The spectrum that will be measured is an average over tine.

A precise terminology has been adopted (ICRU 1971) to describe x-ray spectra and related quantities. The terminology distinguishes between an experimental measurement which is a random quantity and non-stochastic quantities which can be estimated as an average of a series of experiments. The quantities that will be defined here are non-stochastic quantities. The definitions also distinguish between number measurements and energy measurements. Instead of recording the number of photons per channel, the measurement system could record the total energy per channel. This will yield another kind of spectrum.

The fluence, ϕ, of particles at a point is defined to be the quotient of the average number of particles dN which enter a sphere of area da centered at the point.

$$\phi = \frac{dN}{da} \tag{3.2.1}$$

The fluence rate, ψ, is the quotient of $d\phi$ by dt, where $d\phi$ is the increment of fluence in the time interval dt.

$$\psi = \frac{d\phi}{dt} \tag{3.2.2}$$

The definitions for energy fluence and energy fluence rate are exactly analogous.

A spectrum is the distribution of a quantity with respect to another quantity. The sum distribution $\phi(E)$is that part of the fluence rate due to particles with energies between 0 and E. The differential distribution of $\phi(E)$with respect to the particle energy will be called the spectrum $S(E)$.

$$S(E) = \frac{d\phi(E)}{dE} \tag{3.2.3}$$

In words, it is the average number of photons per unit area, per unit time, and per energy interval.

3.3. Extraction of Energy Dependent Information from Integrating Measurements–Deterministic Considerations

By analogy with a color television system, we would hope to be able to calculate the energy dependent information from measurements with detectors that integrate over energy. This leads to a set of integral equations that relate the measurements to the constants that summarize this information. In this section we derive these integral equations and conditions for the existence of a unique solution.

At any energy, the fraction of the photons that are transmitted through an object with linear attenuation coefficient $\mu(x, y, z; E)$is

$$fraction = e^{-\int \mu(x,y,z;E)ds} \tag{3.3.1}$$

If an x-ray beam with spectrum $S(E)$is incident on the object, the average number of photons that pass through the object is

$$N = AT \int S(E) e^{-\int \mu(x,y,z;E)ds} dE \tag{3.3.2}$$

where A is the detector area and T is the measurement time. This will be the number of photons counted by a detector system if its quantum efficiency G(E) is one at all energies in the diagnostic region. Otherwise G(E) must be included in the integral. The efficiency of detectors used in medical systems is close to one.

If two measurements with spectra $S_1(E)$ and $S_2(E)$ are made, the data are

$$N_i = AT \int S_i(E) e^{-\int \mu(x,y,z;E)ds} dE, \quad i = 1, 2 \tag{3.3.3}$$

Introducing the basis set $f_1(E)$ and $f_{KN}(E)$

$$\mu(x, y, z; E) = a_1(x, y, z) f_1(E) + a_2(x, y, z) f_{KN}(E) \tag{3.3.4}$$

so that

$$\int \mu(x, y, z; E) = A_1 f_1(E) + A_2 f_{KN}(E) \tag{3.3.5}$$

where

$$A_i = \int a_i(x, y, z) ds, \quad i = 1, 2. \tag{3.3.6}$$

The A_i are not to be confused with the detector area A. Substituting in equation 3.3.3, the integral equations that must be solved are

$$N_1 = AT \int S_1(E) e^{-A_1 f_1(E) - A_2 f_2(E)} dE \tag{3.3.7}$$

$$N_2 = AT \int S_2(E) e^{-A_1 f_1(E) - A_2 f_2(E)} dE \tag{3.3.8}$$

As discussed in Chapter 1, if only a single projection is used, there will be spatial averaging and only the line integrals of $a_1$and a_2 can be calculated. In Chapter 5, we will discuss the techniques for calculating $a_1$and a_2 from the measurement of many projections.

The spectra, $S_1(E)$ and $S_2(E)$, in equations 3.3.7 and 3.3.8 can be formed in many ways. For example, if an x-ray tube with spectrum $S(E)$ is used, they may be formed by filtering the x-rays from the tube through materials with transmissions $g_1(E)$ and $g_2(E)$ so $S_1(E) = S(E)g_1(E)$ and $S_2(E) = S(E)g_2(E)$). Alternately, the tube voltage can be changed to produce the two spectra. The same model can be used for a detector with simple energy resolution. If single level pulse height analysis is used so $S_1(E)$ is all the counts from 0 to some threshold energy E_T and $S_2(E)$ is all the counts with energy above E_T then the model with $g_1(E)$ and $g_2(E)$ appropriate rectangle functions may be used.

The model can also be generalized to the more realistic case where the threshold energy is not sharply defined.

For any given spectra, the equations 3.3.7 and 3.3.8 must be solved. This is not possible in all cases. A sufficient condition for the solution of these equations may be derived by considering them to define a transformation between (N_1, N_2) and (A_1, A_2). The transformation will be invertible, and thus the equations can be solved if the Jacobian of the transformation is nonzero (Kaplan 1973)

$$J = det \begin{pmatrix} \frac{\partial N_1}{\partial A_1} & \frac{\partial N_1}{\partial A_2} \\ \frac{\partial N_2}{\partial A_1} & \frac{\partial N_2}{\partial A_2} \end{pmatrix} \neq 0 \tag{3.3.9}$$

If the Jacobian is nonzero but has a small absolute value, it will be shown that there will be relatively large errors in the calculated values of (A_1, A_2).

The deterministic considerations for detectors that measure energy instead of the number of photons are essentially the same. The energy spectrum $I(E)$ must be used instead of the photon number spectrum $S(E)$. These are related by

$$I(E) = ES(E). \tag{3.3.10}$$

3.4. Stochastic Models for Measurements With Broad Spectrum Sources

Stochastic considerations are of fundamental importance in x-ray measurements for several reasons. In common with any other experimental procedure, x-ray measurements are random variables because of the influence of small factors that cannot be controlled in the experiment. Measurements on x-rays are random quantities for more fundamental reasons. The x-rays are produced by processes that take place on the atomic or nuclear scale. These processes are described by quantum mechanics and are inherently random. Since x-rays have sufficient energy so a single photon has a measurable effect, measurements on x-rays show the random nature of the processes that produce them.

The Poisson process is generally used to model the arrival times of x-ray photons at a detector. If a random process satisfies the following axioms, it can be shown to be a Poisson process (Parzen 1962). Suppose $N(t)$ is the number of photons that have arrived by time t. The axioms are:

1. Axiom 0: We begin counting at time 0 so N(O) = 0.
2. Axiom 1: The number of counts over disjoint time intervals are independent.
3. Axiom 3: It is not possible for photons to arrive simultaneously.
4. Axiom 4: For any two times $t > s \geq 0$ and any $h > 0$, the random variables $N(t) - N(s)$and $N(t + h) - N(s + h)$ are identically distributed.

These axioms seem to be a reasonable idealization of the random arrival of x-ray photons. By using these axioms the properties of a Poisson random process can be derived. The number of photons arriving at a detector have been experimentally shown to have the properties of a Poisson process.

Suppose a source, such as an x-ray tube, is used which produces photons with many different energies. The arrival times of these photons may still be described as a Poisson process. The energy may be included by using a marked Poisson process (Snyder 1975) . This is a conventional Poisson process plus a random variable. With the occurrence of each photon, the random variable describes its energy. The probability distribution function of the random variable is related to the spectrum by

$$f(E) = \frac{S(E)}{\int_0^\infty S(E)dE} \tag{3.4.1}$$

There are two basic types of x-ray detectors. One kind, such as a Nal scintillation detector used in counting mode, counts the number of photons incident on the detector regardless of their energy. The other kind, such as a Nal detector in current integrating mode or a film screen cassette, measures the total energy of the photons incident during the measurement period. Models for the measurements from both types of detectors will be developed.

Models for measurements with counting detectors are discussed in Parzen, 1962. In general, the counting process of the registered counts will be different from the counting process of the arriving photons because of the nonzero resolving time of the counter system. If two or more photons arrive during this resolving time, not all of them will be counted. The simplest case will be discussed here. In this case, the resolving time is much less than the mean time between the arrival of photons. The registered counts will then also be a Poisson process. If the detector counts for fixed time T, the number of counts will be a Poisson random variable with parameter

$$\beta = AT \int_0^\infty G(E)S(E)dE \tag{3.4.2}$$

In this equation G(E) is the probability of the detector counting a photon of energy E, S(E) is the spectrum incident on the detector and T is the counting time, and A is the area of the detector. For simplicity G(E) will be assumed equal to one.

Two or more measurements with different source spectra are needed to extract energy dependent information. From the axioms of a Poisson process, the measurements will be independent if they are taken at different times or with different detectors. If a detector with energy resolution is used, the measurements may be taken at the same tine. The relationship between measurements of different energy regions is described by the following theorem (Snyder 1975). Partition the energy region into a set of disjoint regions (B_k) and let (N_k) be the set of counting processes associated with the photons with energies in these regions. If the underlying process is Poisson and if the random variables associated

with the occurrence of each photon are independent and identically distributed, then the counting processes (N_k) are mutually independent Poisson counting processes. The k^{th} process will have an average number of photons per unit time

$$\lambda_k = \lambda \int_{B_k} f(E)dE \tag{3.4.3}$$

where f(E) is the probability distribution function of the photon energy and

$$\lambda = A \int_0^\infty S(E)dE \tag{3.4.4}$$

is the average number of photons of any energy per unit time. Measurements from a detector which measures total energy follow a slightly different law. The energy of the photons that are incident on a detector during a time T is

$$Q = \sum_{n=1}^{N(T)} E_n \tag{3.4.5}$$

In this equation N(T) is the Poisson random variable describing the number of photons arriving at the detector during the time T and the E_n are independent identically distributed random variables describing the energy of each photon. This is a compound Poisson process. If the average number of counts in the interval T is large and if $\overline{E^3}/\overline{E^2}$ is finite, Q will be approximately distributed as a normal random variable with mean m and variance σ^2

$$m = \lambda T \overline{E} \tag{3.4.6}$$

$$\sigma^2 = \lambda T \overline{E^2} \tag{3.4.7}$$

In these expressions an overbar denotes an expected value over the probability distribution function of the photon energy $f(E)$. This result is intuitively reasonable from the central limit theorem. Energy measurements share many properties with measurements of the number of photons. They will be independent if they correspond to different detectors, different time intervals, or nonoverlapping photon energy regions.

3.5. Estimation of A_1 and A_2 from Measurements with Counting Detectors

Since measurements with x-rays are random quantities, statistical techniques must be used to calculate the line integrals A_1 and A_2 from these measurements. In this section an optimum procedure, known as maximum likelihood estimation, for carrying out these calculations will be derived. Maximum likelihood estimation is based on choosing the values of A_1 and A_2 that maximize the probability of occurrence of the measured quantities. These estimators have many desirable features for large number of counts.

Suppose photons with a spectrum $S(E)$ are incident on an object. If the detector counts only photons that have not interacted with the object, the probability of a photon being counted is

$$P = e^{-\int \mu(x,y,z:E)ds} \tag{3.5.1}$$

The transmitted spectrum will be

$$S_t(E) = S(E)e^{-\int \mu(x,y,z:E)ds} \tag{3.5.2}$$

Since a Poisson process is preserved under random selection (Parzen 1962), the transmitted process will have the same stochastic properties as the incident spectrum.

The number of counts from measurements with different source spectra, N_1 and N_2, will be independent Poisson random variables with parameters

$$\beta_1 = C \int S_1(E)e^{-A_1 f_1(E) - A_2 f_{KN}(E)}dE \tag{3.5.3}$$

$$\beta_2 = C \int S_2(E)e^{-A_1 f_1(E) - A_2 f_{KN}(E)}dE \tag{3.5.4}$$

where the constant, C, is proportional to the detector area and the counting time. The probability of measuring N1 and N2 given that A_1 and A_2 take on some value is

$$P(N_1, N_2 \mid A_1, A_2) = \frac{\beta_1^{N_1} e^{-\beta_1}}{N_1!} \frac{\beta_2^{N_2} e^{-\beta_2}}{N_2!} \tag{3.5.5}$$

This function, called the likelihood function, must be maximized to give the maximum likelihood estimate. Since the logarithm is a monotonically increasing function it is equivalent, and easier, to maximize the logarithm of the likelihood function L,

$$L = N_1 \ln \beta_1 - \beta_1 + N_2 \ln \beta_2 - \beta_2 - \ln(N_1!\, N_2!) \tag{3.5.6}$$

This function will be maximum when

$$\frac{\partial L}{\partial A_1} = 0 = \frac{\partial \beta_1}{\partial A_1}\left(\frac{N_1}{\beta_1} - 1\right) + \frac{\partial \beta_2}{\partial A_1}\left(\frac{N_2}{\beta_2} - 1\right) \tag{3.5.7}$$

$$\frac{\partial L}{\partial A_2} = 0 = \frac{\partial \beta_1}{\partial A_2}\left(\frac{N_1}{\beta_1} - 1\right) + \frac{\partial \beta_2}{\partial A_2}\left(\frac{N_2}{\beta_2} - 1\right) \tag{3.5.8}$$

Equations (3.5.7) and (3.5.8) are a set of homogeneous linear equations in the quantities $\left(\frac{N_1}{\beta_1} - 1\right)$ and $\left(\frac{N_2}{\beta_2} - 1\right)$. The only unique solution is

$$\left(\frac{N_1}{\beta_1} - 1\right) = 0 \tag{3.5.9}$$

$$\left(\frac{N_2}{\beta_2} - 1\right) = 0 \tag{3.5.10}$$

which occurs when the determinant of the coefficient matrix is nonzero.

$$det\begin{pmatrix} \frac{\partial\beta_1}{\partial A_1} & \frac{\partial\beta_1}{\partial A_2} \\ \frac{\partial\beta_2}{\partial A_1} & \frac{\partial\beta_2}{\partial A_2} \end{pmatrix} \neq 0 \tag{3.5.11}$$

This is equivalent to requiring the Jacobian of the transformation from (β_1, β_2) to $(A_1, A_2)$to be nonzero.

The estimator equations (3.5.9) and (3.5.10) are equivalent to

$$N_1 = \beta_1 = C\int S_1(E)e^{-A_1 f_1(E) - A_2 f_{KN}(E)}dE \tag{3.5.12}$$

$$N_2 = \beta_2 = C\int S_2(E)e^{-A_1 f_1(E) - A_2 f_{KN}(E)}dE \tag{3.5.13}$$

Maximum likelihood estimation thus involves solving the deterministic equations with the measured data.

Maximum likelihood estimators have many desirable asymptotic properties (Van Trees 1968). For a large number of independent trials, the average of the estimates converges to the proper value and the variance approaches the Cramer-Rao bound. In our case, there is only one trial with a large number of counts. An approach based on Taylor's series may be used to calculate the bias and the variance of the estimates (Papoulis 1965).

The integrals in equations (3.5.12) and (3.5.13) define two functions $N_1 = \beta_1(A_1, A_2)$ and $N_2 = \beta_2(A_1, A_2)$. These functions may be inverted to give $A_1 = g_1(N_1, N_2)$ and $A_2 = g_2(N_1, N_2)$. Since $N_1$and N_2 are Poisson random variables, their standard deviation is the square root of the number of counts. As the number of counts increases, the relative spread of the counts decreases. Thus a Taylor's series with a small number of terms gives an accurate approximation to the inverse functions. Consider the Taylor's series about the average values $\bar{N}_1$ and$\bar{N}_2$

$$A_1 = g_1(\overline{N}_1, \overline{N}_2) + \frac{\partial g_1}{\partial N_1}(N_1 - \overline{N_1}) + \frac{\partial g_1}{\partial N_2}(N_2 - \overline{N_2}) + \frac{1}{2}\frac{\partial^2 g_1}{\partial N_1^2}(N_1 - \overline{N_1})^2 + \frac{1}{2}\frac{\partial^2 g_1}{\partial N_2^2}(N_2 - \overline{N_2})^2 + \dots \tag{3.5.14}$$

$$A_2 = g_2(\overline{N}_1, \overline{N}_2) + \frac{\partial g_2}{\partial N_1}(N_1 - \overline{N_1}) + \frac{\partial g_2}{\partial N_2}(N_2 - \overline{N_2}) + \frac{1}{2}\frac{\partial^2 g_2}{\partial N_1^2}(N_1 - \overline{N_1})^2 + \frac{1}{2}\frac{\partial^2 g_2}{\partial N_2^2}(N_2 - \overline{N_2})^2 + \dots \tag{3.5.15}$$

The bias of the estimates may be evaluated by finding the expected value of A_1 and A_2. These should be near $g_1(\overline{N_1}, \overline{N_2})$ and $g_1(\overline{N_1}, \overline{N_2})$ for a small bias. Taking the expected value of both sides of equation (3.5.14)

$$\overline{A_1} = g_1(\overline{N_1}, \overline{N_2}) + \frac{1}{2}\frac{\partial^2 g_1}{\partial N_1^2}\overline{N_1} + \frac{1}{2}\frac{\partial^2 g_1}{\partial N_2^2}\overline{N_2} + \dots \tag{3.5.16}$$

In deriving this expression, the fact that N_1 and N_2 are Poisson was used so $Ex(N_i - \overline{N_i})^2 = \overline{N_i}$. The bias of the estimate of $A_1$is therefore:

$$bias = A_1 - g_1(\overline{N_1}, \overline{N_2}) = \frac{1}{2}\frac{\partial^2 g_1}{\partial N_1^2}\overline{N_1} + \frac{1}{2}\frac{\partial^2 g_1}{\partial N_2^2}\overline{N_2} + \dots \tag{3.5.17}$$

The expression for the bias of A_2 is the same with g_2 substituted for g_1.

The variance of A_1 is $Ex(A_1 - \overline{A_1})^2$. Assuming A_1 is approximately equal to $g_1(\overline{N_1}, \overline{N_2})$, equation (3.5.14) may be used to show

$$Ex(A_1-\overline{A_1})^2 = (\frac{\partial g_1}{\partial N_1})^2\overline{N_1}+(\frac{\partial g_1}{\partial N_2})^2\overline{N_2}+\frac{1}{2}\frac{\partial g_1}{\partial N_1}\frac{\partial^2 g_1}{\partial N_1^2}Ex(N_1-\overline{N_1})^3+\frac{1}{2}\frac{\partial g_1}{\partial N_2}\frac{\partial^2 g_1}{\partial N_2^2}Ex(N_2-\overline{N_2})^3+\ldots \tag{3.5.18}$$

The first two terms are the Cramer-Rao bound. For a Poisson random variable $Ex(N - \overline{N})^3 = \overline{N}$. The variance of A_2 is the same with g_2 substituted for g_1.

The second derivative terms in these expressions are difficult to evaluate for the general case. In order to estimate the relative magnitude of the various terms, a simple case will be assumed. This is the case of measurements with two monoenergetic sources of energies $E_1$and E_2. The number of counts measured will be

$$N_1 = N_{10}e^{-A_1 f_{11} - A_2 f_{12}} \tag{3.5.19}$$

$$N_2 = N_{20}e^{-A_1 f_{21} - A_2 f_{22}} \tag{3.5.20}$$

These expressions result from the integrals in equations (3.5.12) and (3.5.13) when the spectrum S(E) is a delta function. The symbols in these equations are defined as follows: N_{10} and N_{20} are the numbers of photons of energies and incident on the patient during the measurement, $f_{11} = f_1(E_1)$, $f_{12} = f_{KN}(E_1)$, $f_{21} = f_1(E_2)$, and $f_{22} = f_{KN}(E_2)$. These equations can be solved for A_1 and A_2. The results are

$$A_1 = \frac{f_{12}\ln\frac{N_2}{N_{20}} - f_{22}\ln\frac{N_1}{N_{10}}}{(f_{11}f_{22} - f_{12}f_{21})} \tag{3.5.21}$$

$$A_2 = \frac{-f_{11}\ln\frac{N_2}{N_{20}} + f_{21}\ln\frac{N_1}{N_{10}}}{(f_{11}f_{22} - f_{12}f_{21})} \tag{3.5.22}$$

Using these equations, the bias may be calculated from equation (3.5.17). The results are:

$$bias(A_1) = \frac{\frac{f_{22}}{N_1} - \frac{f_{12}}{N_2}}{2(f_{11}f_{22} - f_{12}f_{21})} \tag{3.5.23}$$

$$bias(A_2) = \frac{-\frac{f_{21}}{N_1} + \frac{f_{11}}{N_2}}{2(f_{11}f_{22} - f_{12}f_{21})} \tag{3.5.24}$$

The bias decreases inversely with the number of counts. Since in a medical system, the number of counts is 10^6 or larger, the bias is quite small. Assuming energies of $E_1 = 50 \quad keV$ and $E_2 = 100 \quad keV$ and $N_1 = N_2 = 10^5$, the bias terms will be

$$bias(A_1) = -0.2(keV)^3 \tag{3.5.25}$$

$$bias(A_2) = 10^{-5} \tag{3.5.26}$$

The variance can be calculated using the equations for A_1 and A_2 and the general expression for the mean value of the A_i in (3.5.16). The results are:

$$E(A_1 - \overline{A_1})^2 = \frac{\frac{f_{12}^2}{N_2} + \frac{f_{22}^2}{N_1}}{(f_{11}f_{22} - f_{12}f_{21})^2} - \frac{\frac{f_{22}^2}{N_1^2} + \frac{f_{12}^2}{N_2^2}}{2(f_{11}f_{22} - f_{12}f_{21})^2} + \dots \tag{3.5.27}$$

$$E(A_2 - \overline{A_2})^2 = \frac{\frac{f_{11}^2}{N_2} + \frac{f_{21}^2}{N_1}}{(f_{11}f_{22} - f_{12}f_{21})^2} - \frac{\frac{f_{21}^2}{N_1^2} + \frac{f_{11}^2}{N_2^2}}{2(f_{11}f_{22} - f_{12}f_{21})^2} + \dots \tag{3.5.28}$$

Since N_1 and N_2 are large, the second and subsequent terms are negligible and the variance equals the Cramer-Rao bound. Note that the variance and bias are described by alternating series so the error in dropping terms is less than the absolute value of the first term dropped. Assuming the same energies and numbers of photons as for the bias calculations, the values of the standard deviations of A_1 and $A_2$are:

$$\sigma_{A_1} = 698.4(keV)^3 \tag{3.5.29}$$

$$\sigma_{A_2} = 3.76 \times 10^{-3} \tag{3.5.30}$$

Comparing the values of the standard deviation and the bias, it is clear that the standard deviation contributes a much larger error than the bias. Since the variance is very close to the Cramer-Rao bound, a general expression in terms of β_1 and β_2 may be derived (Van Trees 1968). The variance $\sigma_{A_1}^2$is

$$\sigma_{A_i}^2 = \frac{cofactor(J_{ii})}{det(J)} \tag{3.5.31}$$

where J is the Fisher information matrix with elements

$$J_{ij} = -Ex\left[\frac{\partial^2 L}{\partial A_i \partial A_j}\right] i,j = 1,2 \tag{3.5.32}$$

Evaluating these expressions yields the following for the variances of A_1 and A_2:

$$\sigma_{A_1}^2 = E(A_1 - \overline{A_1})^2 = \frac{\frac{m_{12}^2}{N_2} + \frac{m_{22}^2}{N_1}}{(m_{11}m_{22} - m_{12}m_{21})^2} \tag{3.5.33}$$

$$\sigma_{A_2}^2 = E(A_2 - \overline{A_2})^2 = \frac{\frac{m_{11}^2}{N_2} + \frac{m_{21}^2}{N_1}}{(m_{11}m_{22} - m_{12}m_{21})^2} \tag{3.5.34}$$

where $m_{ij} = \frac{\partial \ln \beta_i}{\partial A_j}, i,j = 1,2$.

Summarizing, the maximum likelihood estimation procedure involves solving the deterministic integral equations using the measured counts. If the number of counts is large, the errors will be small. The main source of error is the variance of the results. This may be estimated using equations (3.5.33) and (3.5.34).

3.6. Estimation of A_1 and A_2 from Measurements with Energy Detectors

As discussed in Section 3.4, measurements with detectors that measure total energy will be independent normal random variables with variances $\sigma_i^2 = \lambda T \overline{E_i^2}$ and means

$$m_i = \lambda T \overline{E_i} = AT \int_0^\infty E S_i(E) e^{-A_1 f_1(E) - A_2 f_{KN}(E)} dE \tag{3.6.1}$$

where $S_i(E)$ are the photon number spectra incident on the patient. In this section, we will derive a maximum likelihood estimator for A_1 and A_2 and evaluate its errors.
Since the measurements are independent normal random variables, the logarithm of the likelihood function is

$$L = \ln(Pr[Q_1, Q_2 | A_1, A_2] = -\frac{(Q_1 - m_1)^2}{2\sigma_1^2} - \frac{(Q_2 - m_2)^2}{2\sigma_2^2} \tag{3.6.2}$$

Now, $L \leq 0$ and achieves its maximum value of zero if and only if $Q_1 = m_1$ and $Q_2 = m_2$. Thus the maximum likelihood estimation procedure involves solving the deterministic equations with the measured data.

The results for the errors with a detector that measures energy are quite similar to the results for a counting detector. By using a Taylor's series as in Section 3.5, the bias of the estimates is

$$bias(A_i) = \frac{1}{2} \frac{\partial^2 g_i}{\partial Q_1^2} \sigma_1^2 + \frac{1}{2} \frac{\partial^2 g_i}{\partial Q_2^2} \sigma_2^2, i = 1, 2 \tag{3.6.3}$$

The Cramer-Rao bound for the variance is

$$\sigma_{A_1}^2 = E(A_1 - \overline{A_1})^2 = \frac{\frac{\mu_{12}^2}{Q_2} + \frac{\mu_{22}^2}{Q_1}}{(\mu_{11}\mu_{22} - \mu_{12}\mu_{21})^2} \tag{3.6.4}$$

$$\sigma_{A_2}^2 = E(A_2 - \overline{A_2})^2 = \frac{\frac{\mu_{11}^2}{Q_2} + \frac{\mu_{21}^2}{Q_1}}{(\mu_{11}\mu_{22} - \mu_{12}\mu_{21})^2} \tag{3.6.5}$$

where $\mu_{ij} = \frac{\partial m_i}{\partial A_j}, i, j = 1, 2$, $A_1 = g_1(Q_1, Q_2)$, $A_2 = g_2(Q_1, Q_2)$.

3.7. Solution of Estimator Equations

For either a counting or energy detector system, two simultaneous nonlinear integral equations must be solved to calculate A_1 and A_2. In general, integral equations are difficult to solve analytically. Even if an analytical solution were possible, the equations would have to be solved again for each spectrum used. In this section, a technique is developed for solving the integral equations which does not require analytical solutions. The validity

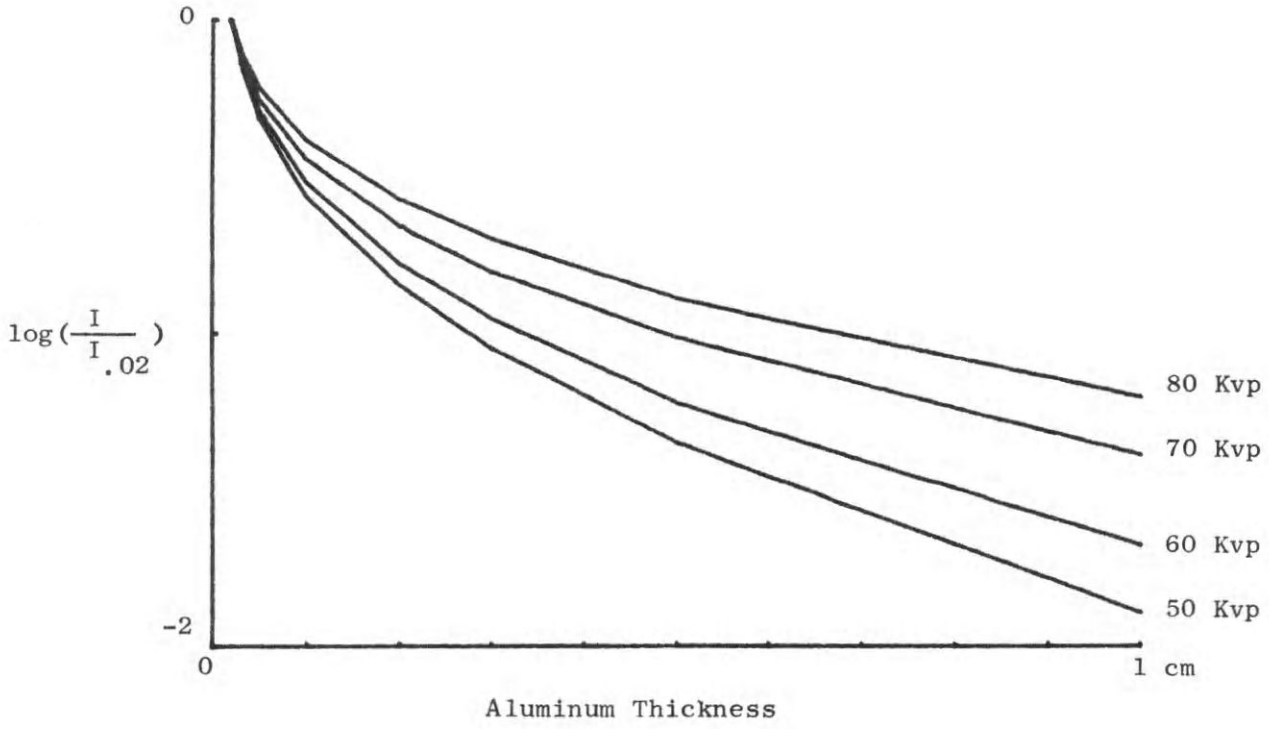

Figure 3.3.: Plot of Logarithm of Total Energy of Transmitted Photons as Function of Aluminum Absorber Thickness (from Thoraeus 1940)

of this technique is shown by computer simulation and by experiment. The technique is based on having an approximation to the equations with undetermined constants. For any particular set of spectra and detector system, the constants are determined by making accurate measurements on an object with known values of $A_1$and A_2. Once the constants are determined, the resulting equations can be used to solve for A_1 and A_2 from measurements on an unknown object.

The search for an approximate general form of the integrals is aided by the fact that they define well-behaved and smoothly varying functions. Figure 3.3 is a plot of the value of the logarithm of the total energy of the transmitted photons as a function of the thickness of an aluminumu absorber. An x-ray tube source was used. The shape of this curve can be explained physically. The slope of this curve is related to the average linear attenuation coefficient

$$\mu_{av} = -\frac{d}{dx} \ln \left(\frac{I}{I_0} \right) \tag{3.7.1}$$

As described in Chapter 2, the linear attenuation coefficient beyond the K absorption edge is a decreasing function of energy. As the absorber thickness increases, the relative

absorption of low energy photons increases and the average energy increases. This is known as "hardening." Thus, the slope of the curve in Fig. 3.3 must decrease as the absorber thickness increases. This slope asymptotically approaches $\mu(E_m)$ where E_m is the maximum energy in the spectrum. Similar results are obtained if numbers of photons are measured. Since the attenuation coefficients are smooth functions, the logarithm of the integrals will also be smooth functions. They can therefore be approximated by power series with a small number of terms

$$\ln I_1(A_1, A_2) = b_0 + b_1 A_1 + b_2 A_2 + b_3 A_1^2 + b_4 A_2^2 + b_5 A_1 A_2 + b_6 A_1^3 + \ldots \tag{3.7.2}$$

$$\ln I_2(A_1, A_2) = c_0 + c_1 A_1 + c_2 A_2 + c_3 A_1^2 + c_4 A_2^2 + c_5 A_1 A_2 + c_6 A_1^3 + \ldots \tag{3.7.3}$$

The symbol I denotes either a total number of photons or their total energy. The sets of coefficients $\{b_i\}$ and $\{c_i\}$ can be determined by curve fitting techniques from measurements an objects with known values of A_1 and A_2. Once these are known, the two simultaneous equations can be solved numerically.

A computer simulation was performed to show the validity of this approximation. The transmission integrals

$$\beta_i(A_1, A_2) = \int S_i(E) e^{-A_1 f_1(E) - A_2 f_2(E)} dE, i = 1, 2 \tag{3.7.4}$$

were evaluated for various values of $A_1$and A_2. An experimentally measured spectrum (Epp and Weiss 1966) was used with a single level pulse height analysis detector. Thus, l represents the number of counts with energy below the threshold E_T. The results were approximated by power series as in equations (3.7.2) and (3.7.3). The coefficients $\{b_i\}$ and $\{c_i\}$ were calculated using least squares techniques. Once the coefficients were known, the two simultaneous cubic equations were solved numerically as described in Appendix B. The results are shown in Table 3.1. The first two columns are the actual values, and the last two columns are the calculated values. Note that the errors are less than 0.1 per cent.

Table 3.1.: ACCURACY OF SOLUTION OF INTEGRAL EQUATIONS

A_1	A_2	$\hat{A}_1$	$\hat{A}_2$
75000	1.5	74963	1.5001
75000	2.7	75029	2.6999
155000	1.5	154959	1.5001
155000	2.7	155039	2.6999

The accuracy of equation (3.7.2) was also tested experimentally. The apparatus shown in Fig. 3.4 was used. This is an EMI scanner. The experiment consisted of making accurate measurements of the transmitted intensity through a step wedge consisting of two materials with accurately known dimensions. The x-ray tube source operated at 100

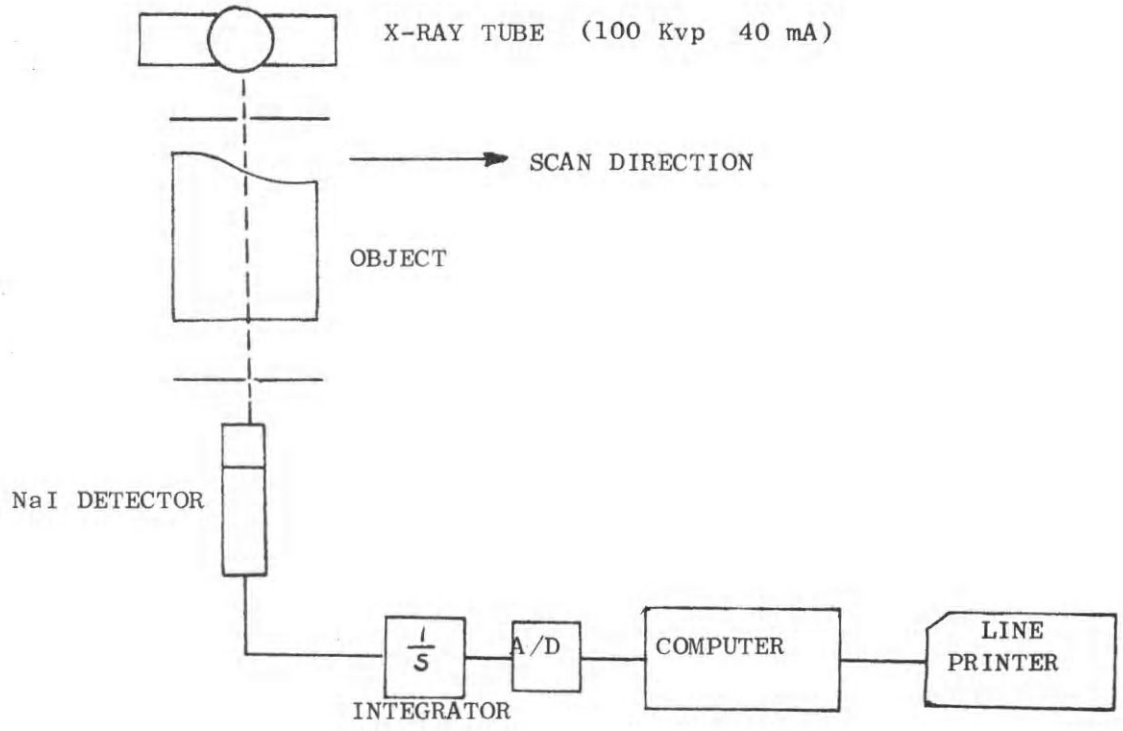

Figure 3.4.: Experimental apparatus for gathering data using a scanned x-ray tube and detector.

Kvp and 40 mA. The tube output was collimated into a thin beam and the intensity of this beam after transmission through the object was measured by a sodium iodide scintillation detector that was operated in the current integrating mode. The detector thus measured total energy. The detector output was measured by an A/D converter and stored in the computer. The x-ray tube and detector were scanned in unison so the beam traversed the object. The measurements of the transmission at 3 mm intervals were stored by the computer and printed on a line printer at the end of a scan.

As noted in Chapter 2, the attenuation coefficients of any two materials may be used as a basis set. In this case the thicknesses of the materials take the place of the line integrals A_1 and A_2. The data were fit to the equation

$$\ln I = a_1 x_{Lu} + a_2 x_{Al} + a_3 x_{Lu}^2 + a_4 x_{Al}^2 + a_5 \tag{3.7.5}$$

The two materials used were aluminum and lucite. The accuracy of this equation is shown in Table 3.2. Several measurements were made for each set of thicknesses. The standard

deviation of these measurements is also shown in this table. The error in the fit of the theoretical equation is about the same as the experimental error of each measurement. There was apparently a drift in the apparatus because the coefficients in (3.7.5) were different for different scans. The accuracy of the fit, for any given scan, was always good.

Table 3.2.: FIT OF EXPERIMENTAL DATA TO APPROXIMATE FORM

X_{Al} (cm)	X_{Lu} (cm)	$\frac{I_0}{I}$	$\left(\frac{I_0}{I}\right)_{calc}$	Error
.635	6.35	1.394±007	1.394	0
.635	5.715	1.227±.006	1.228	.001
1.27	5.08	1. 519±.005	1.517	.002
1.27	4.445	1.338±.007	1.336	.002
1.905	3.81	1.643±.006	1.647	.004
1.905	3.175	1.449±.007	1.449	0
2.54	2.54	1.784±.007	1.782	.002
2.54	1.905	1.565±.009	1.566	.001

3.8. Optimum Filter Functions

The choice of optimum filter functions or optimum incident spectra is a difficult problem. The integral equations involved are nonlinear. The cost function, which in this case is dose, is difficult to calculate for a general object. In this section, optimum filter functions are derived for the case of small changes in $A_1$and A_2. This is a reasonable approximation if a constant path length water bath is used. If only small changes in the A_i are involved, small signal linear analysis may be used. Suppose

$$A_i = A_{i0} + \delta A_i \tag{3.8.1}$$

where $\left|\frac{\delta A_1}{A_1}\right| \ll 1$ and $\left|\frac{\delta A_2}{A_2}\right| \ll 1$. The estimator integral equations for either the photon counting or energy measurement case are

$$I_i = \int_0^\infty g_i(E) S_i(E) e^{-A_1 f_1(E) - A_2 f_{KN}(E)} dE, i = 1, 2 \tag{3.8.2}$$

Using the bracket notation for the inner product,

$$\langle w, h \rangle = \int_0^\infty S(E) e^{-A_1 f_1(E) - A_2 f_{KN}(E)} w(E) h(E) dE \tag{3.8.3}$$

Equations (3.8.2) become (note that we are assuming small δA_i)

$$I_i = \langle g_i, 1 \rangle - \delta A_i \langle g_i, f_1 \rangle - \delta A_i \langle g_i, f_2 \rangle \tag{3.8.4}$$

Suppose we want to minimize $\sigma_1^2 + \sigma_2^2$. Assuming a counting detector is used, the sum of variances will be

$$\sigma_{A_1}^2 + \sigma_{A_2}^2 = \frac{\frac{m_{22}^2+m_{22}^2}{\beta_1} + \frac{m_{12}^2+m_{11}^2}{\beta_2}}{(m_{11}m_{22} - m_{12}m_{21})^2} \tag{3.8.5}$$

Since $I_1 \approx \langle g_1, 1\rangle$, $I_2 \approx \langle g_2, 1\rangle$,

$$m_{ij} \approx \frac{\langle g_i, f_j\rangle}{\langle g_i, 1\rangle}, i, j = 1, 2 \tag{3.8.6}$$

where $f_2(E) = f_{KN}(E)$. Substituting the approximate values of the m_{ij}in equation (3.8.5)

$$\sigma_{A_1}^2 + \sigma_{A_2}^2 = \frac{\langle g_2, 1\rangle \left[\langle g_1, f_1\rangle^2 + \langle g_1, f_2\rangle^2\right] + \langle g_1, 1\rangle \left[\langle g_2, f_1\rangle^2 + \langle g_2, f_2\rangle^2\right]}{\left[\langle g_1, f_1\rangle \langle g_2, f_2\rangle + \langle g_2, f_1\rangle \langle g_1, f_2\rangle\right]^2} \tag{3.8.7}$$

As mentioned in Chapter 2, the set of basis functions is not unique. In this case, it is desirable to choose an orthogonal basis set so $\langle f_1, f_2\rangle = 0$. This may be done by using the Gram-Schmidt procedure with the definition of inner product given in 3.8.3. Assuming this has been done $\langle g_i, f_1\rangle^2 + \langle g_i, f_2\rangle^2 = \langle g_i, g_i\rangle^2$for $i = 1, 2$and Eq. 3.8.3 becomes

$$\sigma_{A_1}^2 + \sigma_{A_2}^2 = \frac{\langle g_2, 1\rangle \langle g_1, g_1\rangle^2 + \langle g_1, 1\rangle \langle g_2, g_2\rangle^2}{\left[\langle g_1, f_1\rangle \langle g_2, f_2\rangle + \langle g_2, f_1\rangle \langle g_1, f_2\rangle\right]^2} \tag{3.8.8}$$

Note that the numerator is independent of f_1 and f_2.

Using a vector interpretation of the inner products, the various terms in the denominator of Eq. 3.8.8 are shown in Fig. 3.5. From this figure one can see that by setting $g_1 = k_1 f_1$ and $g_2 = k_2 f_2$ where k_1 and k_2 are constants, the second term in the denominator is zero and the first is maximized. The optimum values of k_1 and k_2 depend on dose considerations. Once k_1 and k_2 are chosen the denominator is maximized and the total expression is minimized. Since f_1 and f_2 are orthogonal, this means that the optimum g_1 and g_2 are also orthogonal.

3.9. Optimum Threshold Energy for Single Level Pulse Height Analysis

The expressions for the variance of the calculated values are useful not only for general considerations but also to optimize specific situations. In this section, the optimum threshold energy for single level pulse height analysis will be discussed.

In a counting detector system, it is possible to classify the pulses according to their size and hence the energy of the photon. The simplest of such systems classifies the pulses into two groups:those with energy less than some threshold E_t and those with energy greater than E_t. As discussed in Section 3.3, the energy dependent information can be calculated from these measurements. For any given E_t we can calculate the resultant

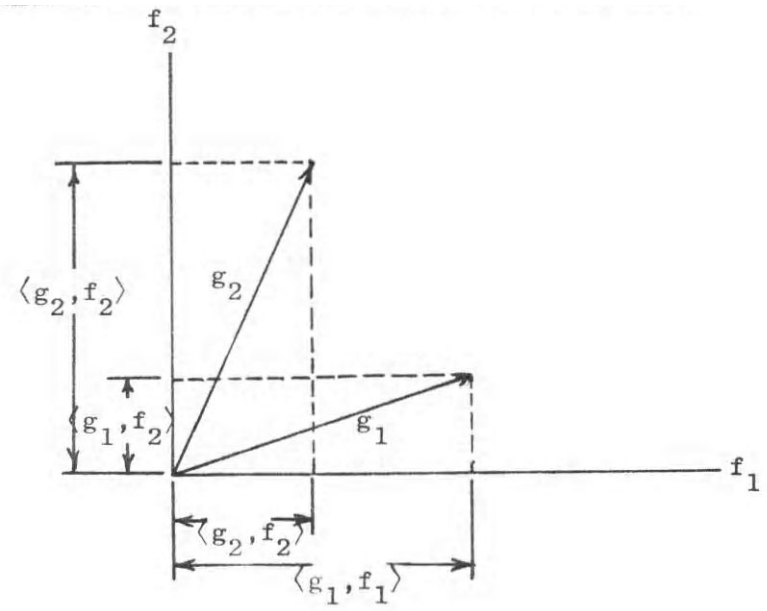

Figure 3.5.: Vector Interpretation of Terms in Denominator

errors in the estimates of the A_i. There should be an optimum value of E_t because if it is too low or too high one of the measurements will have few photons and errors will result.

A computer simulation was performed to calculate these errors. The errors depend on the threshold energy, the incident spectrum, and the body transmission. An experimentally measured 105 Kvp spectrum (Epp and Weiss 1966) was used. It was assumed that $5x10^7$ photons were incident during the measurement. The average energy is 50 Kev so the energy deposited in the patient will be 4 ergs per measurement. This will be shown to produce doses approximately twice those of intensity only systems.

The variance of the estimates is given by Eqs 3.5.33 and 3.5.34. The terms in these expressions can be calculated by using the approximating form of equation (3.7.4). The undetermined coefficients were found by calculating the number of photons in each measurement for several values of A_1 and A_2 and then using least squares curve fitting techniques. The variances were calculated as a function of threshold energy for various body thicknesses. The results are shown in Fig. 3.6. There are several features of interest. First, the minimum as a function of E_t is very broad and not strongly dependent on body thickness. Thus, one can choose a single threshold energy suitable for most applications. Another feature of interest is the relative size of the errors in the photoelectric and Compton line integrals. The photoelectric term corresponds to a function that decreases rapidly with energy. Since low energy photons are more highly attenuated by the body, this term should be expected to have higher errors.

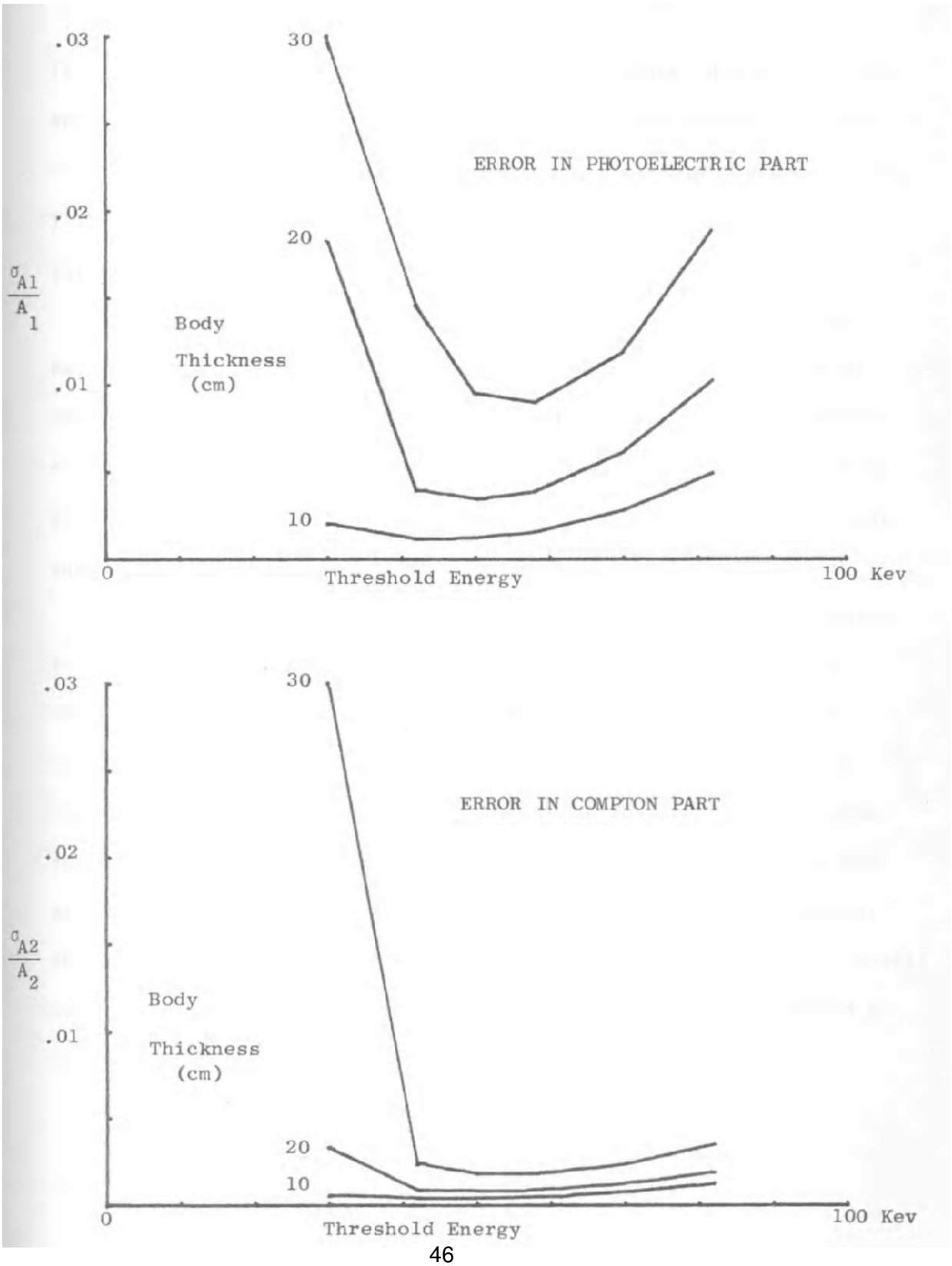

Figure 3.6.: Optimum Threshold for Single Level Pulse Height Analysis

3.10. Other Considerations

There are many practical considerations that must be considered in the implementation of a system to extract energy dependent information. Two important ones are scatter and system stability.

The equations in this chapter assume that once a photon has interacted it is removed from consideration and will not be counted. In fact, a photon can have several Compton scattering interactions and still enter the detector. In general, scattering adds a low spatial frequency noise component which is independent of the directly transmitted photons. In a conventional single projection system with a film cassette detector, relatively large numbers of scattered photons can be tolerated because of their low spatial frequency content. Scatter is more troublesome in a system which derives information from mathematical operations on measurements.

The effects of scatter on a conventional computerized tomography system are discussed by Stonestrom and Macovski (1975). There are two principal effects. The scatter increases counting noise. Also, these systems use nonlinear operations to calculate the line integral from their measurements. The additive scattered component introduces artifacts into the reconstruction. The artifacts are a more serious limitation than the added counting noise.

Energy dependent systems use mathematical operations on measurements and will be affected by scatter in a similar manner. The scatter will produce increased counting noise. Errors will be introduced because nonlinear equations must be solved to calculate the energy dependent information.

Scatter does not seem to be a fundamental problem, however, The successful operation of computerized tomography systems indicates that by proper collimation and other techniques scatter can be reduced to negligible levels.

Another limitation is system stability. The calculations in this chapter assume that the spectra do not change with time. There will be some change and this will introduce errors. Since we are extracting more information, we would expect the stability requirements to be more stringent. The experiments described in subsequent chapters show that, with some care, the stability requirements can be met.

4. Extraction of Energy Dependent Information in Single Projection Radiography

4.1. Introduction

Single projection systems are the most widely used in medical radiography. Even with the introduction of computerized tomography, we would expect these systems to remain popular. Although they do not extract the available information completely, the images of a single projection system are sufficient for many purposes in radiology. Compared to tomographic systems, they offer the advantages of simplicity and the capability of stopping motion by forming an image in a short time interval.

The addition of energy dependent measurements increases the information presented by a single projection system and, therefore, the usefulness of the system to a radiologist. This chapter has two main parts. First, we describe some systems to measure the data necessary to calculate the energy dependent information. These systems are relatively simple modifications of conventional single projection systems and thus keep the advantages of simplicity and "snapshot" operation. Next, we discuss the additional information in an energy dependent system. We present two possible applications of this information and experiments showing the feasibility of these techniques.

4.2. Systems for Measurement of Energy Dependent Information in a Single Projection System

The theory developed in Chapter 3 allows the use of conventional detectors to measure the data necessary to calculate the line integrals of the coefficients a_1 and a_2. The basic data needed at any point in the image are the transmitted intensities with two different incident spectra. This information can be measured in many ways. Two possible techniques will be discussed in this section. They are spatial frequency multiplexing and a double film screen cassette.

Acquisition of energy dependent information by spatial frequency multiplexing was introduced by Macovski (Macovski, Alvarez, Chan, 1974). The technique is illustrated in Fig. 4.1. A grating composed of alternate stripes of materials with transmissions $g_1(E)$ and $g_2(E)$ is placed between the x-ray tube and the patient. The filtered beams of x-rays

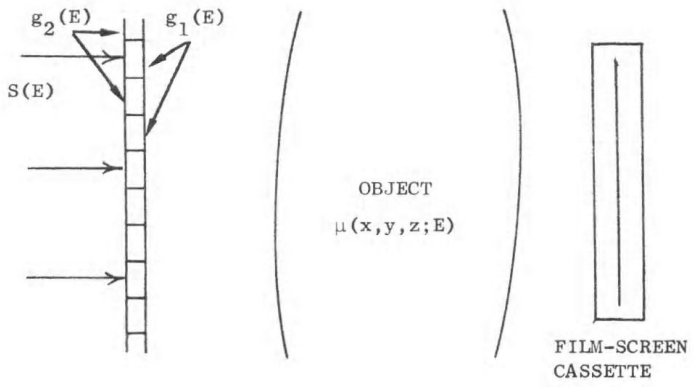

Figure 4.1.: Acquisition of energy dependent information by spatial frequency multiplexing.

are then incident on the patient and the transmitted intensity is recorded on a conventional film-screen cassette. The width of the stripes is assumed to be small enough so the body composition and thickness do not change appreciably from one stripe to the next.

The image recorded by the detector will be as shown in Fig. 4.2. This shows the film density on a typical line across the image. The sinusoidal variation is caused by the grating. The peak values, as illustrated, correspond to the desired quantities. The film density is a nonlinear function of the total energy incident during exposure. If this energy is within the useful range of the film, measurements of the film density can be used to calculate the total energy of the photons.

$$I_1 = h(D_1) = AT \int ES(E) g_1(E) \exp[-A_1 f_1(E) - A_2 f_2(E)] dE \tag{4.2.1}$$

$$I_2 = h(D_2) = AT \int ES(E) g_2(E) \exp[-A_1 f_1(E) - A_2 f_2(E)] dE \tag{4.2.2}$$

In these equations, $h(D)$ is the function relating the film density D to the total energy, A is the area of a resolution element of the system, and T is the exposure time.

Another possibility for the acquisition of energy dependent information is a double film screen cassette. This is illustrated in Fig. 4.3. The light measured by the first photographic film corresponds to the low energy photons. It is proportional to

$$I_1 = AT \int ES(E) \left[1 - e^{-\mu_1(E) d_1}\right] \exp[-A_1 f_1(E) - A_2 f_2(E)] dE \tag{4.2.3}$$

The light gathered by the second film is proportional to

$$I_2 = AT \int ES(E) e^{-\mu_1(E) d_1} \left[1 - e^{-\mu_2(E) d_2}\right] \exp[-A_1 f_1(E) - A_2 f_2(E)] dE \tag{4.2.4}$$

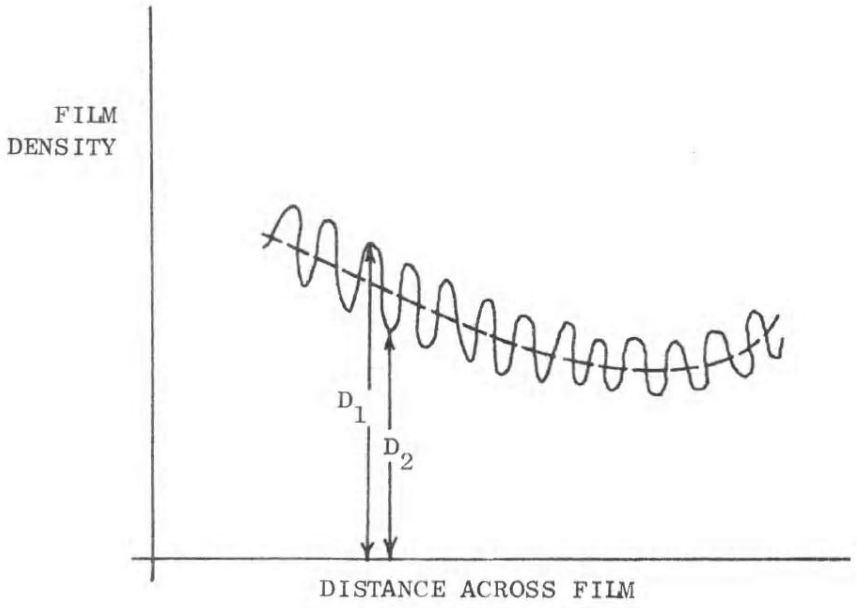

Figure 4.2.: Typical line on film.

The measured quantities are equivalent to filtering with

$$g_1(E) = 1 - e^{-\mu_1(E)d_1} \tag{4.2.5}$$

$$g_2(E) = \left[1 - e^{-\mu_2(E)d_2}\right] e^{-\mu_1(E)d_1} \tag{4.2.6}$$

Other possibilities for the measurement of the data are systems which use scanned detectors or either linear or area arrays of detectors. An experiment with a scanned detector will be described in Section 4.6.

4.3. Energy Dependent Information from a Single Projection System

The information from any single projection system still contains spatial averaging. Thus it consists basically of the line integrals of the linear attenuation coefficient of the object. In an energy dependent system, it will consist of two pieces of information at every resolution element in the image. These will be A_1 and A_2, the line integrals of $a_1(x, y, z)$ and $a_2(x, y, z)$ along a line from a point in the image to the source.

From the values of A_1 and A_2 we can infer two types of information: an indication of the average atomic number and the amount of material along the path. Suppose the object

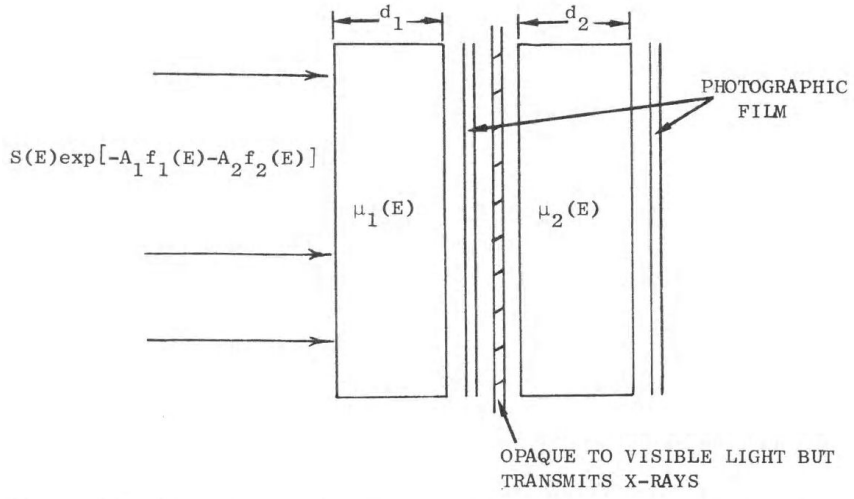

Figure 4.3.: Acquisition of energy dependent information using a double film screen cassette.

consists of a single material with coefficients (a_1, a_2) and thickness d. The line integrals will be

$$A_1 = \int a_1(x, y, z)ds = a_1 d \tag{4.3.1}$$

$$A_2 = \int a_2(x, y, z)ds = a_2 d \tag{4.3.2}$$

As described in Chapter 2, the coefficients a_1 and a_2 depend on the physical properties of the material. The relationships are

$$a_1 \approx K_1 \frac{\rho}{W} Z^4 \tag{4.3.3}$$

$$a_2 \approx K_2 \frac{\rho}{W} Z \tag{4.3.4}$$

where K_1 and K_2 are constants, ρ is the mass density, W is the atomic weight, and Z is the atomic number.

After substituting in equations 4.3.1 and 4.3.2, expressions can be derived for quantities that depend on physical properties.

The ratio A_1/A_2 depends on atomic number only

$$\frac{A_1}{A_2} \approx \frac{K_1}{K_2} Z^3 \tag{4.3.5}$$

Since Z/W is roughly constant for most elements, the line integral A_2 is proportional to

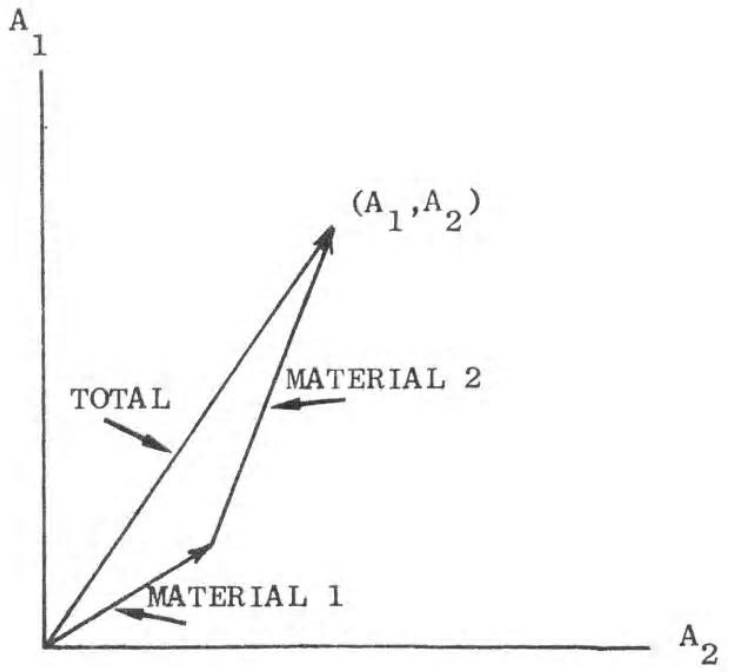

Figure 4.4.: Two-dimensional plot of the line integrals.

the amount of material present ρd.

$$A_2 \approx K_2 \frac{Z}{W} \rho d \approx (\text{constant}) \rho d \tag{4.3.6}$$

Note that ρd has the units of mass per unit area.

The quantities A_1 and A_2 may be plotted as shown in Fig. 4.4. On this plot A_1/A_2 is the slope of the radius vector to the point (A_1, A_2). From equation 4.3.5 the greater this slope, the greater the atomic number. Measurements on materials with the same composition will have the same slope and thus lie along the same line. The distance from the origin along this line

$$r = \sqrt{A_1^2 + A_2^2} = \rho d \sqrt{\left(K_1 \frac{Z^4}{W}\right)^2 + \left(K_2 \frac{Z}{W}\right)^2} \tag{4.3.7}$$

will be proportional to ρd for a given material.

If several materials are present along the x-ray path, one cannot give a precise interpretation to the values of A_1 and A_2. The best that can be done is to infer average properties of the materials. Suppose there are m materials with coefficients $(a_{11}, a_{21}), (a_{12}, a_{22}), \ldots, (a_{1m}, a_{2m})$

and thicknesses $d_1, d_2, \ldots, d_m$. The line integrals will be

$$A_1 = a_{11}d_1 + a_{12}d_2 + \ldots + a_{1m}d_m \tag{4.3.8}$$

$$A_2 = a_{21}d_1 + a_{22}d_2 + \ldots + a_{2m}d_m \tag{4.3.9}$$

Note this is equivalent to stating that the resultant value of (A_1, A_2) in a plot such as Fig. 4.4 is the vector sum of the radius vectors to the points (A_{1i}, A_{2i}) corresponding to each material.

Substituting from equations 4.3.3 and 4.3.4,

$$A_1 = K_1 \left(\frac{\rho_1 d_1}{W_1} Z_1^4 + \frac{\rho_2 d_2}{W_2} Z_2^4 + \ldots + \frac{\rho_m d_m}{W_m} Z_m^4 \right) \tag{4.3.10}$$

$$A_2 = K_2 \left(\frac{\rho_1 d_1}{W_1} Z_1^4 + \frac{\rho_2 d_2}{W_2} Z_2^4 + \ldots + \frac{\rho_m d_m}{W_m} Z_m^4 \right) \tag{4.3.11}$$

Since Z/W is roughly constant, A_2 is proportional to the amount of material along the path of the x-ray beam.

$$A_2 \approx (\text{constant}) \, (\rho_1 d_1 + \rho_2 d_2 + \ldots + \rho_m d_m) \tag{4.3.12}$$

The value of A_1 increases rapidly with atomic number. Thus, the larger A_1/A_2, the larger the average atomic number.

The interpretation of the information from any single projection system is complicated by two geometrical effects: nonzero source size and finite source to detector distance [Macovski l975]. The situation is illustrated in Fig. 4.5. The information in the final image is the convolution of the body transmission with the projection of the source onto the body. Because the source is not infinitesimally small, the resolution of the system is limited. Because of finite source to detector distance, the paths of the x-ray beams from the source are diverging. These geometrical effects do not change the data fundamentally. The source size effect is negligible if the source is made small enough so that its projected size is small compared to details of interest in the object. The effect of finite source to detector distance is to introduce magnification into the final image.

4.4. The Compton Coefficient as a High Voltage Radiograph

The x-ray tube voltages used in most radiology procedures are 150 Kvp or less. Higher voltages have been suggested for some examinations to improve the visualization of soft tissue structures overlying bone [Tuddenham 1953]. At conventional energies the photoelectric effect makes a substantial contribution to the attenuation coefficient of bone. Its mass attenuation coefficient is therefore much higher than that of soft tissue and the visibility of soft tissue structures which overly bone is greatly reduced. At higher energies, the photoelectric contribution becomes negligible and the mass attenuation coefficients

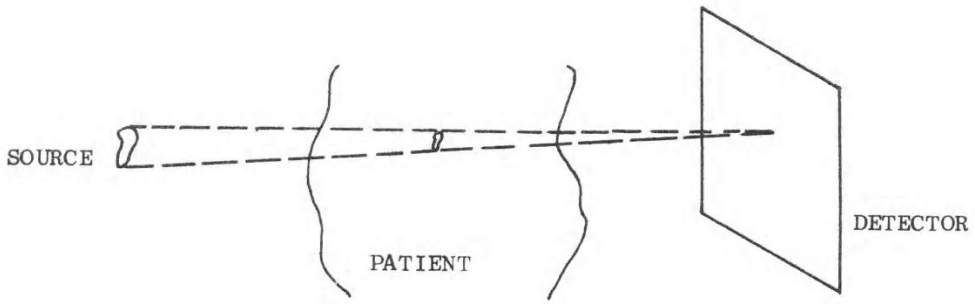

Figure 4.5.: Geometrical effects in single projection systems.

of these materials become almost equal. There will be a difference between the transmission of bone and soft tissue due to their different densities, but this difference will be much smaller than at lower energies. Thus the visibility of the soft tissue structures will be increased.

While high voltage radiography improves the visualization of these structures, it has serious limitations. As shown in Chapter 2, at higher energies the contrast per unit dose decreases. Also, the differential cross section for Compton scattering becomes increasingly peaked in the forward direction as energy is increased. Thus it becomes more difficult to remove scattered photons using collimators. Finally, the dose is increased because at higher energies the efficiency of the detector decreases [Ter-Pogossian 1967].

By displaying the line integral of the Compton scattering coefficient A_2, an image equivalent to a high voltage radiograph can be produced. In this image the differences between structures will be determined mainly by differences in density. Thus, the visualization of soft tissue structures will be increased. The spectra used to extract the energy dependent information can correspond to conventional x-ray energies and many of the physical limitations of high voltage radiography can be avoided. The energy dependent system will also measure the photoelectric coefficient line integral and this can be used for selective material imaging.

4.5. Selective Material Imaging

Selective material imaging can be defined as the calculation of the amounts of particular materials along the path between the source and a point in the image. In this section, we show this is strictly possible only under restrictive conditions in a single projection system. However, by using the ideas of Chapter 2, we develop a slightly different interpretation of selective material imaging which is generally applicable and which provides a great deal of information.

Since there are only two pieces of information and these result from spatial averaging,

selective material imaging in a single projection system is possible only if the object is composed of two materials of known composition. The information available is described by equations 4.3.8 and 4.3.9. These equations can be solved for the amounts of materials $d_1, d_2, \ldots, d_m$ only if there are two materials and if the values of (a_{11}, a_{21}) and (a_{12}, a_{22}) are known.

This limitation has been encountered in practice [Alberi, Kraner, Bradley-Moore, Atkins 1974]. The techniques described in Chapter 1 for measuring the amounts of different materials using measurements with isotope sources in single projections have never been able to isolate more than two materials. Even if measurements are made at many energies, the equations that must be solved to determine the amounts of three materials become ill-conditioned. The only exception to this rule is materials with K edges in the diagnostic region. Their discontinuous attenuation coefficient functions cannot be represented with a two function basis set over the entire diagnostic energy region.

The limitation does not exist in systems, such as will be described in Chapter 5, which remove spatial averaging. These systems can calculate the values of (a_1, a_2) at points within the object. So long as the materials have different average atomic number and density, the capability of the system to distinguish between materials in different resolution elements is determined by measurement accuracy.

By changing the interpretation somewhat, the concept of selective material imaging in a single projection system can be useful even if there are more than two materials present. This may be seen from the following example. For many purposes, an image of soft tissue only or bone only would be useful. In a single projection system, this could be produced only if the body were known to consist of these two materials.

However, we can choose the attenuation coefficient function of any two materials as a basis set. Suppose we pick water and a particular composition of bone. From the discussion in Chapter 2, we are guaranteed that the attenuation coefficient function of any body material can be expressed as a linear combination of our functions

$$\mu(E) = c_1\mu_b(E) + c_2\mu_W(E) \tag{4.5.1}$$

where $\mu_b(E)$ and $\mu_W(E)$ are the attenuation coefficient functions of bone and water. Images of the line integrals C_1 or C_2 would be close to bone only or soft tissue only images. Actual soft tissue would contain a contribution from bone and actual bone would contain a contribution from water, but these would be small.

Because of the theoretical framework that has been developed, the contributions from the two materials can be interpreted. For example, by looking at the relative contributions of bone and water, we can decide if a lesion is calcified or simply high density.

4.6. Experimental Tests

The feasibility of selective material imaging with two materials is shown by an experiment described in Chan, Alvarez, Macovski 1976. This experiment shows that the amounts of

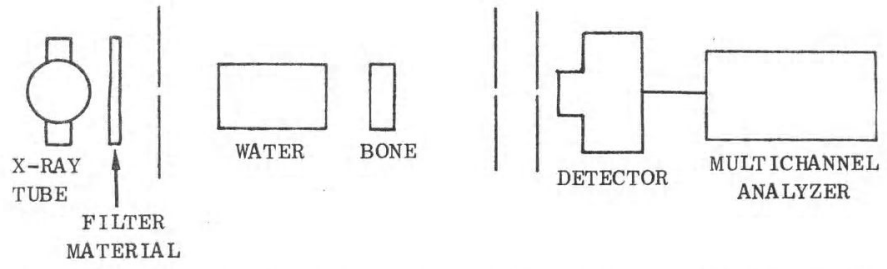

Figure 4.6.: Apparatus for experiment showing the feasibility of selective material imaging.

bone and soft tissue along the path of an x-ray beam can be accurately calculated from broad spectrum measurements. The experimental apparatus is shown in Fig. 4.6. It consists of the x-ray tube source, a filter, an object consisting of bone and water, and a germanium detector with a multichannel analyzer. The detector was used to measure the transmitted spectrum. Two measurements were made with different filter materials placed between the source and the object. The measured spectra were then integrated as a function of energy to yield the raw data. From this data, the amounts of bone and water were calculated as described in Chapter 3. A principal source of error was the instability of the x-ray tube.

The feasibility of the generalized approach to selective material imaging was shown by an experiment using a scanned system. The experimental apparatus was the scanned x-ray tube and detector of the EMI machine at the Stanford Medical Center. This apparatus was described previously in Fig. 3.4. The machine produces two beams as shown in Fig. 4.7. By placing a filter in each beam and using an object that is constant across the two beams, the data necessary to calculate the line integrals can be measured. Gadolinium and molybdenum filters were used. Spectra similar to those incident on the object are shown in Fig. 4.7. These spectra were actually measured on a different tube operated at the same voltage. The tube in the EMI scanner is not readily accessible for measurements.

The objects that were scanned are shown in Fig. 4.8. The first object scanned was a test wedge consisting of aluminum and lucite with accurately known dimensions. The measurements on this object were used to calculate the coefficients in the approximations to the integral equations as described in Chapter 3. Instead of using the photoelectric and Compton scattering basis set, the attenuation coefficient functions of aluminum and lucite were used. The results for an unknown object are then equivalent amounts of these two materials which have the same attenuation coefficient.

The unknown object was then scanned. The raw data consisted of the transmissions of the filtered beams at 3 millimeter intervals. At each point, the equivalent amounts of aluminum and lucite were calculated by solving the approximations to the integral equations. Typical results are shown in Fig. 4.9. From the equivalent amounts of aluminum and lucite, the photoelectric and Compton scattering line integrals can be calculated. These

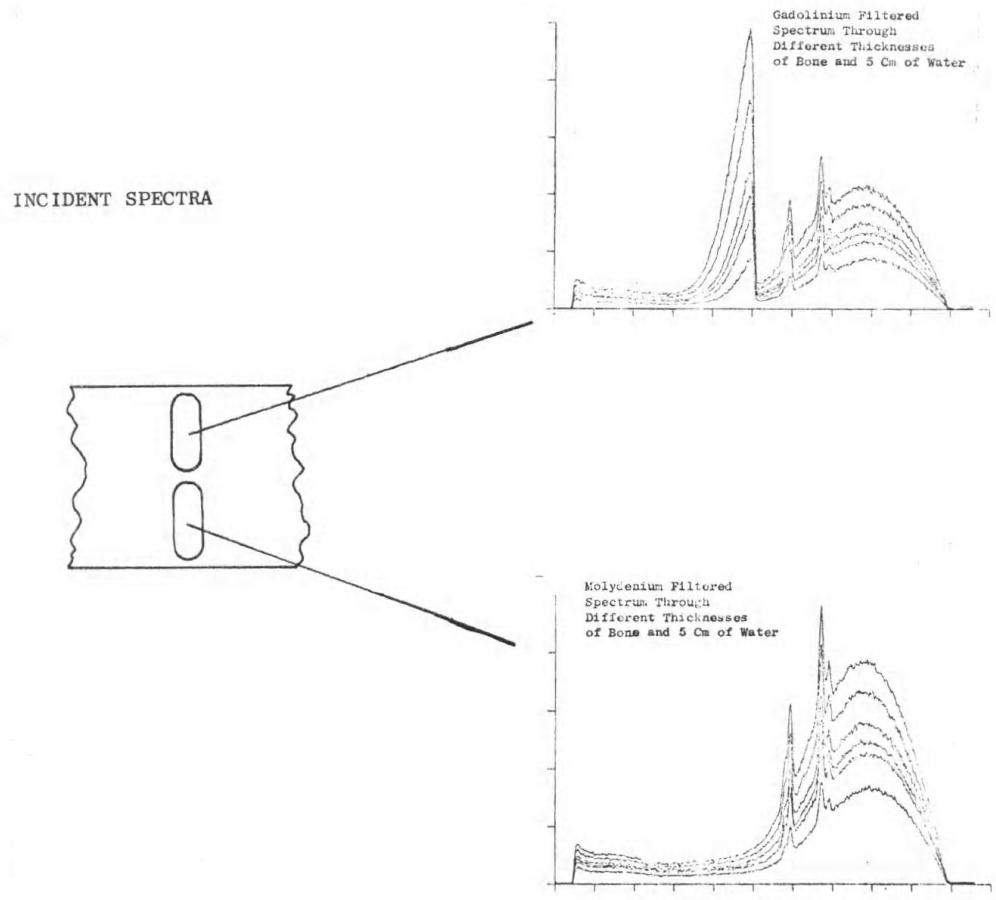

Figure 4.7.: Spectra in Scanned System

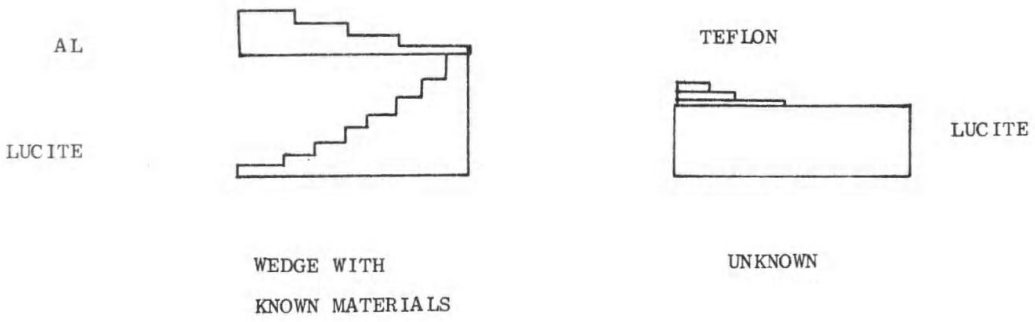

Figure 4.8.: Object scanned in experimental test.

are also shown in Fig. 4.9.

The unknown object was a piece of lucite with three thicknesses of teflon slabs placed on it. The features of this object are evident in Fig. 4.9. The "spikes" at the edges of the teflon slabs are caused by imperfect alignment of the x-ray beam and the pieces of teflon. At the edges, the two beams are not passing through equivalent materials and the data is inconsistent. This causes errors in the results. It is also evident that the photoelectric line integral is noisier than the Compton line integral. This is to be expected from the theoretical results in Chapter 3.

The consistency of the data can be checked by combining the results so the effect of the teflon disappears. Suppose the teflon has coefficients (a_{1T}, a_{2T}) and the lucite (a_{1L}, a_{2L}). The photoelectric and Compton line integrals at any point will be

$$A_1 = a_{1T}d_T + a_{1L}d_L \tag{4.6.1}$$

$$A_2 = a_{2T}d_T + a_{2L}d_L \tag{4.6.2}$$

where d_T and d_L are the teflon and lucite thicknesses. The quantity $A_1 - bA_2$ where b is a constant, can be calculated from the line integrals. It is

$$A_1 - bA_2 = (a_{1T} - ba_{2T})d_T + (a_{1L} - ba_{2L})d_L \tag{4.6.3}$$

By setting $b = a_{lT}/a_{2T}$, the effect of the teflon will disappear and the quantity

$$A_1 - bA_2 = (a_{1L} - ba_{2L})d_L \tag{4.6.4}$$

will depend only on the lucite. Figure 4.10 shows $A_1 - bA_2$ for various values of b. For some value of b, we would expect the result to be constant because the lucite thickness is constant. Even though the data is somewhat noisy, this condition occurs as shown in Fig. 4.10.

There was considerable drift in the apparatus and the results from trial to trial were not the same. The EMI scanner is not intended for experimental purposes and it was not possible to check the quantities of interest for drift during the course of the experiment. Although there are errors in the results, the experiment demonstrates the feasibility of generalized selective material imaging.

4.7. Noise Properties of Single Projection Systems

Assuming that Poisson counting noise is the limiting factor, the errors in the estimates of the line integrals may be calculated as described in Sections 3.5 and 3.6. Poisson counting noise is the limiting factor for common detectors such as NaT scintillation detectors and film-screen cassettes [Ter-Pogossian 1967]. These detectors convert the x-ray photons to visible light. The number of light photons produced by an x-ray photon is a random variable. However, a large number of visible light photons are produced for every x-ray

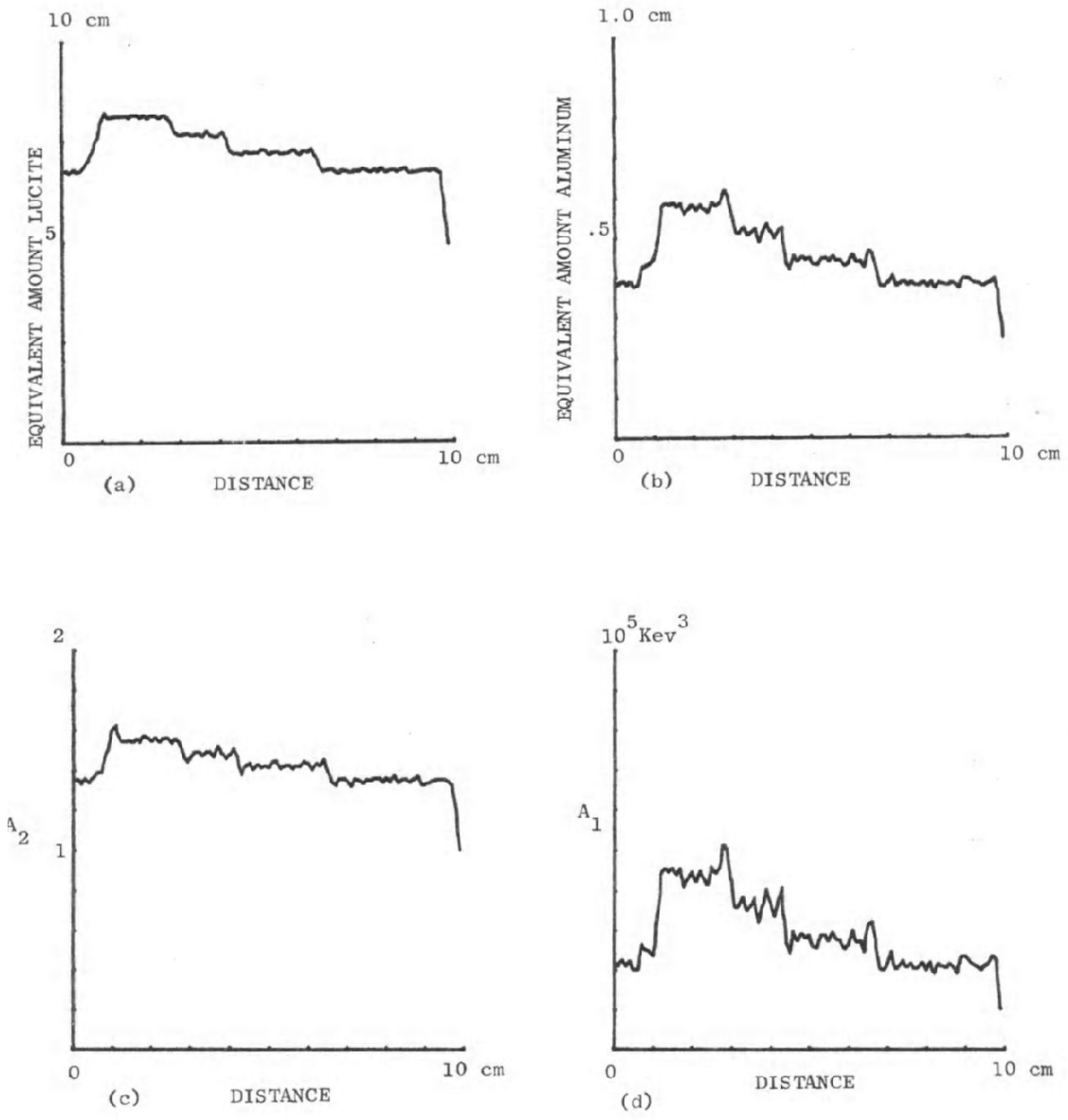

Figure 4.9.: Typical results for scans of a teflon and lucite object. Parts (a) and (b) show the equivalent amounts of lucite and aluminum. Parts (c) and (a) show the line integrals of the Compton and photoelectric coefficients.

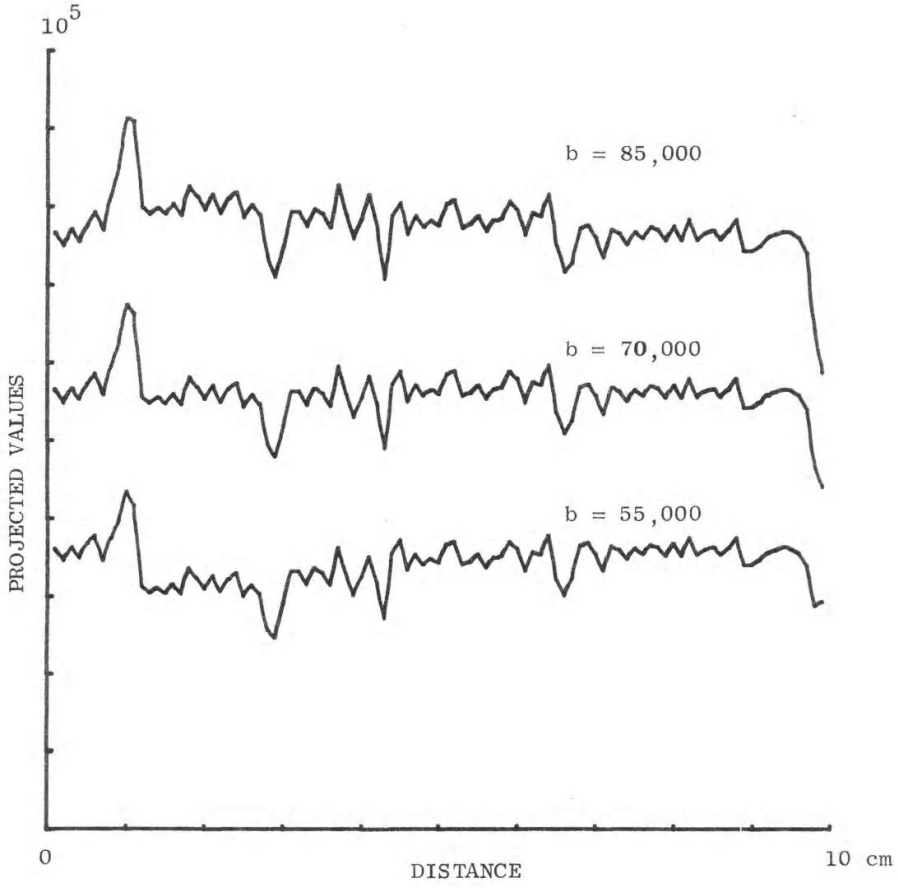

Figure 4.10.: Selective material imaging of lucite. By choosing the proper value of the constant b, the effect of the teflon can be eliminated and the result is a horizontal line. The theoretical value for b is approximately 50,000.

photon and the statistical fluctuations in the measured quantities are determined mainly by the x-ray photons.

The details of the calculation of errors depend on the particular detector system used. In general, the detector output will be a nonlinear function of the energy, or the total number of photons incident during the measurement period. So long as the nonlinear function is invertible, the maximum likelihood estimate will be the solution of the deterministic equations with the measured quantities [Van Trees, 1968, p. 70]. Once the nonlinear function is specified, the errors can be calculated using the Taylor's series approach of Section 3.5.

5. Extraction of Energy Dependent Information in Computerized Tomography

5.1. Introduction

The information in a single projection system represents the projection of the transmission of a three-dimensional object onto a two-dimensional image. This is an undesirable situation since structures of interest can be obscured by other parts of the patient along the same line of sight. Various types of tomography systems have been invented to remove the spatial averaging.

Recently, a highly successful form of tomography, known as computerized tomography, has been introduced. This technique uses a scanned x-ray beam, an electronic detector, and a computer to calculate an image of a cross section slice through the object. The technique offers two main advantages. Conventional tomography systems blur the contribution of intervening parts of the object. Computerized tomography systems remove their effect almost completely. Conventional tomography systems use photographic film as a detector and, thus, their measurements have limited accuracy. Computerized tomography systems use electronic detectors and calculate the linear attenuation coefficient extremely accurately. This allows the radiologist to distinguish various body tissues and fluids by the values of their linear attenuation coefficient.

Conventional computerized tomography systems attempt to calculate the value of the linear attenuation coefficient at a single average energy. In this chapter, we discuss techniques for the extraction of energy dependent information in computerized tomography. This allows the calculation of the values of a_1 and a_2 at every resolution element in a cross section slice through the object. An energy dependent computerized tomography system thus removes both the averaging over energy and depth and extracts the information available from an x-ray transmission measurement completely.

5.2. Mathematical Techniques for the Reconstruction of a Function From its Line Integrals

The image produced by a computerized tomography system is calculated by using the mathematical technique of the reconstruction of a function from its line integrals. This

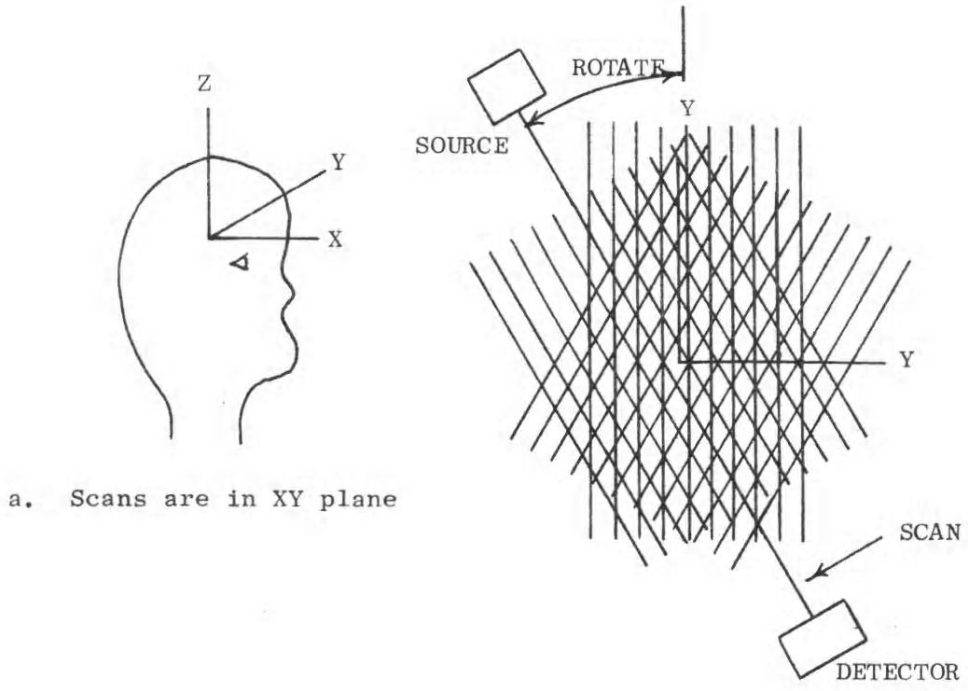

Figure 5.1.: Simple x-ray computerized tomography system.

technique requires the measurement of line integrals through the object at every possible position and orientation. In a simple system, this is accomplished by simultaneously scanning a pencil x-ray beam and detector as shown in Fig. 5.1. The detector measures the total energy of the transmitted photons at each position for a fixed measurement time and the line integral of the linear attenuation coefficient is calculated from this measurement. For a fixed angle the line integrals are measured by scanning the x-ray tube and detector across the patient. The apparatus is rotated by a small angle and another set of measurements are taken. The computer takes the sets of line integrals and calculates the value of the linear attenuation coefficient at every resolution element in the cross section of the object. In this section we review the mathematical basis for this calculation.

The variables used in this section are defined in Fig 5.2. The line integrals $g_\varphi(t)$ are measured for all angles φ, $0 \leq \varphi < \pi$, and all displacements t. From these measurements, the two-dimensional function $f(x, y)$ is to be calculated.

This problem was considered and solved rigorously by Radon in 1917. A theorem developed by Bracewell gives a great deal of insight into the problem. This theorem states that the Fourier transform of $g_\varphi(t)$, for constant φ, gives the values of the two-dimensional Fourier transform of $f(x, y)$ along a line through the origin at angle $\varphi + \pi/2$. Thus, it is called the central section theorem (Bracewell 1956).

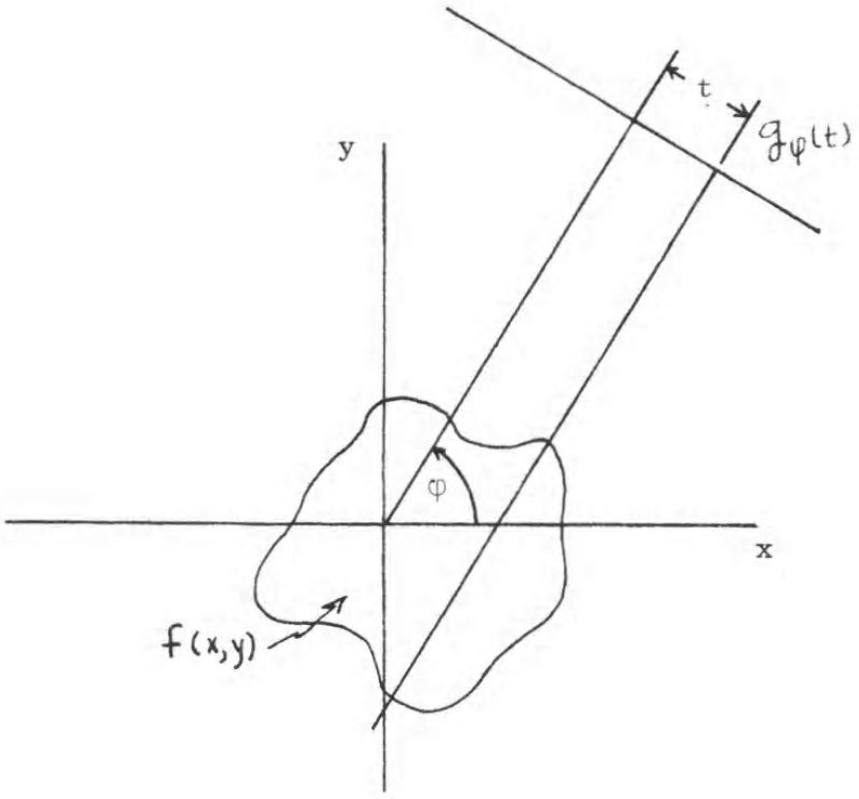

Figure 5.2.: Definition of variables in problem of reconstruction from line integrals.

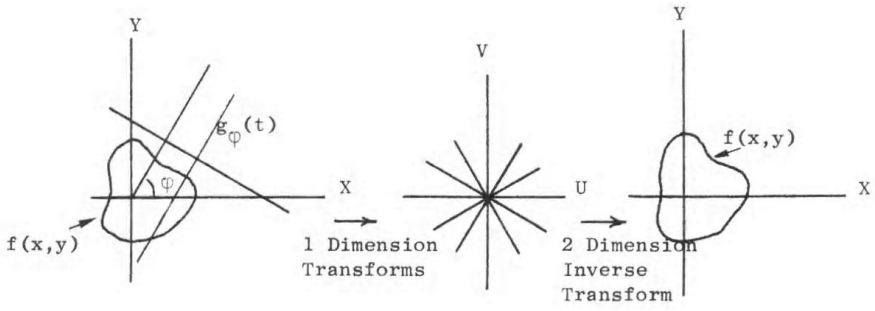

Figure 5.3.: Fourier transform technique to reconstruct a function from its line integrals.

The theorem may be derived by considering the definition of $F(u,v)$, the Fourier transform of $f(x,y)$:

$$F(u,v) = \iint_{-\infty}^{\infty} f(x,y) \exp[-j2\pi(ux+vy)]dxdy \tag{5.2.1}$$

The value of this function along the u axis (which is the line $v=0$) is

$$F(u,0) = \int_{-\infty}^{\infty} \left[\int_{-\infty}^{\infty} f(x,y)dy\right] \exp[-j2\pi ux]dx. \tag{5.2.2}$$

The integral in brackets is a line integral along a line parallel to the y axis and a distance x from it. It is therefore equal to $g_{\pi/2}(x)$

$$F(u,0) = \int_{-\infty}^{\infty} g_{\pi/2}(x) \exp[-j2\pi ux]dx = G_{\pi/2}(x) \tag{5.2.3}$$

This result can be easily generalized to give the central section theorem.

This theorem gives an existence proof for the solution of the problem of the reconstruction of a function from its line integrals. By measuring $g(t)$ for all φ and t and then Fourier transforming for constant φ, the values of $F(u,v)$ along all lines through the origin can be calculated. This gives $F(u,v)$ at all points on the (u,v) plane and by inverse transforming $f(x,y)$ is uniquely determined for all functions encountered in practical applications. This technique is actually used to reconstruct $f(x,y)$ in some cases. It is illustrated in Fig. 5.3.

The method in Fig. 5.3 uses two successive Fourier transforms to calculate $f(x,y)$. From the properties of the Fourier transform, it should be possible to reconstruct $f(x,y)$ directly from the line integrals by a convolution technique. This can indeed be done (Bracewell and Riddle 1967) and is illustrated in Fig. 5.4.

Consider the two-dimensional inverse Fourier transform in polar coordinates

$$f(r,\theta) = \int_0^{\pi} \int_{-\infty}^{\infty} |\rho| F(\rho,\varphi) e^{-j2\pi\rho r\cos(\theta-\varphi)} d\rho d\varphi. \tag{5.2.4}$$

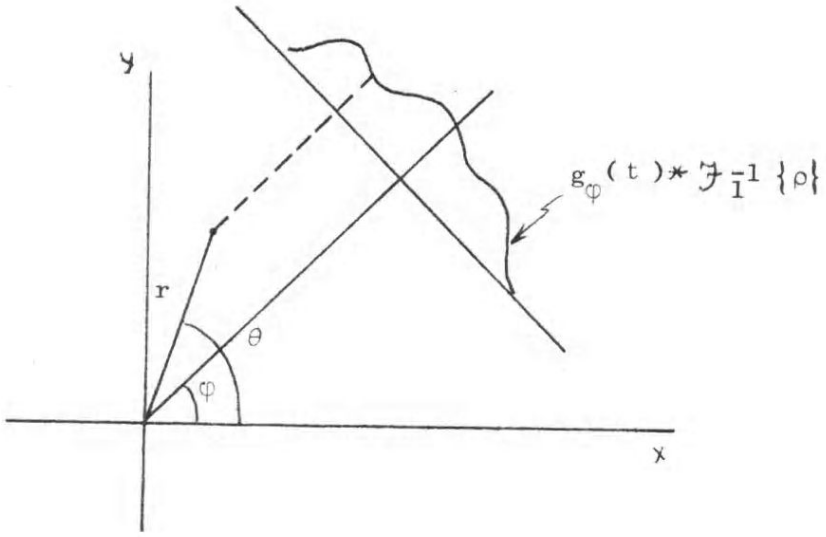

Figure 5.4.: Reconstruction from line integrals by convolution plus back projection.

From the central section theorem

$$F(\rho, \varphi) = G_{\varphi'}(\rho), \qquad \varphi' = \varphi + \pi/2 \tag{5.2.5}$$

Substituting this in equation 5.2.4

$$f(r, \theta) = \int_0^\pi \int_{-\infty}^\infty |\rho| G_{\varphi'}(\rho) e^{-j2\pi\rho w} d\rho d\varphi. \tag{5.2.6}$$

where $w = -r\cos(\theta - \varphi) = r\sin(\theta - \varphi - \pi/2) = r\sin(\theta - \varphi')$. Changing the variable of integration to $\varphi' = \varphi + \pi/2$

$$f(r, \theta) = \int_0^\pi \left[\int_{-\infty}^\infty |\rho| G_{\varphi'}(\rho) e^{-j2\pi\rho w} d\rho \right] d\varphi' \tag{5.2.7}$$

The integral in brackets is the one-dimensional Fourier transform of $|\rho| G_{\varphi'}(\rho)$. Applying the convolution theorem, equation 5.2.7 is:

$$f(r, \theta) = \int_0^\pi \left[\mathcal{F}_1^{-1}\{|\rho|\} * g_{\varphi'} \right] d\varphi' \tag{5.2.8}$$

This equation is the mathematical statement of the convolution back projection technique. In words, the reconstruction is carried out as follows. For any angle φ' convolve the line integrals with a function $h(t)$ whose transform is $|\rho|$. To reconstruct $f(r, \theta)$, at a

point (r, θ), project the value of the convolved function along a line through (r, θ) parallel to a line through the origin at angle φ as illustrated in Fig. 5.4. Do this for all angles φ and sum the projected values of the convolved functions to give the value of $f(r, \theta)$.

The results presented so far assume that measurements at all possible angles φ and all displacements t are available. In a practical system, there will only be a finite number of measurements with a beam of nonzero width. The effect of nonzero beamwidth in a linear system is to give a reconstructed image which is the convolution of the desired object with a two-dimensional spatial impulse response [Bracewell 1975]. In a nonlinear system, such as an x-ray transmission system, there will be some artifacts at discontinuities in the object [Macovski and Stonestrorn 1975].

If the object is spatially bandlimited, it can be accurately reconstructed with a finite number of measurements. Of course, any object of finite spatial extent will not be ideally bandlimited, but its spectrum will drop to negligible values for high enough spatial frequencies. The number of measurements necessary to reconstruct an object may be derived by using the sampling theorem [Goodman 1968].

Suppose the object has a maximum dimension L and we want to reconstruct it with a spatial resolution Δl. Assume the object is then bandlimited with a maximum significant spatial frequency $1/\Delta l$. The object and its transform are shown in Fig. 5.5. From the central section theorem, the one-dimensional Fourier transform of the line integrals gives a line through the two-dimensional Fourier transform of the object. Since the object has a maximum spatial frequency $1/\Delta l$, by the sampling theorem, it must be sampled with period $\Delta l/2$ to prevent aliasing. The number of measurements per projection is then

$$N = \frac{L}{\Delta l/2} = \frac{2L}{\Delta l}. \tag{5.2.9}$$

Similarly, in order to calculate an inverse Fourier transform accurately, the transform must be sampled on a grid of side $2/L$, where L is the maximum dimension of the object. Thus, from Fig. 5.5, the angle between projections must be $\Delta\theta = 2\Delta l/L$ to give the proper sampling at the edge of the transform. The number of projection angles is

$$M = \frac{\pi}{\Delta\theta} = 2\pi L \Delta l. \tag{5.2.10}$$

Note that this gives an oversampled system towards the center of the transform and fewer angles might be tolerated. Equations 5.2.9 and 5.2.10 give good estimates within a factor of 2 or 3.

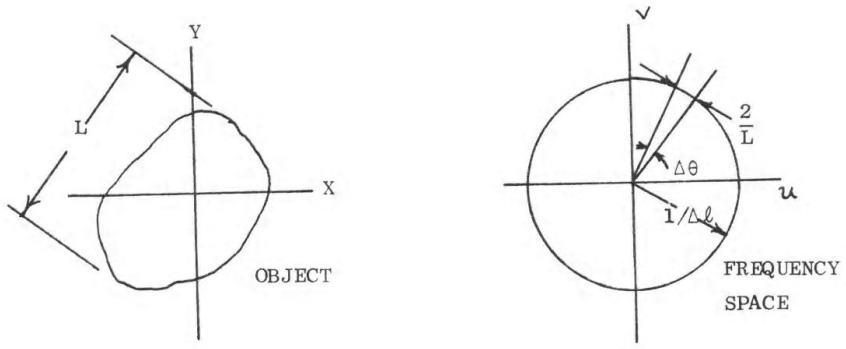

Figure 5.5.: Number of measurements necessary to reconstruct a spatially bandlimited object.

5.3. Computer Simulation of Extraction of Energy Dependent Information Using Computerized Tomography

A computer simulation was performed to illustrate the procedure for extracting energy dependent information using computerized tomography. The general procedure described in Chapter 3 was followed. The integral equations were approximated by a power series with undetermined coefficients. The coefficients were calculated from the values of the number of transmitted photons through an object with known values of A_1 and A_2. The approximations to the integral equations were then solved to give the line integrals A_1 and A_2 of the object. From these line integrals, the values of a_1 and a_2 were calculated using the techniques described in the previous section.

The object assumed is shown in Fig. 5.6. It is circularly symmetric so only one set of line integrals had to be calculated. It consists of a bone annulus filled with brain tissue except for a “lesion” at the center. The lesion was assumed to have an attenuation coefficient similar to fat. Experimentally measured attenuation coefficients were used for the tissues [Phelps, Hoffman, Ter-Pogossian 1975] and the bone [ICRU 1970].

The data consisted of the number of photons transmitted calculated at 160 points across the object. An experimentally measured 105 Kvp x-ray tube spection [Epp and Weiss 1966] was assumed. The detector used single level pulse height analysis with a 58 Kev threshold energy. This sharp threshold is an idealization which can be almost fully realized by a semiconductor detector. A lower resolution detector will have a spectral response equal to the convolution of the assumed rectangular response functions with its energy resolution impulse response. So long as the Jacobian of the integral equations is not zero, this will not affect this deterministic simulation. As discussed in Chapter 3, the lower resolution system will have a somewhat larger error due to counting noise.

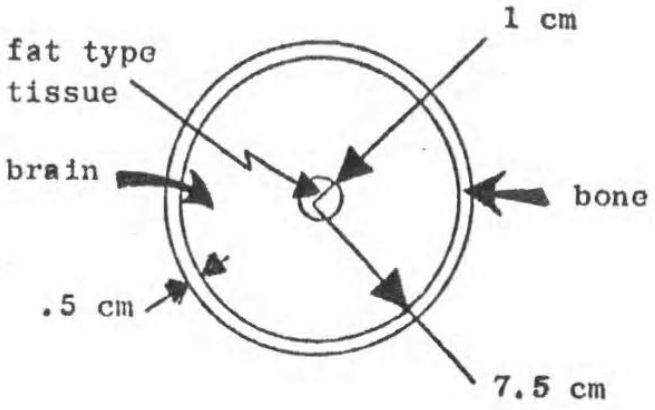

Figure 5.6.: Object used in computer simulation

At each point across the object, the equations

$$I_1 = \int S(E)g_1(E)\exp[-A_1 f_1(E) - A_2 f_{\mathrm{KN}}(E)dE \tag{5.3.1}$$

$$I_2 = \int S(E)g_2(E)\exp[-A_1 f_1(E) - A_2 f_{\mathrm{KN}}(E)dE \tag{5.3.2}$$

had to be solved. This was carried out by approximating them by:

$$lnI_1 = b_1A_1 + b_2A_2 + b_3A_1^2 + b_4A_2^2 + b_5A_1A_2 + b_6A_1^3 + b7 \tag{5.3.3}$$

$$lnI_2 = c_1A_1 + c_2A_2 + c_3A_1^2 + c_4A_2^2 + c_5A_1A_2 + c_6A_1^3 + c7 \tag{5.3.4}$$

As discussed in Section 3.7, this gives accurate results. The coefficients $\{b_i\}$ and $\{c_i\}$ were calculated by fitting the values of I_1 and I_2 for objects with known values of A_1 and A_2 with least squares techniques. The resultant cubic equations were then solved numerically at every point using the technique described in Appendix B.

Three reconstructions were carried out. They are the values of a_1 and a_2 at points in the cross section and a reconstruction assuming $ln(I_1 + I_2)$ is a line integral. The latter simulates a conventional intensity only reconstruction. The results are shown in Fig. 5.7.

The density of the lesion at the center was adjusted so that at the average energy of the transmitted spectrum, 65 Kev, its attenuation coefficient is equal to that of the surrounding tissue. The lesion is therefore not visible in the intensity only reconstruction. Since its attenuation coefficient is different at other energies, it is quite visible in the photoelectric and Compton scattering reconstructions.

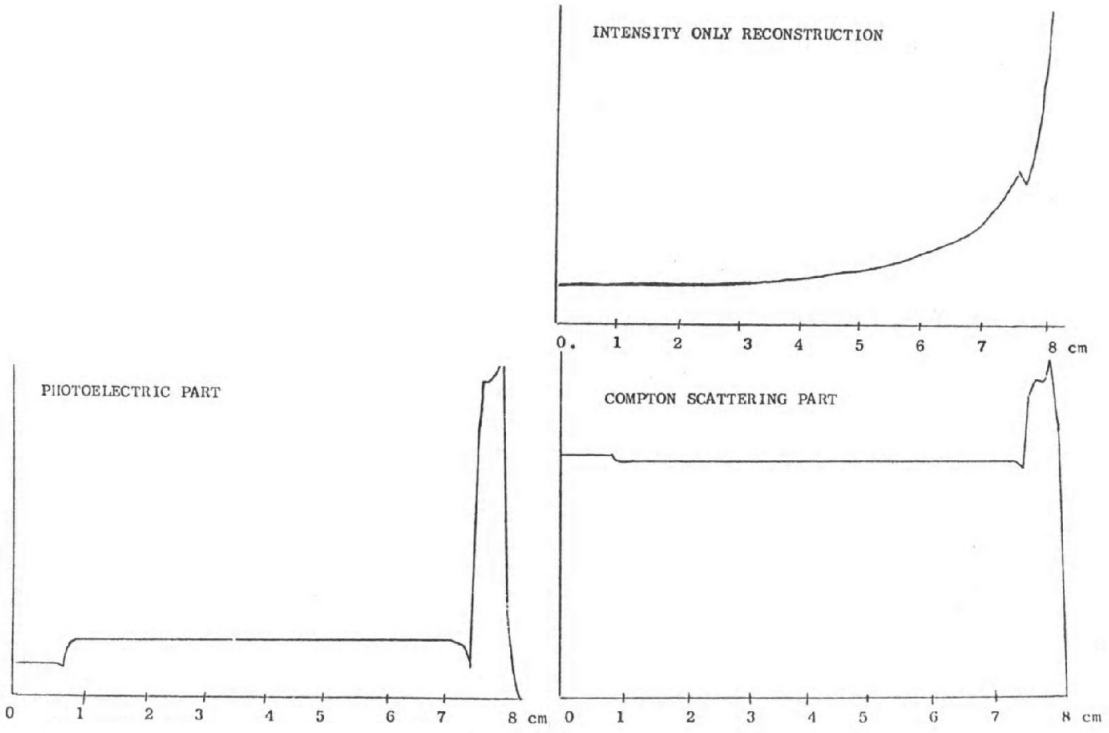

Figure 5.7.: Results of computer simulation

Also evident in the intensity only reconstruction is a "cupping" near the edge of the skull. This is a spectrul shift artifact. By reconstructing $ln(I_1 + I_2)$ we are assuming a single average energy exists so that the transmission integral is approximated by

$$I_1 + I_2 = \int S(E) \exp\left[-\int \mu(x, y; E) ds\right] dE \approx I_0 \exp\left[-\int \mu(x, y; \overline{E}) ds\right] \qquad (5.3.5)$$

Because of beam hardening, the average energy increases after the bean traverses large amounts of material. The single average energy approximation is thus inaccurate and leads to artifacts in the reconstruction. Energy dependent techniques provide a general method of computerized tomography which does not contain this artifact. Corrections for spectral shift artifacts are important features of computerized tomography systems and are discussed in Chapter 6.

The spikes evident at the junctions of different structures are artifacts of the reconstruction algorithm. As discussed in the previous section, this assumes a spatially bandlimited object. Because of the sharp edges, the object is not bandlimited and this causes the artifact. The phenomenon is quite similar to "ringing" in temporal systems.

5.4. Display of Energy Dependent Information

The results of an energy dependent computerized tomography system are two images. At every resolution element in the cross section there are associated the values of a_1 and a_2 for the material in that volume, The information may be displayed as two separate images or combined in various ways.

One possibility is a color display. One primary color might represent a_1 and another a_2. The result at any point will be a shade of color which is indicative of the values of a_1 and a_2 at that point.

Another possibility is to use the values of a_1 and a_2 and the functions $f_1(E)$ and $f_{\mathsf{KN}}(E)$ to calculate the linear attenuation coefficient at any point

$$\mu(E) = a_1 f_1(E) + a_2 f_{\mathsf{KN}}(E). \qquad (5.4.1)$$

Any energy within the diagnostic region may be used. Figure 5.8 shows the attenuation coefficient in the computer simulation described in the previous section calculated at 40 Kev.

Selective material imaging is also possible. The data can be combined in such a way that the contribution of any particular material is zero. This may be done by taking a linear combination $a_1 - ba_2$ with $b = a_{1m}/a_{2m}$ where (a_{1m}, a_{2m}) are the coefficients of the material. Figure 5.9 shows the results when b is chosen so the contribution of water is zero.

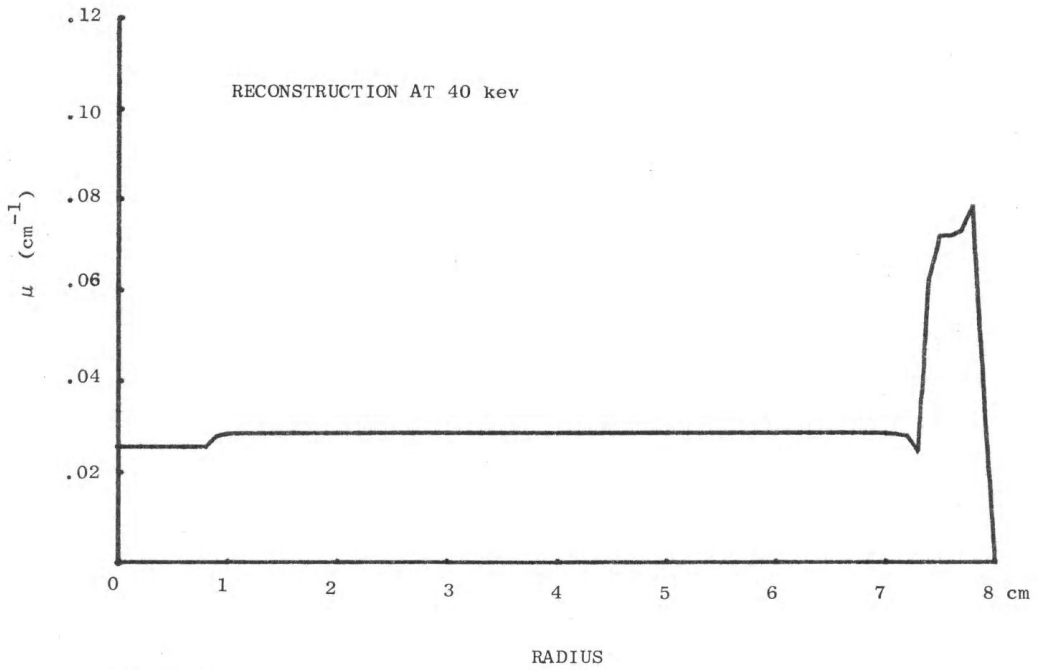

Figure 5.8.: Reconstructed image valuesalong a radial line.

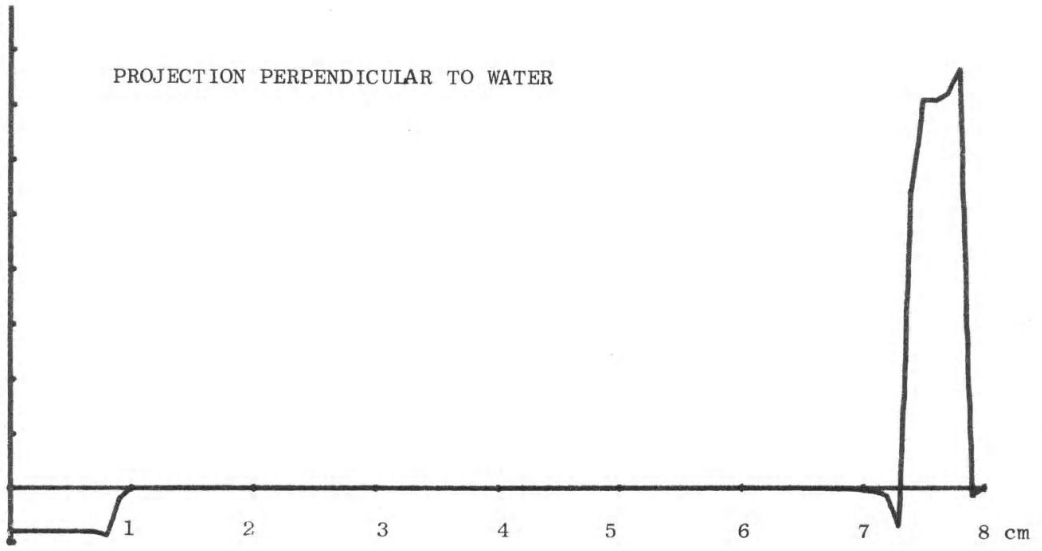

Figure 5.9.: Linear combination of reconstructed values along a radial line. The cofficients were chosen to elmininate water as discussed in the text.

5.5. Counting Noise in Energy Dependent Computerized Tomography Systems

The values of a_1 and a_2 for typical body materials should be as shown in Fig. 2.13. The diagnostic utility of this information cannot be determined unless the errors in the measurements are known. In this section we consider the errors in the measurement of a_1 and a_2 due to counting noise.

In terms of noise properties, the linear reconstruction techniques such as convolution plus back projection, the Fourier transform method, and others are similar [Barrett, Gordon, Hershel 1976]. The convolution plus back projection technique is perhaps the most widely used in x-ray computerized tomography and will be discussed here. This technique consists of convolving the line integrals at any particular angle with a function h. The convolved functions are then back projected and summed to yield the reconstructed image at any point.

Unfortunately, the noise in the reconstructed value depends on the original object. In order to get an estimate of the noise some assumptions must be made. The noise at the center of a large uniform object will be calculated. If $A_\varphi(k)$ are the line integrals at angle φ and position k, the reconstructed value at the center of the image in discrete form will be

$$a = \sum_{l=1}^{M} \sum_{k=-N/2}^{N/L} A_{\varphi l}(k) h(k) \tag{5.5.1}$$

Assuming the object is large and uniform, $\sigma_A^2(k)$ will be constant over the region where $h^2(k)$ is nonzero. Thus for independent measurements

$$\sigma_a = \sigma_A^2 M \sum_{k=-N/2}^{N/L} h^2(k) \tag{5.5.2}$$

Since h is known, M and N can be calculated from the formulas in Section 5.2, and can be calculated using the techniques of Chapter 3, the expression for the variance of the estimate can be evaluated for any particular situation. From the discussion in Chapter 3, the bias will be negligible compared to the standard deviation of the error.

In an energy dependent system, there are two numbers associated with each measurement. The errors in these numbers can be used to define regions around each point in a plot such as Fig. 2.13 where a measured value is likely to occur. If these probable regions are small compared to the distance between points, the measurement system can distinguish the materials.

These regions may be considered to be contour lines of a probability distribution. For large numbers of counts, the errors will be jointly normally distributed for two reasons. First, for large numbers of counts, the relative spread of the number of counts decreases and a linear approximation accurately describes the system. Also, as the number of counts

increases, their distribution becomes closer to a Gaussian. Therefore, the errors will be normally distributed since they become linear combinations of normal random variables. The functions $f_1(E)$ and $f_{\mathsf{KN}}(E)$ are not orthogonal so the errors are correlated and the contours of equal probability are ellipses with major axes not parallel to the a_1 or a_2 axes. These ellipses will be approximated by rectangles.

Figure 5.10 shows the data of Fig. 2.13. Also shown is a rectangle with sides σ_{a_1} and σ_{a_2} as an error estimate. The system assumed is the same as that described in Section 3.9. An object $20\,$cm thick was assumed.

The dose may be roughly approximated as follows. The total energy deposited is $(4\,\text{ergs}) \times M \times N$. Assuming $2\,$mm resolution, $M = 157$ and $N = 200$. An object $20\,$cm in diameter, $1\,$cm thick with an average density near $1\,\text{gm/cm}^3$ is also assumed. The average dose will then be approximately

$$\text{Dose} = \frac{\text{Energy}}{\text{Mass}} \approx 4\,\text{rad}. \tag{5.5.3}$$

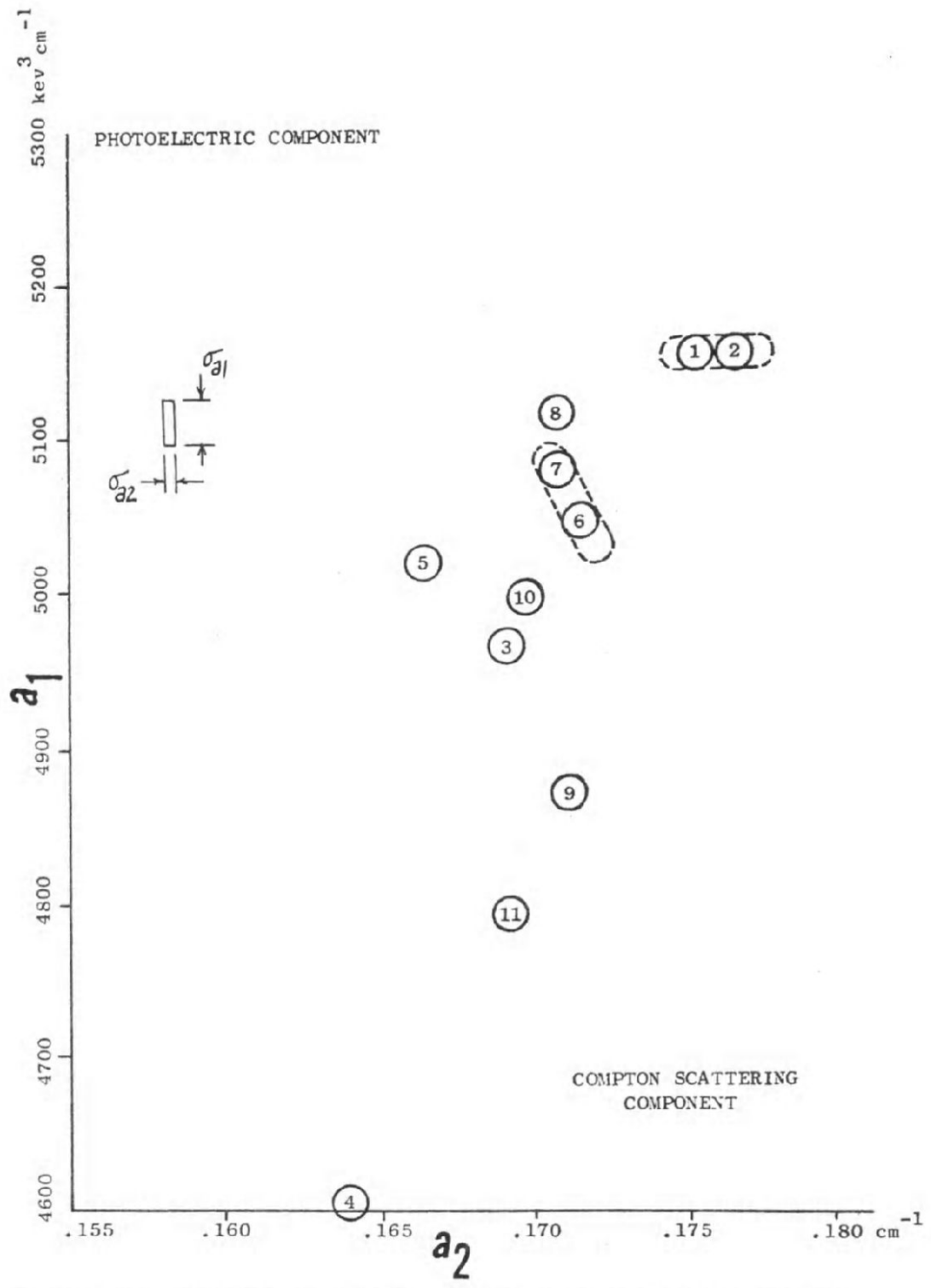

Figure 5.10.: Values of a_1 and a_2 for various tissues with estimate of error in a typical system. The standard deviation of the errors for each quantity are shown in the rectangle at the upper left.

6. Spectral Shift Artifacts In X-Ray Computerized Tomography

6.1. Introduction

The data needed by a computerized tomography system are the line integrals of the linear attenuation coefficient. The quantity actually measured by the detectors used in these systems is the intensity I of the photons transmitted through the body. From this measurement the line integrals $\int \mu(x, y; E)ds$ must be calculated. If a monoenergetic source were used with a zero width beam, then these quantities would be related by

$$I = I_0 \exp\left[-\int \mu(x, y; E)ds\right] \tag{6.1.1}$$

and it would be relatively simple to calculate the line integral from the measured quantity. Monoenergetic sources, however, do not produce a sufficient number of photons per second to permit accurate measurements on objects of medical interest in a sufficiently short time. Thus broad spectrum x-ray tube sources must be used. In this case, the line integral and the intensity are related by the integral equation

$$I = \int S(E) \exp\left[-\int \mu(x, y; E)ds\right] dE \tag{6.1.2}$$

and it is a difficult problem to solve for the line integral.

A technique for attempting to solve this equation for the line integral is to assume that an average energy $\overline{E}$ exists so that equation 6.1.2 may be approximated by

$$I = I_0 \exp\left[-\int \mu(x, y; \overline{E})ds\right] \tag{6.1.3}$$

This is not a good approximation. Because of beam hardening, the average energy is not constant but increases as the beam traverses more material. This is shown in Fig. 6.1. The spectrum of an x-ray beam is plotted after transmission through various thicknesses of bone. Note that the average energy increases as the bone thickness increases.

The errors caused by making a single average energy approximation can lead to significant artifacts in the reconstruction [Macovski, Alvarez, Chan, Stonestrom 1975]. Since the attenuation coefficient is a function of energy, its apparent value will be different for beams that have passed through different amounts of material. As shown in Fig. 6.2,

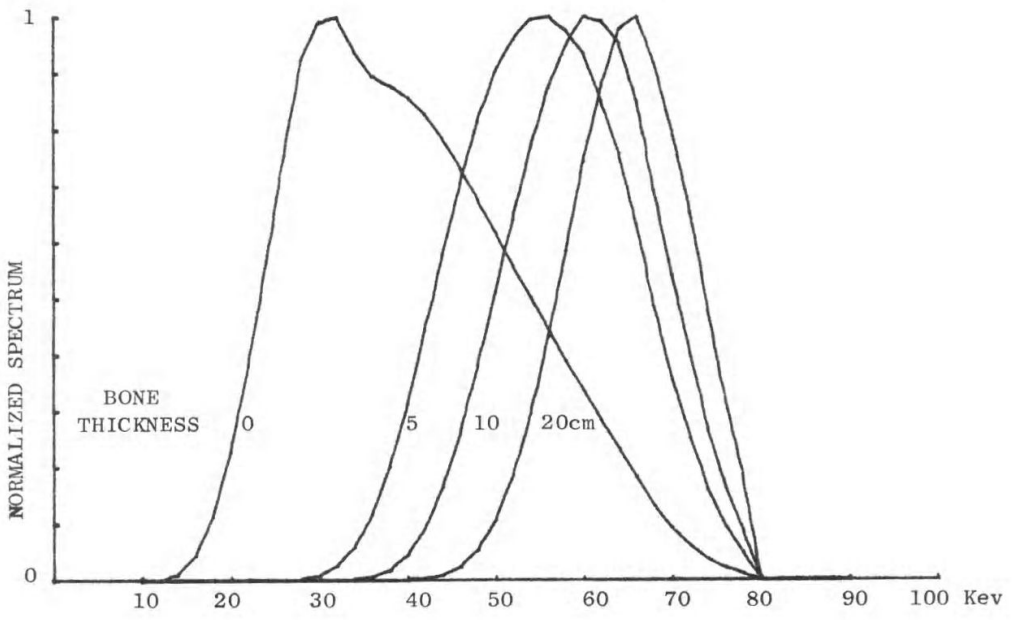

Figure 6.1.: X-Ray spectrum after transmission through various thicknesses of bone. The spectra are normalized to have the same maximum value.

this will lead to inconsistent values in different measurements of line integrals and thus to errors in the reconstruction. In a scan of the head, the errors should be greatest near the skull. In this region, rays tangential to the skull pass through large amounts of bone while perpendicular rays have much less bone in their paths. As shown in Fig. 6.3, this leads to a “cupping” artifact in the reconstruction near the skull. In part a, a cross section of the reconstruction with a monoenergetic source is shown. Part b shows the cross section of the reconstruction with a broad spectrum source using a single average energy assumption. This artifact has been seen experimentally. Figure 6.4 shows reconstructions of a brain and skull on an EMI machine [Gado and Phelps 1975]. Reconstructions with the skull have significant artifacts. The EMI machine makes some attempt to correct the artifact [Hounsfield 1975] but apparently it is not completely effective.

In this chapter we discuss techniques for calculating line integrals from broad spectrum measurements. We present a unified analysis of the techniques currently used which shows the effects of various system parameters on their accuracy. We consider the general problem of calculating the line integral and show that it cannot be calculated from a single broad spectrum intensity measurement. Finally, we show that energy spectral analysis provides an accurate general technique for calculating the line integral.

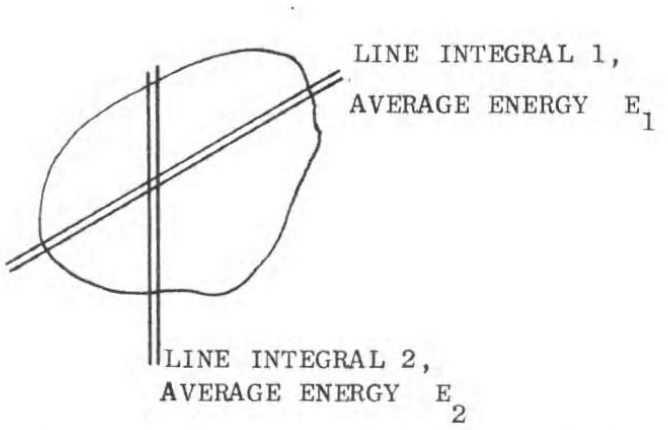

Figure 6.2.: Measurement of line integrals through different object thicknesses.

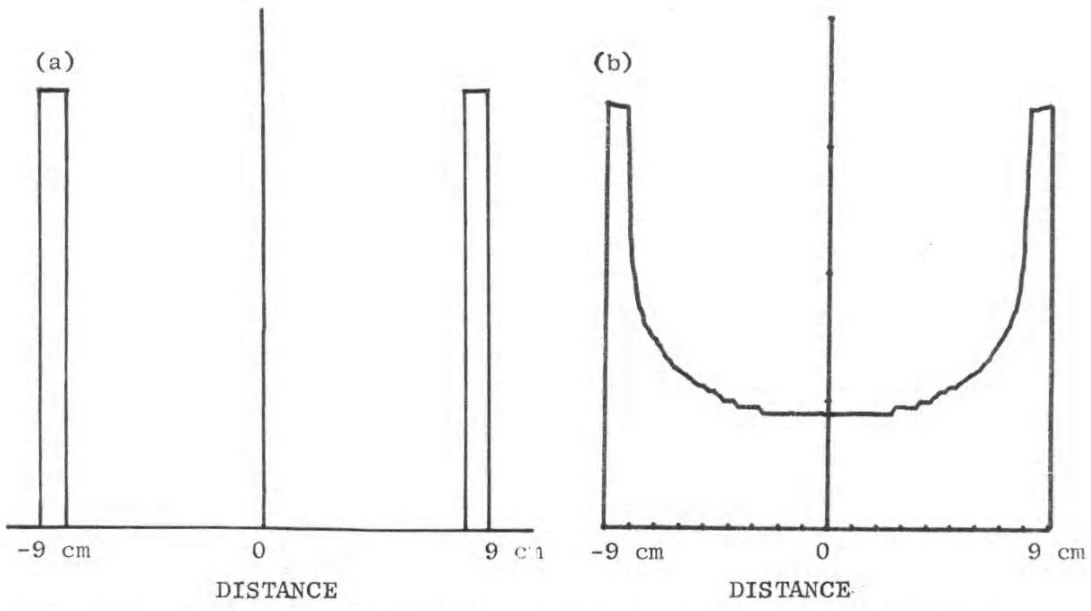

Figure 6.3.: Artifacts for annulus object. (a) Reconstruction with accurate line integrals. (b) Reconstruction using single average energy approximation. A logarithmic vertical scale is used.

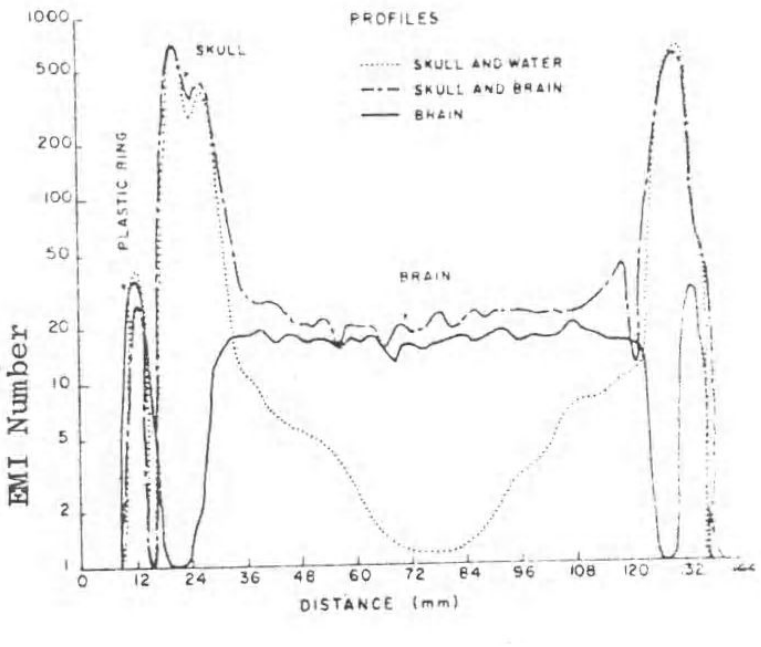

Figure 6.4.: Reconstructions on an EMI brain scanner showing artifacts.

6.2. Techniques Currently Used For Calculating Line Integrals

Most of the techniques currently used for calculating line integrals are based on making the average energy approximation more accurate. The techniques that will be discussed are prefiltering, constant path length water baths, and linearization.

As shown in Fig. 6.1, an x-ray spectrum becomes more monoenergetic after passing through a material. Since a narrow spectrum beam produces smaller spectral shift artifacts, the technique of prefiltering consists of placing a filter material between the x-ray tube and the patient. This technique reduces spectral shift artifacts, but it introduces several problems. One problem is that it reduces the available intensity of the x-ray source. Because of the desirability of shortened scan times, the source intensity is an important limiting factor in the design of a computerized tomography system. Another problem is that prefiltering raises the average energy of the incident spectrum. As discussed in Chapter 2, the contrast per unit dose has a maximum as a function of energy. Depending somewhat on the object thickness, most computerized tomography systems operate with energies above this maximum so increasing the average energy decreases the available contrast per unit dose.

Another technique for decreasing spectral shift artifacts is the use of a constant path length water bath. This is illustrated in Fig. 6.5. The effectiveness of this technique may be seen by writing the expression for the transmitted intensity. Assume the object has

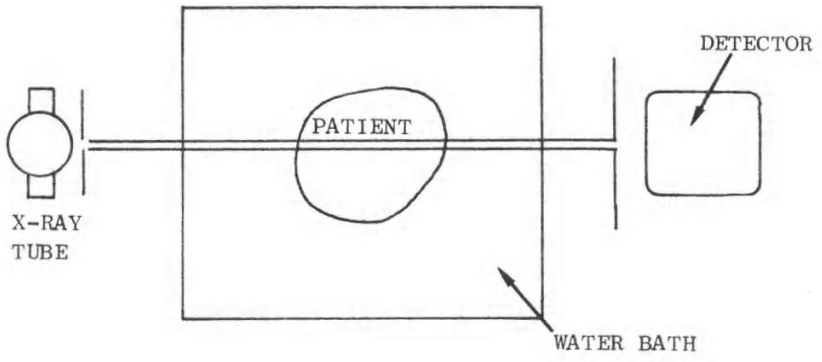

Figure 6.5.: Use of a constant path length water bath in a computerized tomography system.

attenuation coefficient $\mu(E)$, length l, and is placed in a water bath with total length d. The transmitted intensity will be

$$I = \int S(E) \exp\left[-l\mu(E) - (d-l)\mu_w(E)\right] dE \tag{6.2.1}$$

In this expression, $\mu_w(E)$ is the linear attenuation coefficient of water. Rewriting the equation:

$$I = \int S(E) \exp\left[-d\mu_w(E) - l[\mu(E) - \mu_w(E)]\right] dE \tag{6.2.2}$$

From this equation, we can see that the water bath has two effects. The first term in the exponential shows that a water bath is equivalent to having a water prefilter of thickness d. The second term in the exponential shows that the object reconstructed will not be the original object. It will be an equivalent object with an attenuation coefficient equal to the difference between that of the original object and water. For biological materials, this tends to reduce the dynamic range of the quantity reconstructed. This decreases the shift in the average energy and, therefore, the magnitude of the spectral shift artifact.

A constant path length water bath is effective in reducing spectral shift artifacts, but it also has some problems. It increases the dose because of the attenuation of the water between the patient and the detector. It is cumbersome to implement especially in a body scanner configuration.

In the single average energy approximation, the line integral is calculated by taking the logarithm of the measured intensity. If an object consisting of a single material is measured with a broad spectrum source, the logarithm will be a nonlinear function of the line integral. In this case the line integral is

$$\int \mu(x, y; E) ds = l\mu(E) \tag{6.2.3}$$

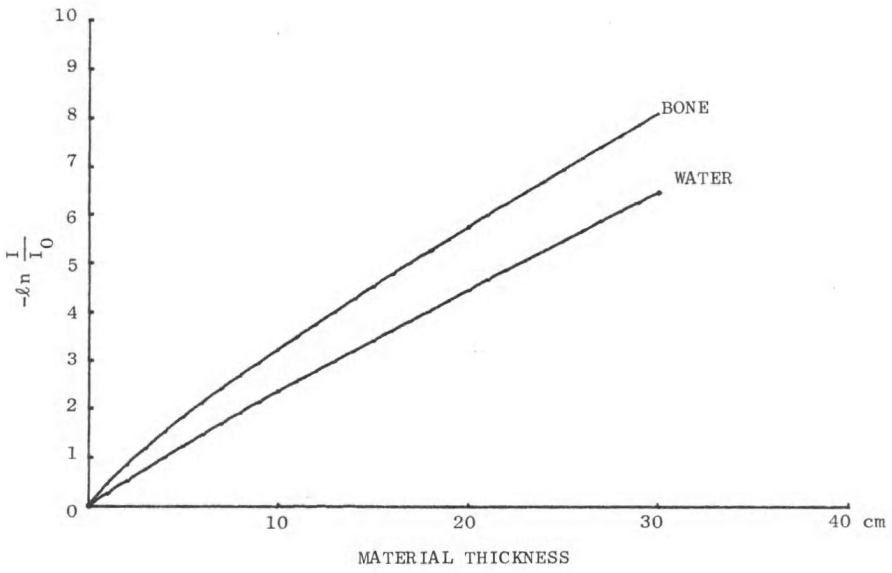

Figure 6.6.: Nonlinear relationship between line integral and logarithm of intensity for a broad spectrum source.

where l is the length of the material along the x-ray beam path. This nonlinearity is shown in Fig. 6.6. Since the function is very well-behaved it is easy to find an inverse and solve for the length, and, hence, the line integral. This is the technique of linearization.

This technique has several theoretical and practical difficulties. First, it assumes the object consists of a single material. This is certainly not the case for the human body. If a water bath is used, the body might be modeled as consisting of bone and water for the purpose of correcting spectral shift artifact. In this approximation, the object reconstructed will be bone since the system will reconstruct an object equal to the difference between the original object and water. Thus we have a single material system and an inverse function can be found to correct the line integrals. The bone-water approximation is only for the purpose of correcting artifacts. Once the line integrals are corrected for large errors due to spectral shift, the original variations in the object are reconstructed.

Even with a water bath system, there are difficulties. The inverse function depends on the composition of the bone which is not the same in all individuals. We will show in Section 6.4 that it is not possible to define a single inverse function which will be accurate for all compositions of materials. Therefore, linearization can be applied only under very restrictive assumptions. There are two cases. The object consists of a single material. The object consists of water plus another material and a constant path length water bath is used. The inverse function will depend on the tube voltage, spectrum, and the material.

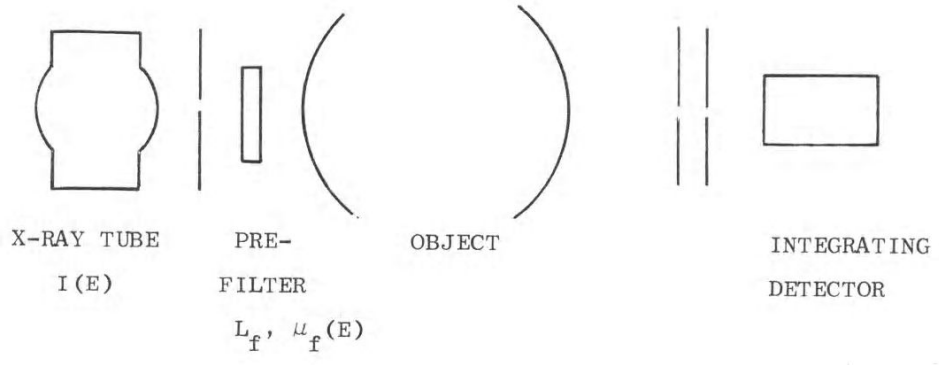

Figure 6.7.: Experimental configuration assumed in analysis.

6.3. Analysis of Conventional Techniques for Calculating Line Integrals

The efficiency and accuracy of the techniques described in the previous section will be analyzed in this section. This will be done by deriving an expression for the logarithm of the transmitted intensity. The expression contains a term linear in the line integral which yields an artifact free reconstruction and a nonlinear term which leads to spectral shift artifacts. This technique is useful because it deals with the source of artifacts at the line integrals and is independent of the reconstruction technique.

The situation analyzed is shown in Fig. 6.7. There is a prefilter with thickness l_f and attenuation coefficient $\mu_f(E)$. The x-ray tube spectrum is $I(E)$ and the detector is assumed to measure the total energy of the photons.

For a given line, the line integral is a function of energy only:

$$L(E) = \int \mu(x, y, z; E) ds \tag{6.3.1}$$

The intensity of the transmitted beam is then

$$I = \int_0^{E_m} I(E) e^{-L(E)} e^{-l_f \mu_f(E)} dE. \tag{6.3.2}$$

where E_m is the maximum energy of the incident spectrum. This is a Laplace integral [Copson 1965]. As the filter attenuation becomes large, the main contributions to the transmitted intensity come from the point where $\mu_f(E)$ attains its minimum value. Since $\mu_f(E)$ is a decreasing function, the minimum occurs at the end point of the region of interest, E_m. We can derive an asymptotic approximation to the integral which is accurate for large attenuation. Since the attenuation must be large or spectral shift artifacts will

ruin the reconstruction, this assumption is valid and the approximation will be accurate for practical systems.

In Section 6.6 of this chapter, we calculate an approximation to the logarithm of the transmitted intensity. The resultant expression is

$$-ln\frac{I}{I_{L=0}} = L(E_m) + \frac{2L'(E_m)}{l_f\mu'_f(E_m)} - \left[\frac{L'(E_m)}{l_f\mu'_f(E_m)}\right]^2 \tag{6.3.3}$$

where a primed quantity denotes a derivative with respect to energy. Although this expression is valid for the case of many materials, its interpretation is made easier by considering the case of an object consisting of a single material. In this case

$$L(E) = l\mu(E) \tag{6.3.4}$$

where $\mu(E)$ is the linear attenuation coefficient of the object and l is the thickness of material along the x-ray beam path. This thickness is the variable quantity. The computerized tomography system attempts to measure the thickness for all orientations and positions across the object and reconstruct the object from these measurements.

For the single material case, the logarithm of the transmitted intensity is:

$$-ln\frac{I}{I_{L=0}} = l\left[\mu(E_m) + \frac{2\mu'(E_m)}{l_f\mu'_f(E_m)}\right] - l^2\left[\frac{\mu'(E_m)}{l_f\mu'_f(E_m)}\right]^2 \tag{6.3.5}$$

The first term is proportional to the desired quantity l. It shows that the average energy will be somewhat less than E_m. This is physically reasonable. The first term is linear so it leads to an artifact free reconstruction. The second term is proportional to l^2. Since this is nonlinear, it leads to artifacts in the reconstruction.

The accuracy of this approximation is shown in Fig. 6.8. This shows the computer simulation of the reconstruction of an annular object in three cases. In part b the object is reconstructed with accurate line integrals. In part c the line integrals are calculated by taking the logarithm of the transmitted intensity. In part d a quadratic approximation such as equation 6.3.5 is used. Note the cupping near the annular ring in parts c and d. This is due to spectral shift. The size of the artifact is the same in c and d so the approximation is accurate. The coefficient of the quadratic term used in these calculations is $.0026\,\text{cm}^2$ while that predicted by equation 6.3.5 is $.0018\,\text{cm}^2$. The expressions developed from the asymptotic approximation do not give the magnitude of the error term exactly. They are valuable because they show the functional of the behavior of the error term with the system parameters.

The effectiveness of prefiltering can be seen directly from equation 6.3.3. The magnitude of the artifact will decrease as the square of the inverse of the filter thickness. Since the transmission of the filter decreases exponentially with its thickness, there is a tradeoff between the size of the artifact and the effective intensity of the source. The dependence

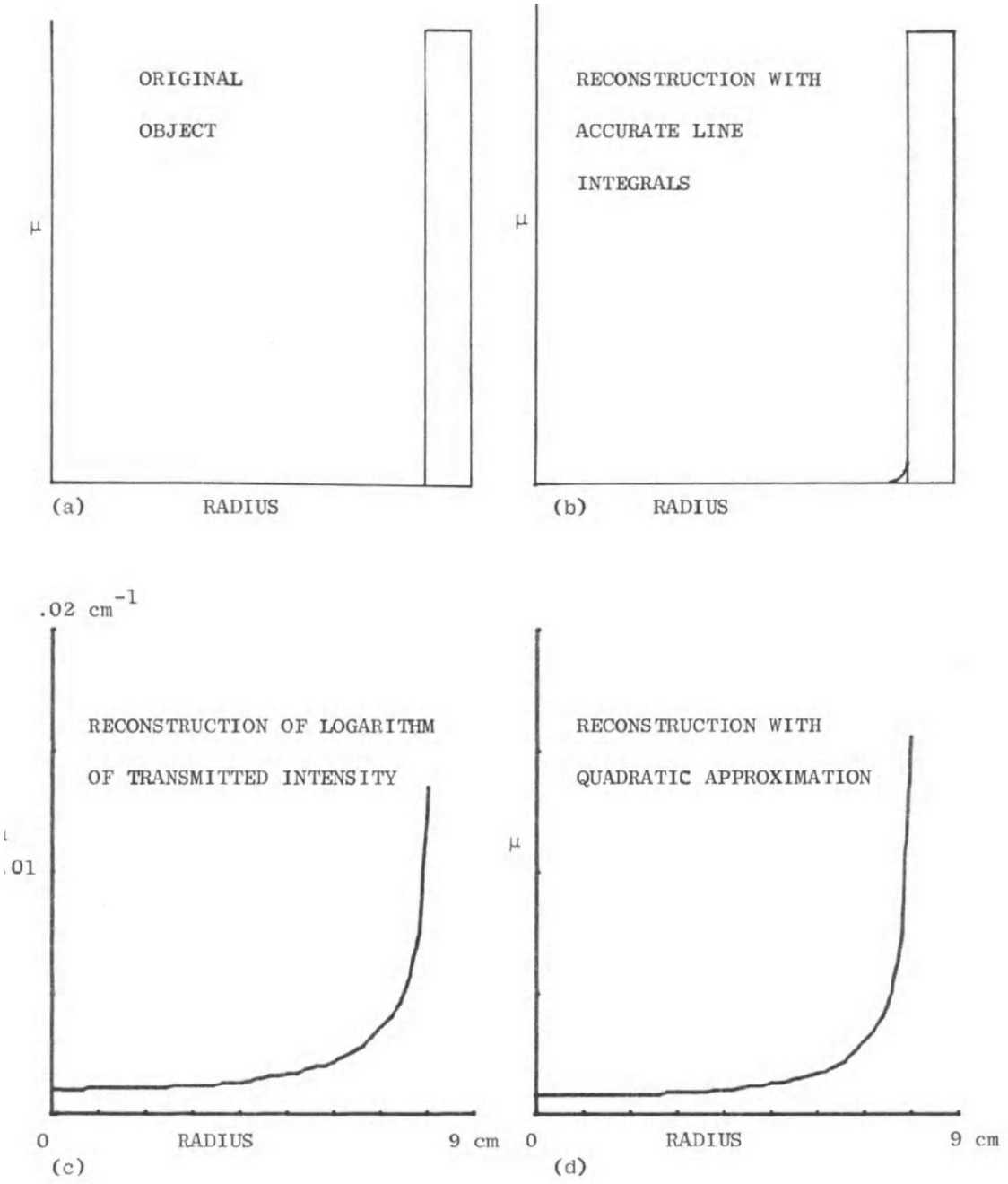

Figure 6.8.: Accuracy of quadratic approximation to logarithm of transmitted intensity.

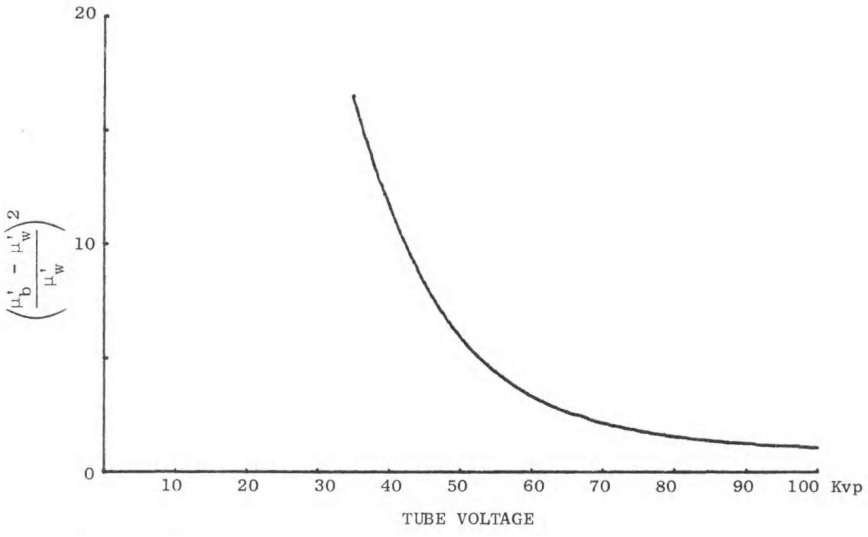

Figure 6.9.: Magnitude of artifact as a function of tube voltage. The object is ICRU bone and a water bath is assumed.

of the artifact with prefiltering on tube voltage is shown in Fig. 6.9. The artifact decreases with increasing tube voltage. Increasing the tube voltage, however, increases the average energy and thus decreases the contrast per unit dose.

If a constant path length water bath is used equation 6.3.3 is still applicable with

$$L(E) = \int \mu(x, y, z; E)ds - d\mu_w(E) \tag{6.3.6}$$

and

$$l_f \mu_f(E) = d\mu_w(E) \tag{6.3.7}$$

where d is the length of the water bath. Substituting these in equation 6.3.3 yields an expression for the logarithm of the transmitted intensity. The quadratic term will be

$$\text{Quadratic term} = \left[\frac{\int \mu'(x, y, z; E_m)ds - \mu'_w(E_m)}{d\mu'_w(E_m)}\right]^2 \tag{6.3.8}$$

The term decreases as l/d^2. The nonlinear term is also smaller than in a system without a water bath because of the subtraction of the $\mu'_w(E_m)$ term.

The effectiveness of linearization is also evident from 6.3.3 and 6.3.5. The coefficient of the quadratic term depends on $[\mu'_w(E_m)]^2$ and therefore on the composition of the material. An inverse function suitable for one material will be inaccurate for a different material.

6.4. Calculation of Line Integrals From Broad Spectrum Data

The discussion of the previous section was based on techniques which attempt to calculate the line integral by making the single average energy approximation more accurate. Are there other techniques which can be used to calculate the line integral. In this section we show that the line integral cannot be calculated from a single intensity measurement except in the situations described in Section 6.2, where linearization is possible or if a monoenergetic source is used.

The proof of this statement is simplified by using the two function basis set introduced in Chapter 2. In terms of A_1 and A_2, the line integral of the linear attenuation coefficient is

$$\int \mu(x, y, z; e)ds = A_1 f_1(E) + A_2 f_{\mathsf{KN}}(E) \tag{6.4.1}$$

The line integral at a fixed energy will be a linear combination of A_1 and A_2. The problem may then be stated mathematically as follows. Is there any way to calculate a linear combination of A_1 and A_2 from a single intensity measurement, I ?

$$I(A_1, A_2) = \int S(E) \exp\left[-A_1 f_1(E) - A_2 f_{\mathsf{KN}}(E)\right] dE. \tag{6.4.2}$$

We will show that an invertible function g does not exist such that

$$g\left[I(A1, A2)\right] = k_1 A_1 + k_2 A_2 \tag{6.4.3}$$

for the case where the object consists of more than one material. The k_1 and k_2 are constants. The proof is done in two steps. First, we will show that if g exists, then the contour lines of $I(A_1, A_2)$ must be straight lines. Next we will show that the contour lines of $I(A_1, A_2)$ are not straight lines. This completes the proof by contradiction.

Consider the composite function $h(A_1, A_2)$ defined by

$$h(A_1, A_2) = g\left[I(A_1, A_2)\right] \tag{6.4.4}$$

If g exists then $h(A_1, A_2) = g[I(A_1, A_2)] = k_1 A_1 + k_2 A_2$. The contour lines of h defined by $h(A_1, A_2) =$ constant are straight lines. The function g is assumed to be invertible so, if $h(A_1, A_2)$ is equal to a constant, then $I(A_1, A_2)$ must also be equal to a unique constant. Conversely, if $I(A_1, A_2)$ is equal to a constant, then, since g is invertible, $h(A_1, A_2)$ must be a unique constant. This shows that if g exists and is invertible then the sets of points $[A_1, A_2|I(A_1, A_2) = K_1 =$ constant] and $[A_1, A_2|h(A_1, A_2) = g(K_1) =$ constant] are included in each other. They must then be identical and the contour lines of $I(A_1, A_2)$ are straight lines.

The contour lines of $I(A_1, A_2)$, however, are not straight lines in general. This is evident empirically from the fact that a power series with quadratic and cubic terms must be used to accurately represent $lnI(A_1, A_2)$ if a broad spectrum source is used. It will be shown

to result from the fact that $f_1(E)$ and $f_{\mathsf{KN}}(E)$ are linearly independent. Any set of basis functions must be linearly independent.

The equation of the contour lines of I is

$$I(A_1, A_2) = \int S(E) \exp\left[-A_1 f_1(E) - A_2 f_{\mathsf{KN}}(E)\right] dE = K_1 = \text{constant} \tag{6.4.5}$$

Differentiating this expression implicitly gives the value of the slope of the contour line through any point $(A1, A2)$

$$\frac{dA_1}{dA_2} = -\frac{\int f_{\mathsf{KN}}(E) S(E) \exp\left[-A_1 f_1(E) - A_2 f_{\mathsf{KN}}(E)\right] dE}{\int f_1(E) S(E) \exp\left[-A_1 f_1(E) - A_2 f_{\mathsf{KN}}(E)\right] dE} \tag{6.4.6}$$

If a contour line is a straight line then this slope must be a constant and equal to, say, α along the straight line $A_2 = \alpha A_1 + \beta$. That is

$$\frac{dA_1}{dA_2} = \alpha = -\frac{\int f_{\mathsf{KN}}(E) S(E) \exp\left[-A_1 f_1(E) - A_2 f_{\mathsf{KN}}(E)\right] dE}{\int f_1(E) S(E) \exp\left[-A_1 f_1(E) - A_2 f_{\mathsf{KN}}(E)\right] dE} \tag{6.4.7}$$

for all A_1. Defining

$$u(E) = S(E) \exp\left[-A_1 f_1(E) - \alpha A_1 f_{\mathsf{KN}}(E) - \beta f_{\mathsf{KN}}(E)\right] \tag{6.4.8}$$

this equation may be written in bracket notation as

$$\alpha = -\frac{\langle f_{\mathsf{KN}}, u \rangle}{\langle f_1, u \rangle} = \text{constant} \tag{6.4.9}$$

This must be true for all possible functions u. In words, this states that in the space of all possible u functions f_1 and f_{KN} are linearly dependent. This will not be true unless the space is degenerate. Thus the contour lines are not straight lines and g does not exist.

The cases where the line integral can be calculated from an intensity measurement are instructive. There are two cases. The spectrum is monoenergetic or the object effectively consists of one known material. If the spectrum is monoenergetic, then the contour lines of $I(A_1, A_2)$ are straight lines. From 6.4.8 their slope will be

$$\text{slope} = -\frac{f_{\mathsf{KN}}(E_0)}{f_1(E_0)} = \frac{dA_2}{dA_1} \tag{6.4.10}$$

where E_0 is the energy of the spectrum. If the object consists of one material then A_1 and A_2 must lie on a straight line through the origin and the space $\{u\}$ is degenerate.

6.5. Calculation of Line Integrals Using Energy Spectral Analysis

The techniques presented in Chapter 5 for extracting energy dependent information in computerized tomography may also be considered to be techniques for accurately calculating a reconstructed image free of spectral shift artifacts. As such, the techniques have several advantages. They are general techniques which are effective for all body materials. They extract more information than conventional techniques. They do not require prefiltering or constant path length water baths and therefore make better use of the source intensity.

Another consideration is patient dose. This is a complicated situation. At first glance, more dose seems necessary to achieve useable accuracy with an energy dependent system than with a conventional system. This is not necessarily true. For example, a constant path length water bath is used in some conventional systems. The water between the patient and the detector absorbs x-rays and, for a given accuracy in the measurement, causes more patient dose. For example, a distance of 3 cm of water approximately doubles the dose. Also, the extra information extracted by energy dependent techniques may eliminate some procedures which cause extra dose. This is the case with conventional computerized tomography.

6.6. Application of Asymptotic Approximation Theory to the Transmission Integral

The integral that must be evaluated is given in equation 6.3.2

$$I = \int_0^{E_m} I(E) e^{-L(E)} e^{-l_f \mu_f(E)} dE. \tag{6.6.1}$$

We can use Watson's Lemma to derive an approximation to this integral which becomes more accurate as the filter attenuation $l_f \mu_f(E_m)$ becomes large. This theorem [Copson 1965] states that if $\Phi(t)$ is analytic for $|t| < R$ and $|\Phi(t)| < Ke^{bt}$ for fixed K and b when $|t| \geq R$ then

$$\int_0^{\infty} \Phi(t) e^{-zt} dt \sim \sum_{m=1}^{\infty} \alpha_m \Gamma(m) z^{-m} \tag{6.6.2}$$

where the α_m are the coefficients in the Taylor's series of $\Phi(t)$

$$\Phi(t) = \sum_{m=1}^{\infty} \alpha_m t^{m-1} \quad \text{for} \quad |t| < R. \tag{6.6.3}$$

The symbol $\sim$ denotes an asymptotic approximation and $\Gamma(m)$ is the gamma function which for integers has the value $\Gamma(m+1) = m!$

In order to apply the theorem, equation 6.6.1 has to be manipulated to the form of the left hand side of equation 6.6.2. This may be done by making the substitutions:

$$\tau = \mu_f(E) \tag{6.6.4}$$

$$t = \tau - \mu_f(E_m). \tag{6.6.5}$$

The result is

$$I = e^{-l_f \mu_f(E_m)} \int_0^{\Delta\mu} \frac{I[E(t)]}{-\mu_f'[E(t)]} e^{-L[E(t)]} e^{-l_f t} dt \tag{6.6.6}$$

where a prime denotes a derivative with respect to E and where $\Delta\mu = \mu_f(0) - \mu_f(E_m)$. But for any material $\mu_f(O) = \infty$, thus $\Delta\mu = \infty$ and the integral in 6.6.6 is in the form necessary to apply Watson's Lemma with

$$\Phi(t) = \frac{I[E(t)]}{-\mu_f'[E(t)]} e^{-L[E(t)]} \tag{6.6.7}$$

As $t \to 0$, $E \to E_m$ and the functions I, μ_f', L are differentiable if the attenuation coefficients do not have K edges in this region. This is certainly the case for body materials. As $t \to \infty$, $E \to 0$ and both $\mu_f'(E)$ and $L(E)$ approach infinity while $I(E)$ remains finite. Thus $\Phi(t) \to 0$ as $t \to \infty$ and $|\Phi(t)| < Ke^{bt}$ for a finite K and $b = 0$ when $|t| \geq R$. Both hypotheses of Watson's Lemma are thus satisfied.

The coefficients $\{\alpha_m\}$ are given by Taylor's Theorem

$$\begin{aligned} \alpha_1 &= \Phi(0) \\ \alpha_2 &= \left.\frac{d\Phi}{dt}\right|_{t=0} \\ \alpha_3 &= \left.\frac{1}{2}\frac{d^2\Phi}{dt^2}\right|_{t=0} \\ \alpha_4 &= \left.\frac{1}{6}\frac{d^3\Phi}{dt^3}\right|_{t=0} \end{aligned} \tag{6.6.8}$$

The region near $t = 0$ corresponds to the energy region near the upper cutoff E_m of the spectrum. As shown in Fig. 6.1 , the spectrum in this region is very accurately approximated by a linear function

$$I(E) = \beta(E_m - E) \tag{6.6.9}$$

Since we are only interested in the behavior for $E < E_m$, the approximation is valid. The constant β depends on the anode material. Using this result, the derivatives in equation 6.6.8 may be evaluated. The results are

$$\alpha_1 = 0 \tag{6.6.10}$$

$$\alpha_2 = \frac{\beta e^{-L(E_m)}}{[\mu'_f(E_m)]^2} \tag{6.6.11}$$

$$\alpha_3 = \frac{1}{2}\left[3\beta h(E_m) + 2\beta L'(E_m)\right]\frac{e^{-L(E_m)}}{[\mu'_f(E_m)]^3} \quad \text{where} \quad h(E) = \frac{\mu''_f(E)}{\mu'_f(E)} \tag{6.6.12}$$

$$\alpha_4 = \frac{1}{6}\Big[-3\beta h'(E_m) + 11\beta h(E_m)^2 - 3\beta L''(E_m) + 12\beta h(E_m)L'(E_m) + 3\beta L'^2(E_m)\Big]\frac{e^{-L(E_m)}}{[\mu'_f(E_m)]^4} \tag{6.6.13}$$

Substituting these results in 6.6.2 yields

$$I = \frac{\beta}{[l_f\mu'_f(E_m)]^2}[1+\gamma(L)]\exp\left[-l_f\mu_f(E_m) - L(E_m)\right] \tag{6.6.14}$$

where

$$\gamma(L) = -[3h(E_m) + 2L'(E_m)]\frac{1}{l_f\mu'_f(E_m)} + \left[-3h'(E_m) + 11h(E_m)^2 - 3\beta L''(E_m) + 12h(E_m)L'(E_m)\right] \times \frac{1}{[l_f\mu'_f(E_m)]^2} + 3\left[\frac{L'(E_m)}{l_f\mu'_f(E_m)}\right]^2$$

The quantity reconstructed in a computerized tomography system is $-ln\ I/I_{L=0}$. This is, from equation 6.6.14

$$-\ ln\frac{I}{I_{L=0}} = L(E_m) - ln[1+\gamma(L)] + ln[1+\gamma(0)] \tag{6.6.15}$$

If $l_f\mu_f$ is large then $\gamma(L)$ is small and

$$ln[1+\gamma(L)] = \gamma - \frac{1}{2}\gamma^2 \tag{6.6.16}$$

Thus 6.6.15 becomes

$$-\ ln\frac{I}{I_{L=0}} = L(E_m) + \frac{2L'(E_m)}{l_f\mu'_f(E_m)} - \left[\frac{L'(E_m)}{l_f\mu'_f(E_m)}\right]^2 \tag{6.6.17}$$

where terms of order $(1/l_f\mu'_f)^2$ are neglected in the linear part and order $(1/l_f\mu'_f)^4$ are neglected in the quadratic part.

7. Conclusion

The main contribution of this thesis is the formulation of a theoretical framework for the problem of extracting energy dependent from x-ray transmission measurements. This formulation can be used in two ways. First, it shows the limitations of the information that can be derived from energy dependent measurements. Also, it can be used to derive techniques for calculating complete energy dependent information from relatively simple low resolution measurements.

A statistical model for the problem of estimating energy dependent information from measurements with low energy resolution is another contribution of this thesis. The statistical model is used to derive an optimum procedure for calculating the energy dependent information. It is also used to calculate errors in the measurement for a given patient dose. The considerations of system complexity and patient dose are of major importance in a medical radiography system.

A third contribution of this thesis is a set of techniques for the extraction and utilization of energy dependent information in single projection and computerized tomography systems. These techniques require relatively simple modifications of the conventional systems and produce a great deal more information.

In computerized tomography, energy dependent techniques can be used to eliminate a major problem: the spectral shift artifact. An analysis of the techniques used to correct this artifact in conventional systems is a fourth contribution of this thesis. The analysis is independent of the reconstruction technique and shows the dependence of the magnitude of the artifact on the parameters of the system.

Future work in this field should have two main emphases: the design of practical medical radiography systems using the results in this thesis and the extension of the results. The application of the results can also lead to interesting theoretical problems such as the characterization of instabilities in x-ray systems and techniques for the solution of the estimator equations in the presence of these instabilities. The results in this thesis can be extended to include high atomic number materials and energy regions larger than the currently used diagnostic energy region.

Bibliography

[1]

Alberi, J.L., H.W. Kraner, P. Bradley-Moore, H.L. Atkins, 1974, "Transmission scanning II," IEEE Trans. Nuc. Sci. , NS-21, 635-644.

Ambrose, J. and G. Hounsfield, 1973, "Computerized transverse axial tomography, Brit. J. Radiol. 46, 148 (abstract).

Barrett, H.H. S.K. Gordon, R.S. Hershel, 1975, "Statistical limitations in transaxial tomography," to be published.

Bernstein, A. and A.K. Mann, 1956, "Summary of recent measurements of the Compton effect," Am. J. of Phys., 24, 445.

Bracewell, R.N. , class notes, "Image formation and Interference," Dept. of Elec. Engrg. , Stanford University, Stanford, California.

Bracewell, R.N., 1956, "Strip integration in radio astronomy," Australian J. Phys. , 9, 198-217.

Cameron, J.R. and J. Sorenson, 1963, "Measurement of bone mineral in vivo: an improved method," Science, 142, 230-232.

Chan, J. L.-H., R.E. Alvarez, A. Macovski, 1976, "Measurement of soft tissue overlying bone utilizing broad band energy spectrum techniques," IEEE Trans. Nuc. Sci., NS-23, 551-554.

Cho, Z.H., C.M. Tsai, G. Wilson, 1975, "Study of contrast and modulation mechanisms in x-ray/photon transverse axial transmission tomography," Phys. Med. Biol. , 20, 879-889.

Copson, E.T., 1965, Asymptotic Expansions, (Cambridge University Press, Cambridge), Chapter 6.

Deslattes, R.D. , 1969, "Estimates of x-ray attenuation coefficients for the elements and their compounds," Acta Cryst., A25, 89-93.

Donovan, G.E., 1951, "Radiography in colour," Lancet, 1, 832-833.

Donovan, G.E. and G. Jones, 1951, "Colour in radiography," Proc. Roy. Soc. Med., 44, 816-818.

Dyson, N,A., 1973, X-Rays in Atomic and Nuclear Physics, (Longman Group Limited, London).

Epp, E.R. and H. Weiss, 1966, "Experimental study of the photon energy spectrum of primary diagnostic x-rays," Phys. Med. Biol, 11, 225-238.

Evans, R.13., 1955, The Atomic Nucleus, (McGraw-Hill, New York).

Fano, U., 1953, "Gamma ray attenuation - basic processes," Nucleonics, 11, No. 8, 8-12.

Gado, M. and M. Phelps, 1975, "The peripheral zone of increased density in cranial computed tomography," Radiology, 117, 71-74.

Glocker, R. and W. Frohnmayer, 1925, "Uber die rontgenspektrosopische Bestim mung des Gewichtsanteiles eines Elementes in Gemengen und Verbindungen," Ann. Physik [4], 76, 369-395.

Goodman, J.W., 1968, Introduction to Fourier Optics, (McGraw-Hill, New York), 21-25,

Hounsfield, G.N., 1975, in Reconstructive Tomography in Diagnostic Radiology and Nuclear Medicine, edited by M.M. Ter-Pogossian (Baltimore University Park Press) in press.

ICRU, 1971, Radiation Quantities and Units, International Comm. on Radiation Units and Measurements, Washington, D.C., Report #19, July 1, 1971.

ICRU, 1970, "Radiation Dosimetry: X-Rays Generated at Potentials of 5 to 150 Kv," International Comm. on Radiation Units and Measurements, Washington, D.C. Report No. 17.

Jacobson, B., 1958, "Dichromography-method for in-vivo quantitative analysis of certain elements," Science, 128, 1346.

Jacobson, B. and R.S. MacKay, 1958, "Radiological contrast enhancing methods," Advances in Biological & Medical Physics, edited by C.A. Tobias and J.H. Lawrence (Academic Press, New York/London, 1958), Vol. VI, 201-261.

Kaplan,W., 1973, Advanced Calculus, (Addison-Wesley, Reading, Mass.).

Klein, 0. and Y. Nishina, 1929, "Uber die Streuung von Strahlung durch freie Elektronen nach der neuen relativistischen Quantendynamik von Dirac," Zeit. fur Physik, 52, 853.

Macovski, A., 1975, class notes, "Medical Imaging Systems," Dept. of Elec. Engrg., Stanford University, Stanford, California.

Macovski, A., R.E. Alvarez, J. L.-H. Chan, 1974, "Selective material x-ray imaging using spatial frequency multiplexing," Applied Optics, 13, 2202-2208.

Macovski, A., R.E. Alvarez, J. L.-H. Chan, J.P. Stonestrom, 1975, "Correction for spectral shift artifacts in x-ray computerized tomography," in Technical Digest, Image Processing for 2D & 3D Reconstruction from Projections, (Optical Soc. of Am, Washington, D.C.) paper MB1.

Macovski, A. and J.P. Stonestrom, 1975, private communication.

Mazess, R.B., J.R. Cameron, J.A. Sorenson, 1970, "Determining body composition by radiation absorption spectrometry," Nature, 228, 771-772.

McCracken, D.D. and W.S. Dorn, 1964, Numerical Methods and Fortran Programming, (Wiley, New York).

Mistretta, C.A., F. Kelcz, M.G. Ort, M.P. Siedband, J.R. Cameron, A.B. Crummy, R.E. Polcyn, 1974, "Absorption edge fluoroscopy," IEEE Trans. Nuc. Sci., NS-21, 645-651.

Papoulis, A., 1965, Probability, Random Variables, and Stochastic Processes, (McGraw-Hill, New York).

Parzen, F., 1962, Stochastic Processes, (Holden-Day, San Francisco).

Phelps, M.E., E.J. Hoffman, M.M. Ter-Pogossian, 1975, "Attenuation coefficients of various body tissues, fluids and lesions at photon energies of 18 to 136 Kev," Radiology, 117, 573-583.

Radon, J., 1917, "Uber die Bestimmung von Funktionen durch ihre integralwerte langs gewisser Manningfaltigkeiten," Ber. Saechs. Akad. Wiss. Leipzig, Math. Phys., Kl 69, 262-277.

Rushton, W.A.H., 1969, "Colour perception in man," in Processing of Optical Data by Organisms and Machines, edited by W. Reichardt Academic Press, New York/London) 565-577.

Snyder, D.L., 1975, Random Point Processes, (Wiley, New York).

Stonestrom, J.P. and A. Macovski, 1975, "The Scatter Problem in Fan-Beam Computerized Tomographic Systems," in Technical Digest, Image Processing for 2D & 3D Reconstruction from Projections, (Optical Society of America, Washington, D.C.) paper WE 3.

Takahashi, S., 1952, "Chromatoroentgenography A method of taking the colored roentgenogram on the multilayer color film," Tohoku J. Exptl. Med., 56, 43-45.

Ter-Pogossian, M.M., 1967, The Physical Aspects of Diagnostic Radiology, (Harper and Row, Inc., New York) 179-183, 202-203.

Thoraeus, R., 1940, "Standard curves of the absorption of Roentgen rays in aluminum and their employment for estimating the equivalent of the initial filtration in Roentgen tubes," Acta. Radiol., 21, 603-614.

Tuddenham, W.J., J.F. Hale, E.P. Pendergrass, 1953, "Supervoltage diagnostic roentgenography," Amer. J. Roentgen., 70, 759-765.

Van Trees, H.L., 1968, Detection, Estimation and Modulation Theory, Part I, (Wiley, New York).

Zatz, L.M., 1976, "The effect of changing Kvp in the EMI scanner and its use for selective material imaging," Radiology, 119, 683-688.

A. Solution of Estimator Equations by Newton-Raphson Method

The Newton-Raphson method for finding the root of an equation is discussed in most calculus textbooks. The method is iterative. In attempting to solve the equation,

$$F(x) = 0 \tag{A.0.1}$$

if the nth estimate of the root is x, the $(n+l)$st estimate is

$$x_{n+1} = x_n - \frac{F(x_n)}{F'(x_n)} \tag{A.0.2}$$

The prime denotes a derivative with respect to x. The conditions for convergence of this method are [McCracken and Dorn, 1964]:

1. the initial guess is sufficiently close to a root of $F(x) = 0$.
2. $F''(x)$ is not excessively large.
3. $F'(x)$ is not too close to zero.

The Newton-Raphson method may be generalized to solve two equations in two unknowns

$$F(x, y) = 0 \tag{A.0.3}$$
$$G(x, y) = 0 \tag{A.0.4}$$

Suppose the nth guess is (x, y). Expanding F and G in Taylor's series about this point:

$$F(x, y) = F(x_n, y_n) + (x - x_n)\frac{\partial F}{\partial x} + (y - y_n)\frac{\partial F}{\partial y} + \dots \tag{A.0.5}$$

$$F(x, y) = G(x_n, y_n) + (x - x_n)\frac{\partial G}{\partial x} + (y - y_n)\frac{\partial G}{\partial y} + \dots \tag{A.0.6}$$

If these series are truncated as written and $F(x, y) = 0$ and $G(x, y) = 0$, two simultaneous linear equations for $(x - x_n)$ and $(y - y_n)$ result. Their solution gives the value for the $(n+l)$st iteration:

$$x_{n+1} = x_n - \left[F(x_n, y_n)\frac{\partial G}{\partial y} - G(x_n, y_n)\frac{\partial F}{\partial y}\right]/J \tag{A.0.7}$$

$$y_{n+1} = x_n - \left[F(x_n, y_n)\frac{\partial G}{\partial x} - G(x_n, y_n)\frac{\partial F}{\partial x}\right]/J \tag{A.0.8}$$

where

$$J = \frac{\partial F}{\partial x}\frac{\partial G}{\partial y} - \frac{\partial F}{\partial y}\frac{\partial G}{\partial x}$$

The estimator equations are:

$$F(A_1, A_2) = lnI_1 + b_1A_1 + b_2A_2 + b_3A_1^2 + b_4A_2^2 + b_5A_1A_2 + b_6A_1^3 + b7 = 0 \quad \text{(A.0.9)}$$

$$G(A_1, A_2) = lnI_1 + c_1A_1 + c_2A_2 + c_3A_1^2 + c_4A_2^2 + c_5A_1A_2 + c_6A_1^3 + c7 = 0 \quad \text{(A.0.10)}$$

The values of lnI_1 and lnI_2 are known and these equations must be solved for A_1 and A_2. Since these are polynomials, the expressions for the derivatives can be easily derived.

The initial guesses $A_{1,0}$ and $A_{2,0}$ were derived from these equations by dropping all the nonlinear terms. The resultant linear equations

$$b_1A_1 + b_2A_2 = lnI_1 - b_7 \quad \text{(A.0.11)}$$

$$c_1A_1 + c_2A_2 = lnI_2 - c_7 \quad \text{(A.0.12)}$$

can be easily solved.

B. Least Squares Curve Fitting for Determining Values of a_1 and a_2 from Experimental Data

The values of a_1 and a_2 may be determined from experimental measurements of the linear attenuation coefficient at different energies. Since there are only two coefficients, measurements at two energies are sufficient to determine their values. Usually, measurements at many more than two energies are available and some kind of curve fitting may be used to increase the accuracy of the values of a_1 and a_2.

In this appendix, the technique for least squares curve fitting is described [Hamming, 1973]. This technique is widely used and easy to apply. The justification for the use of this technique is the fit to the experimental data. This should be about as accurate as the measurements themselves.

Suppose that measurements of the linear attenuation coefficient $\mu(E_j)$ are available at energies E_j, $j = l, 2, \ldots, N$. The problem is to choose values of a_1 and a_2 that minimize the sum of the squares of the difference between $\mu(E_j)$ and

$$\hat{\mu}(E_j) = a_1 f_1(E_j) + a_2 f_2(E_j). \tag{B.0.1}$$

In our case, $f_1(E) = 1/E^3$ and $f_2(E) = f_{\text{KN}}(E)$. The squared error is

$$\text{Error} = x^2 = \sum_{j=1}^{N} \left[\sum_{i=1}^{2} a_i f_i(E_j) - \mu(E_j) \right]^2 W_j \tag{B.0.2}$$

where W_j are weighting factors to be set later. Differentiating with respect to a_1 and a_2 and setting the result equal to zero yields the set of equations

$$\sum_{j=1}^{N} \sum_{i=1}^{2} a_i W_j f_i(E_j) f_k(E_j) = \sum_{j=1}^{N} \sum_{i=1}^{2} \mu(E_j) f_k(E_j) W_j, \qquad k = 1, 2 \tag{B.0.3}$$

Defining the matrix U with elements $u_{i,k} = \sum_{j=1}^{N} f_i(E_j) f_k(E_j) W_j$ and the vectors and $\vec{a}$ and $\vec{T}$ with elements a_1 and a_2, and $T_k = \sum_{j=1} N \mu(E_j) f_k(E_j) W_j$, equations B.0.3 may be written

$$U\vec{a} = \vec{T} \tag{B.0.4}$$

so long as the basis functions $f_1(E)$ and $f_2(E)$ are linearly independent over the set of energies $\{E_j\}$, the determinant of U is nonzero [Hamming, 1973] and equation B.0.4 can be solved for a_1 and a_2.

Because of the large dynamic range of the data, a set of weights equal to the measured values of the attenuation coefficients was used. That is $W_j = 1/\mu(E_j)$. The curve fitting procedure thus tends to minimize the square of the fractional error.